Improvement of the Performance of Direct Electron Transfer-Type Bioelectrocatalysis Based on the Understanding of the Interaction between Redox Enzymes and Electrodes

Hong-qi Xia

2017

Table of contents

General Introduction

Direct electron transfer (DET)-type bioelectrocatalysis is an ideal system in which the electron is transferred directly from electrodes to the substrate molecule (or *vice versa*) via the redox active site of an enzyme (Fig. 1). Since the DET-type system is constructed only with an enzyme and an electrode without any mediator, it is possible to miniaturize devices to extremely small size and to minimize the thermodynamic over potential required in electron transfer between an enzyme and a mediator, thereby making it very suitable for a variety of bioelectrochemical devices including biofuel cells and biosensors. However, interfacial electron transfer (IET) between an enzyme and a solid electrode often has a high kinetic barrier because the redox active sites of enzymes are usually deeply buried in peptides and the IET rate constant decreases exponentially with an increase in the distance between the electrode surface and the redox active site of the enzyme.

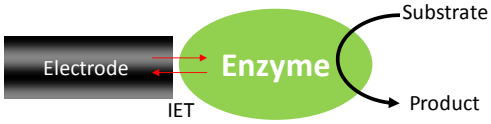

Fig. 1 Schematic illustration of DET-type booelectrocatalysis

Several redox enzymes are capable of direct electrochemical communication with suitable electrodes, although the number of DET-type enzymes is limited. There must be several factors governing the DET-type bioelectrocatalysis, but the factors have not yet clearly elucidated. Understanding the interaction between redox enzymes and electrodes is essential for improving the performance of DET-type bioelectrocatalysis as well as for exploring novel DET-type enzyme. In this thesis, the author attempted to investigate the factors of the electrode surface and enzymes affecting the performance of DET-type bioelectrocatalysis. The author also attempted to improve the performance of DET-type bioelectrocatalysis with oriented immobilization of the redox enzymes at functionalized electrode surfaces based on the understanding of the interaction between the redox enzymes and the electrodes.

In chapter 1, the author focuses on siginificance the mesoporous structure for promoting the performance of DET-type bioelectrocatalysis. Peroxidase (POD) was used as a model enzyme for reduction of H_2O_2. Bare glassy carbon (GC) electrode and ketjen black modified glassy carbon (KB/GC) electrode were used as platforms for adsorption of POD, respectively. Electrochemical methods were used to inversitgated DET-type bioelectrocatalysis of POD. Furthermore, the author also tried to constructe an bienzyme electrode by coupling of the H_2O_2-generated oxidase (for example, glucose oxidase) and POD for substrate of H_2O_2-generated oxidase determination.

In chapter 2, the author focuses on the effects of the electrostatic interaction between enzymes and electrodes on the performance of DET-type bioelectrocatalysis. Three types of CNTs with different lengths were used as platform for adsorption of bilirubin oxidase (BOD), copper efflux

oxidase (CueO) and hydrogenase (H_2ase). Several factors of CNTs and enzymes affect the adsorption of enzymes have been investigated and discussed in the viewpoint of DET-type bioelectrocatalysis.

In chapter 3, based on the understanding of the interaction between the enzyme and electrode, the author attempt to improve the proformance of DET-type bioelectrocatalysis by oriented-immobilization of redox enzymes onto functionalized electrode surfacecs. Charged surfaces were constructed by modification of aminobenzoic acid and *p*-phenylenediamine onto KB electrode for oriented-adsorption of BOD and H_2ase. On the other hand, in consideration of the specific interaction between methoxy substituent and the electron-donating heme *c* moiety of D-fructose dehydrogenase (FDH), the author also attempt to construct several methoxy-substituent-functionalized surfaces and assess DET-type bioelectrocatalytic performance of FDH adsorbed on these electrodes.

Chapter 1

Significances of mesoporous structure for promoting DET-type bioelectrocatalysis

1-1 Direct electron transfer-type bioelectrocatalysis of peroxidase at mesoporous carbon electrodes and its application for glucose determination based on bienzyme system

Abstract

Non-catalytic direct electron transfer (DET) signal of Compound I of horseradish peroxidase (POD) was first detected at 0.7 V on POD/carbon nanotube mixture-modified electrodes. Excellent performance of DET-type bioelectrocatalysis was achieved with POD immobilized with glutaraldehyde on Ketjen Black (KB)-modified electrodes for H_2O_2 reduction with an onset potential of 0.65 V (vs. Ag|AgCl|sat. KCl) without any electrode surface modification. The POD-immobilized KB electrode was found to be suitable for detecting H_2O_2 with a low detection limit (0.1 μM at *S*/*N* = 3) at −0.1 V. By co-immobilizing glucose oxidase (GOD) and POD on the KB-modified electrode, a bienzyme electrode was constructed to couple the oxidase reaction of GOD with the DET-type bioelectrocatalytic reduction of H_2O_2 by POD. The amperometric detection of glucose was performed with a high sensitivity (0.33 ± 0.01 μA cm^{-2} μM^{-1}) and a low detection limit (2 μM at *S*/*N* = 3).

1. Introduction

Peroxidases (POD) are ubiquitous in the living world. The catalytic center of POD is a protoheme at which hydrogen peroxide (H_2O_2) is reduced to water in the presence of suitable electron donors. The ferric state of POD is oxidized to Compound I by H_2O_2 in a one-step two-electron reaction:

$$POD(Fe^{3+}) + H_2O_2 \rightarrow \text{Compound I} + H_2O \quad (1)$$

Compound I is re-reduced to the ferric state via Compound II as an intermediate:

$$\text{Compound I} + H^+ + e^- \rightarrow \text{Compound II} \quad (2)$$

$$\text{Compound II} + H^+ + e^- \rightarrow POD(Fe^{3+}) \quad (3)$$

The electrochemistry of horseradish POD has been extensively studied.[1] H_2O_2 is not the exclusive electron acceptor to provide Compound I from the ferric state. Actually, the ferric form is easily oxidized to Compound I (as well as Compound II) by suitable electron acceptors such as $IrCl_6^{2-}$. The three redox states are reversible and the formal potential of the reactions given by Eqs. (2) and (3) were spectroelectrochemically determined as 0.75 and 0.72 V (vs. Ag|AgCl at pH 7.0), respectively.[2] Since the electrochemical oxidation of H_2O_2 frequently requires high electrode

potentials in the absence of catalysts, the situation leads to co-oxidation of other electroactive metabolites in the physiological fluids to cause positive interference. Therefore, POD is frequently used in biosensors for determination of H_2O_2 .

Many papers have reported non-catalytic direct electron transfer (DET) of POD and bioelectrocatalytic reduction of H_2O_2.[3–6] However, most non-catalytic DET signals of POD are assigned to the redox reaction of Fe^{3+}/Fe^{2+} of the protoheme at −0.2 V (vs. Ag|AgCl) and the Fe^{3+}/Fe^{2+} redox reaction is entirely unrelated to the catalytic redox cycle described in Eqs. (1)–(3). In addition, the current densities of the catalytic waves of the H_2O_2 reduction at POD-adsorbed electrodes are very low, and the onset potentials are in a large variety in the literature and are usually much more negative than the redox potential of Compound I. Therefore, several artificial mediators have been proposed for the reduction of Compound I to construct mediated electron transfer- (MET-) type biosensors for H_2O_2 detection.[7,8] MET-type POD sensors have been frequently combined with an H_2O_2-generating oxidase for determination of the first substrate of the oxidase.[9–15] One of the issues to be considered for such MET-type POD/oxidase bienzyme-electrode reactions may be that the oxidized form of a mediator generated in the POD reaction frequently works as an electron acceptor of the oxidase in the bienzyme system (due to the dehydrogenase activity), [13] which results in negative interferences.

Recently, catalytic waves of H_2O_2 reduction by POD on electrodes with positive onset potentials of approximately 0.5–0.6 V (vs. Ag|AgCl) were reported at carbon nanotube- (CNT-) modified graphite electrodes, although the mechanism remains unclear.[16,17] It has been proposed that mesoporous structures with porous radii close to the radius of an enzyme[18–20] and electrostatic interaction between the redox center of an enzyme and an electrode surface[21–26] are important to improve the performance of DET-type bioelectrocatalysis. Therefore, there seems to be some possibility to construct mesoporous electrodes suitable for DET reaction of POD.

On the other hand, glucose oxidase (GOD) is one of the key enzymes for determination of glucose. Although there are a countable number of papers claiming DET-type bioelectrocatalysis of GOD, a recent conclusion is that native GOD does not undergo DET reaction.[27] Therefore, GOD-based biosensors should detect H_2O_2 generated in the oxidase reaction or the reduced mediator in MET-type bioelectrocatalysis of GOD using its dehydrogenase activity.

In this work, Ketjen Black (KB) and water-soluble carbon nano tubes (CNTs) were used to construct mesoporous structured carbon electrodes suitable for DET-type bioelectrocatalysis of POD. As a result, a pair of weak but clear waves of non-catalytic DET reaction of POD embedded in CNTs was for the first time recorded at a POD/CNT mixture-modified electrode. In addition, great performance of mediator-free DET-type bioelectrocatalysis of POD was realized for two-electron reduction of H_2O_2 at KB-modified electrodes without any special electrode surface modification. The high catalytic efficiency and high stability of POD-immobilized KB-modified electrodes was

useful to reductively detect H_2O_2. In addition, the POD-electrode was used to detect H_2O_2 generated in the GOD reaction to construct semi-DET-type bienzyme biosensor for glucose determination, as shown in Scheme 1.

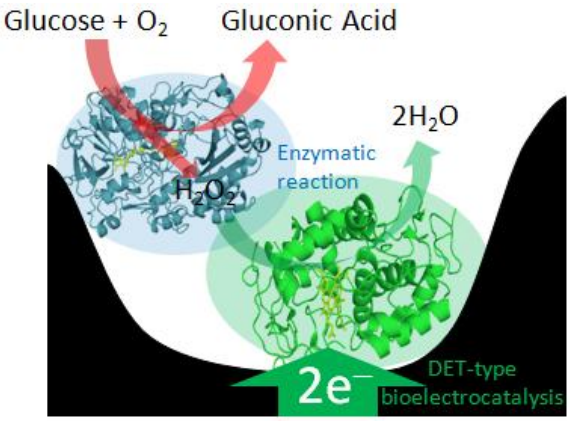

Scheme 1.

Proposed DET-type bienzymatic mesoporous electrode for glucose determination

2. Experimental

2.1 Materials and reagents

Ketjen Black EC300J (KB) was donated by Lion Co. (Japan). Poly(tetrafluoroethylene) fine powder (PTFE, 6-J) was obtained from DuPont Mitsui Fluorochemicals (Japan). Water-dispersed carbon nanotubes (CNTs, outer diameter: 10–15 nm, length: 1–4 μm) were donated by Nitta Corp. (Japan). Ascorbic acid (AA), uric acid (UA), glutaraldehyde (GA, 20%), glucose, and H_2O_2 were obtained from Wako Chemicals Co. (Osaka, Japan). Peroxidase from horseradish (POD, EC 1.11.1.7, 292 U mg^{-1}) and glucose oxidase from *Aspergillus sp*. (GOD, EC 1.1.3.4, 163 U mg^{-1}) were purchased from Toyobo Co. (Japan) and used without further purification. UA solution was prepared with 0.1 M KOH (1 M = 1 mol dm^{-3}), and the enzymes, substrates, AA, and GA solutions were prepared with a 0.1 M phosphate buffer (pH 7.0). All other chemicals used in this study were of analytical grade and all solutions were prepared with distilled water.

2.2 Preparation of POD modified electrode and POD/GOD bienzyme-modified electrode

A KB-modified glassy carbon electrode (KB/GCE) was prepared according to a previously described method.[28] In brief, a 3-μL KB slurry (PTFE:KB = 1:4, w/w) was dropped onto a rotating disk GCE surface (diameter = 3 mm) and dried at room temperature (1 L = 1 dm^3). For enzyme immobilization, a 20-μL enzyme solution (POD: 5 mg mL^{-1}) containing 5% (w/v) of GA was

applied on the KB/GCE and dried at room temperature for 2 h. The electrode was washed with a phosphate buffer (0.1 M, pH 7.0) and used for electrochemical measurements.

When CNTs were used as a platform for enzyme immobilization, the POD solution was mixed with a water soluble CNT suspension (0.3%) to form a POD/CNT mixture (POD:CNT = 1:2, w/w). A 20-μL POD/CNT mixture was applied on a polished GCE and dried under reduced pressure at room temperature for 30 min. This is a new method for enzyme immobilization using CNTs without any reagents. CNTs would be immobilized on GCE with π–π stacking and also seem to enfold the enzyme to minimize the length between the redox center of the enzyme and a CNT.

For the POD/GOD bienzyme-modified electrode, a 20-μL enzyme solution containing POD, GOD, and GA was applied on a KB/GCE surface and dried for 2 h at room temperature. For long-term storage, the enzyme electrode was stored at 4 °C in a water-saturated atmosphere.

2.3 Electrochemical measurement

Cyclic voltammetry and chronoamperometry were performed using an electrochemical analyzer ALS 701 E with a rotating disk GCE as a working electrode, a Pt wire as a counter electrode, and an Ag|AgCl|KCl (sat.) electrode as a reference electrode. Rotating disk voltammetry was performed at a rotating rate of 4000 rpm to obtain steady-state currents. All potentials were referenced against the reference electrode.

3. Results and Discussion

3.1 Non-catalytic and catalytic DET-type signals POD on mesoporous carbon electrodes

Fig. 1A shows a cyclic voltammogram (CV) of a POD/CNT mixture-modified GCE in a 0.1 M phosphate buffer solution (25 ± 1 °C, pH 7.0). A pair of small but visible surface-confined redox waves of POD was observed. The midpoint potential is approximately 0.7 V and very close to the average (0.73_5 V) of the two redox potentials determined spectroelectrochemically for the reactions of Eqs. (2) and (3).[2] The negative shift of the midpoint potential indicates that Compound I is embedded in CNTs more stably than the ferric form, most probably due to electrostatic interaction of Compound I with negatively charged CNTs. This is the first report of a non-catalytic DET signal of POD. In the presence of H_2O_2, a steady-state catalytic wave of H_2O_2 reduction was observed at potentials more negative than 0.6 V on a rotating disk CV (Fig. 1B). As expected, no catalytic reduction wave was observed in the absence of POD (Fig. 1B, inset) and at a POD-immobilized GCE (data not shown). Therefore, the reduction wave is assigned to a DET-type bioelectrocatalytic reduction of H_2O_2 by POD embedded in CNTs. Because direct oxidation currents of H_2O_2 were

observed at potentials more positive than 0.6 V (Fig. 1B), the zero current potential (0.6 V) is determined by the POD-catalyzed reduction of H_2O_2 and the non-catalytic direct oxidation of H_2O_2. This is the reason why the zero current potential is slightly more negative than the midpoint potential of POD (Compound I) embedded in CNTs.

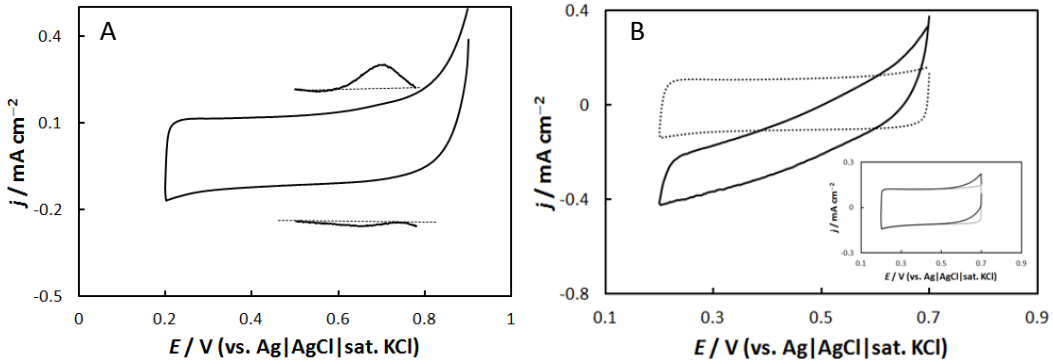

Fig. 1

A) Non-catalytic CV of POD/CNT mixture-modified GCE in the absence of H_2O_2 in 0.1 M phosphate buffer (pH 7) at a scan rate of 5 mV s^{-1}. The redox waves are shown after the capacitive background signal subtraction and are multiplied by a factor of 15 for the sake of clarity.

B) Rotating disk CVs of POD/CNT mixture-modified GCE in the absence (dotted line) and presence (solid line) of 0.1 mM H_2O_2. The inset shows rotating disk CVs at CNT-modified GCE in the absence and presence of 0.1 mM H_2O_2.

Fig. 2A shows rotating disk CVs at a POD-immobilized KB/GCE in a 0.1 M phosphate buffer solution in the absence and presence of H_2O_2. A well-defined sigmoidal catalytic reduction wave was obtained with an onset potential of approximately 0.65 V. The steady-state current density reached a limiting value of 0.7 ± 0.1 mA cm^{-2} at 0.1 mM H_2O_2. The signal was very stable even at a high rotating rate (4000 rpm) because POD is stably immobilized in the mesoporous structure of KB/GCE. Since the potential window of KB/GCE was limited to ca. 0.5 V (Fig. 2B), it was impossible to detect a non-catalytic DET signal of POD immobilized on the KB/GCE. However, very fast electron transfer from KB to Compound I must occur compared with CNTs, because the rising portion of the catalytic wave is sharper at KB/GCE than that at CNT/GCE. The limiting current density is also larger at KB/GCE than that at CNT/GCE. The three dimensional meso/micro structures of KB on the GCE seem to be one of the most important factors in improving the performance of the DET-type bioelectrocatalysis of POD, as predicted in our previous studies.[18–20] The fast catalytic reduction of H_2O_2 was realized at the POD-immobilized KB/GCE without any extra mediator or special surface modification at such high potentials.

We used GA as a cross-linker to form a stable enzyme layer for DET-type

bioelectrocatalysis. Such DET-type catalytic H_2O_2 reduction wave was obtained at POD-modified KB/GCE electrode in the absence of GA. However, the current decreased with time, and the catalytic current density was smaller than that in the presence of GA. If multi-layer POD molecules are formed on the electrodes when GA is used, POD molecules in the second and upper layers (if any) would not work as DET-type electrocatalysts.

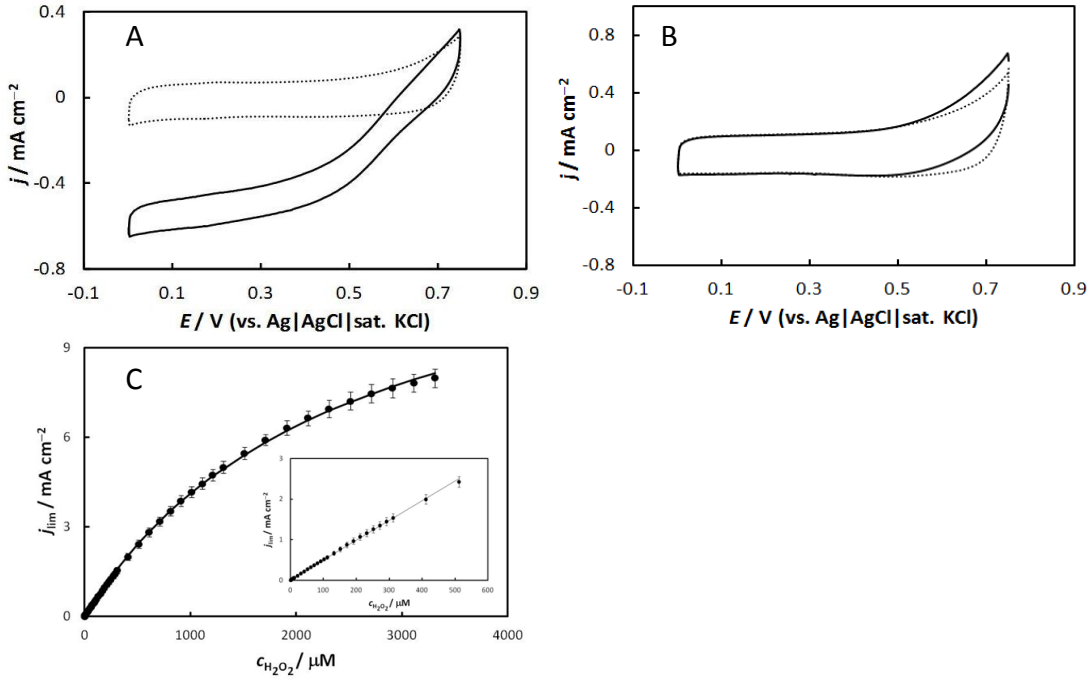

Fig. 2

Rotating disk CVs at (A)POD/KB/GCE and (B) KB/GCE in the absence (dotted line) and in the presence (solid line) of 0.1 mM H_2O_2 in 0.1 M phosphate buffer (pH 7) at a scan rate of 5 mV s^{-1} and a rotating rate of 4000 rpm.

(C) Dependence of the limiting steady-state current response (j_{lim}) on the concentration of H_2O_2 ($c_{H_2O_2}$) at 0 V. The solid line was evaluated by a nonlinear regression analysis with Eq. (4), and the inset shows a linear dependence of j_{lim} on $c_{H_2O_2}$ at low $c_{H_2O_2}$.

Fig. 2C shows the relationship between the limiting reduction current density (j_{lim}) at the POD/KB/GCE and the H_2O_2 concentration ($c_{H_2O_2}$).The value of j_{lim} was measured at 0 V. The j_{lim} value increased almost linearly with $c_{H_2O_2}$ up to 0.5 mM and showed a Michaelis–Menten-type curved characteristic at increased$c_{H_2O_2}$:

$$j_{lim} = \frac{j_{lim,max}}{1+K_{M,app}/c_{H_2O_2}} \quad , \qquad (4)$$

where $j_{lim,max}$ and $K_{M,app}$ represent the maximum value of j_{lim} and the apparent Michaelis-Menten constant, respectively. Using $j_{lim,max}$ and $K_{M,app}$ as adjustable parameters, the data were fitted to eq.

(4) through a non-linear regression analysis with Gnuplot© 5.0. The refined $K_{M,app}$ of POD immobilized on the KB/GCE was 2.4 ± 0.6 mM. The detection limit of H_2O_2 with the POD/KB/GCE was as low as 0.1 μM (S/N > 3), and the linear range was from 0.5 μM to 500 μM with a slope of 4.8 ± 0.4 μA cm^{-2} μM^{-1}. The biosensor prepared has high sensitivity and is suitable for the detection of extremely low concentrations of H_2O_2.

3.2 GOD/POD bienzyme-immobilized electrode for glucose determination

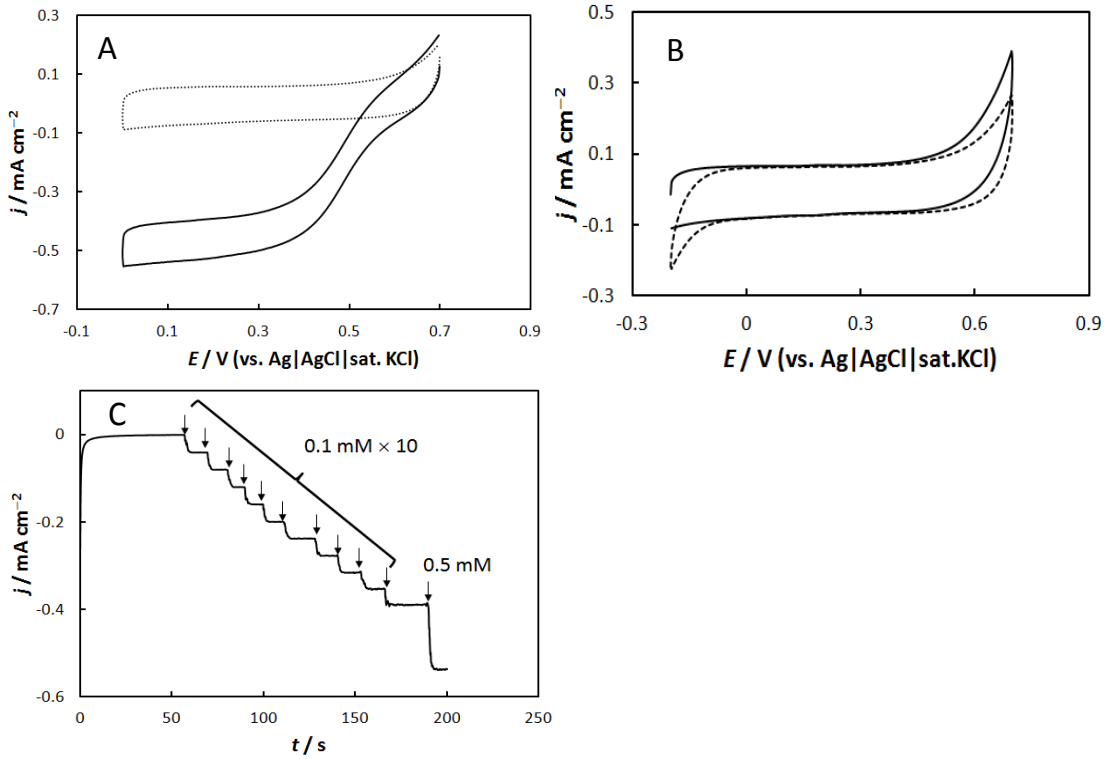

Fig. 3

Rotating disk CVs at (A)GOD/POD/KB/GCE and (B)GOD/KB/GCE in the absence (dotted line) and in the presence (solid line) of 1 mM glucose in 0.1 M phosphate buffer (pH 7) at a scan rate of 5 mV s^{-1} and a rotating rate of 4000 rpm.

(C)Steady-state current response at the rotating GOD/POD-immobilized KB/GCE upon the successive addition of glucose at 0 V. The measurement was carried out in 0.1 M phosphate buffer (25 °C, pH 7) at a rotating rate of 4000 rpm.

Fig. 3A shows typical rotating-disk CVs obtained at a GOD/POD-immobilized KB/GCE in the presence and absence of glucose. A clear catalytic reduction wave was observed at the bienzyme electrode in the presence of glucose. As expected, the similar reduction wave was also

obtained at the GOD/POD-immobilized KB/GCE when H_2O_2 was added (data not shown). Such reduction wave was not observed in the absence of POD on the electrode even in the presence of glucose (Fig. 3B). These results indicate that the reduction wave at the GOD/POD-immobilized KB/GCE is ascribed to the reduction of H_2O_2 (Eqs. (1)-(3)) generated in the GOD-catalyzed two-electron reduction of O_2 with glucose as an electron donor.

Fig. 3C shows a typical current–time curve at the GOD/POD-immobilized KB/GCE with the successive addition of a glucose solution into an air-saturated buffer solution at a detection potential of 0 V. The catalytic current density increased with the addition of glucose and reached a steady-state within 2 s. Such fast response may be attributed to two factors: 1) the excellent electron-transfer kinetics from the KB-modified electrode to POD (Compound I), and 2) the fast mass-transfer of H_2O_2 generated by the GOD reaction in the immobilized bi-enzyme layer.

Considering the fact that the composition of POD and an H_2O_2-generated oxidase may affect the biosensing performance of bienzyme biosensors,[11,12] the ratio of POD to GOD was examined. Fig. 4A shows the effects of the POD/GOD ratio on the relative current response to 1 mM glucose (ratios from 0.05 to 0.30 at a constant GOD concentration of 5 mg mL^{-1}) in the mixed enzyme/reagent solutions for immobilization. The relative response increased with the POD/GOD ratio and reached a maximum at a POD/GOD ratio (w/w) of 0.15. Then, it gradually decreased with increasing the POD/GOD ratio. Therefore, a POD/GOD ratio (w/w) of 0.15 was selected for the following experiments to obtain optimal sensitivity. The value was simply optimized here, but it would become very important in near future to describe the situation by numerical simulation based on the kinetics and the mass transfer of the substrate, O_2, and H_2O_2.

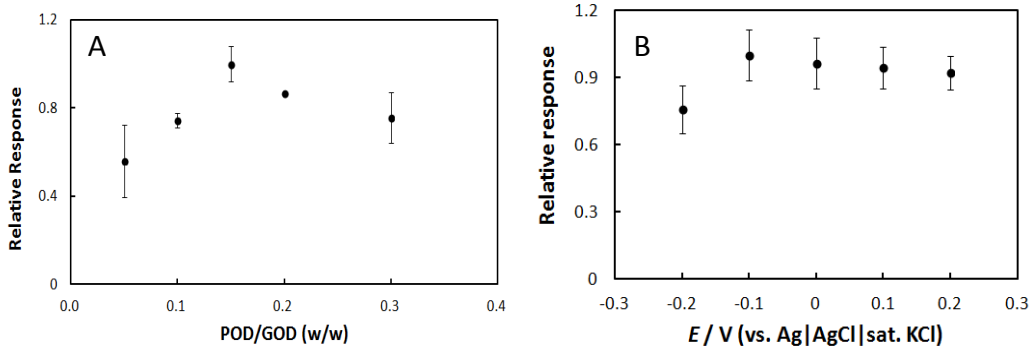

Fig. 4

Dependence of the limiting steady-state current response on (A) the weight ratio of POD to GOD and (B)the electrode potential for the detection of 1 mM glucose at 0 V and at a rotating rate of 4000 rpm. The currents are depicted as relative values.

The effect of the detection potential was also investigated in the range from −0.2 to 0.2 V

on the response of the biosensor in the presence of 1 mM glucose (Fig. 4B). With decreasing the detection potential from 0.2 V, the reduction current gradually increased and reached a maximum at −0.1 V. For more negative detection potential values (such as −0.2 V), the current decreased, probably because of the progressive inactivation of POD.[10] In addition, at potentials more negative than −0.15 V, the influence of non-catalytic direct reduction of O_2 at electrodes appeared. On the other hand, several reduced compounds such as AA and UA will be non-catalytically oxidized at carbon electrodes at potentials more positive than 0 V and interfere with the amperometric detection of glucose. Thus, the detection potential was set at −0.1 V for the glucose-sensing bienzyme electrode.

3.3 Glucose sensing

The characteristics of the biosensor were investigated by chronoamperometric measurements under the optimum conditions obtained above. Fig. 5A shows a calibration curve. The data showed a linear dependence of the limiting catalytic current density on the glucose concentration (c_{glc}) from 5 μM to 1500 μM and a Michaelis–Menten-type relation at increased c_{glc}. The apparent Michaelis-Menten constant ($K_{M,app}$) for glucose was estimated to be 3.5 ± 0.3 mM, which is much lower than the true Michaelis constant reported for GOD (33 mM with O_2 as an electron acceptor in a solution under air-saturated conditions).[29] This is most probably because of the lower $K_{M,app}$ value (2.4 ± 0.6 mM) of POD against H_2O_2 than that of GOD against glucose. The lowest glucose detection limit with the proposed bienzyme biosensor was estimated at 2 μM (S/N > 3) with a slope of 0.33 ± 0.01 μA cm^{-2} μM^{-1}.

GOD shows highly specific catalytic activity toward glucose even in the presence of other carbohydrates. However, some interferences such as AA may react with POD (Compound I) as electron donors resulting in negative interferences.[30] The effects of the presence of UA (0.5 mM) and AA (0.5 mM) as probable interfering species on glucose detection were examined. These compounds caused negligible decreases of less than 1% and 2%, respectively, for the reduction current of 0.5 mM glucose. Therefore, these substances hardly interfered with the response of the biosensor due to low detection potential and high specificity of the enzymes.

In addition, the stability of the proposed bienzyme biosensor was investigated with chronoamperometry at −0.1 V for 7200 s. Only a slight decrease (< 8%) in the current response (at 0.5 mM glucose) was observed for the continuous measurements. For long-term storage stability, the prepared biosensor was stored at 4 °C for two weeks. The current response to 0.5 mM glucose still remained above 90%. The results verify the high stability of the bienzyme biosensor.

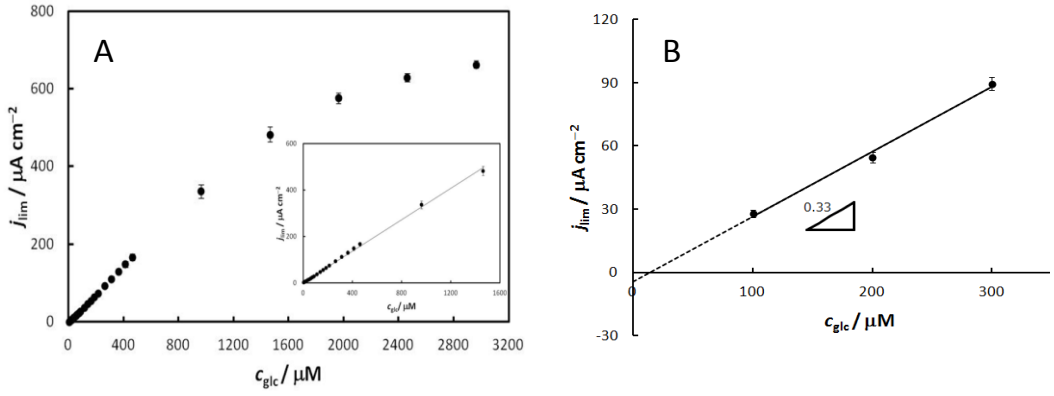

Fig. 5

(A)Dependence of the limiting steady-state current density (j_{lim}) on the concentration of glucose (c_{glc}) at −0.1 V at a rotating rate of 4000 rpm. The inset shows the linear dependence of j_{lim} on c_{glc}.

(B) Calibration line for glucose detection in the presence of 1 mg mL^{-1} BSA in 0.1 M phosphate buffer (pH 7.0) as a diluted serum mimic with a GOD/POD-immobilized KB/GCE bienzyme sensor. The slope (0.33 μA cm^{-2} μM^{-1}) indicates the sensitivity of the bienzyme biosensor in 0.1 M phosphate buffer (pH 7.0) without BSA.

The low detection limit and high stability is suitable for glucose determination in real samples, for example, in serum. Since the glucose concentration in human serum (c_{glc} = 4.4–6.6 mM[31]) is higher than the upper limit of the linear range, we supposed to detect glucose in a diluted serum sample. Therefore, glucose determination was performed in a phosphate buffer (pH 7) containing 1 mg mL^{-1} bovine serum albumin (BSA) as a diluted serum mimic. The current responses were recorded with the successive addition of a standard glucose solution. Fig. 5B shows the relationship between j_{lim} and c_{glc}. The slope (0.31 ± 0.03 μA cm^{-2} μM^{-1}) was similar to that obtained for the standard glucose solution (0.33 ± 0.01 μA cm^{-2} μM^{-1})). The result indicates that the proposed bienzyme biosensor works properly even in the presence of BSA (1 mg mL^{-1}). Therefore, the proposed bienzyme biosensor is applicable for clinical diagnosis.

4. Conclusion

Thanks to the three-dimensional structure of mesoporous materials, a non-catalytic DET signal of POD was detected at the POD/CNT mixture-modified electrode with a redox potential of approximately 0.7 V. To the best of the authors' knowledge, this is the first case of the voltammetric detection of the non-catalytic wave of POD (Compound I). Great performance of DET-type

bioelectrocatalysis of immobilized POD was realized at KB-modified electrodes without any surface modification at such positive electrode potentials up to 0.6 V. The POD-immobilized KB/GCE can be utilized for detecting H_2O_2 with a low detection limit and high sensitivity. GOD as an H_2O_2-generated oxidase was co-immobilized with POD on KB/GCE for glucose determination. The proposed bienzyme glucose biosensor showed high sensitivity and high stability.

The proposed bienzyme system can be applied to the detection of several substrates by just replacing GOD with the corresponding oxidase, such as D-amino acid oxidase,[11] sarcosine oxidase,[12] and glutamate oxidase.[14] In addition, the reduction of H_2O_2 at such high electrode potentials on POD-immobilized mesoporous carbon electrodes can be utilized as bio-cathodes in biofuel cells in place of multi-copper oxidase-based bio-cathodes, since the activity of the latter bio-cathodes are liable to be inhibited by H_2O_2 and halogen ions.[32, 33] The positive onset potential for the H_2O_2 reduction at POD-immobilized electrodes is also one of the benefits as bio-cathodes in biofuel cells.

5. References

1 T. Ruzgas, L. Gorton, J. Emnéus, G. Marko-Varga, Kinetic models of horseradish peroxidase action on a graphite electrode, J. Electroanal. Chem. 391 (1995) 41–49.

2 M. Torimura, M. Mochizuki, K. Kano, T. Ikeda, T. Ueda, Mediator-assisted continuous-flow column electrolytic spectroelectrochemical technique for the measurement of protein redox potentials. Application to peroxidase, Anal. Chem. 70 (1998) 4690–4695.

3 Y.D. Zhao, W.D. Zhang, H. Chen, Q.M. Luo, S.F.Y. Li, Direct electrochemistry of horseradish peroxidase at carbon nanotube powder microelectrode, Sens. Actuators B 87 (2002) 168–172.

4 Y.T. Kong, M. Boopathi, Y.B. Shim, Direct electrochemistry of horseradish peroxidase bonded on a conducting polymer modified glassy carbon electrode, Biosens. Bioelectron. 19 (2003) 227–232.

5 T. Gu, J. Wang, H. Xia, S. Wang, X. Yu, Direct electrochemistry and electrocatalysis of horseradish peroxidase immobilized in a DNA/chitosan-Fe_3O_4 magnetic nanoparticle bio-complex film, Materials 7 (2014) 1069–1083.

6 K. Komori,T. Tatsuma, Y. Sakai, Direct electron transfer kinetics of peroxidase at edge plane sites of cup-stacked carbon nanofibers and their comparison with single-walled carbon nanotubes, Langmuir 32 (2016) 9163–9170.

7 T. Gu, Y. Hasebe, Peroxidase and methylene blue-incorporated double stranded DNA–polyamine complex membrane for electrochemical sensing of hydrogen peroxide, Anal. Chim. Acta 525 (2004) 191–198.

8 R. Katsube,Y. Kitazumi, O. Shirai, M. Yamamoto, K. Kano, Potentiometric coulometry using a liquid-film-modified electrode as a reversible surface-confined system, J. Electroanal. Chem. 780 (2016) 114–118.

9 L. Zhu, R. Yang, J. Zhai, C. Tian, Bienzymatic glucose biosensor based on co-immobilization of peroxidase and glucose oxidase on a carbon nanotubes electrode, Biosens. Bioelectron. 23 (2007) 528–535.

10 G.E. De Benedetto, F. Palmisano, P.G. Zambonin, One-step fabrication of a bienzyme glucose sensor based on glucose oxidase and peroxidase immobilized onto a poly (pyrrole) modified glassy carbon electrode, Biosens. Bioelectron. 11 (1996) 1001–1008.

11 C.H. Nieh, Y. Kitazumi, O. Shirai, K. Kano, Sensitive d-amino acid biosensor based on oxidase/peroxidase system mediated by pentacyanoferrate-bound polymer, Biosens. Bioelectron. 47 (2013) 350–355.

12 C.H. Nieh, S. Tsujimura, O. Shirai, K. Kano, Amperometric biosensor based on reductive H_2O_2 detection using pentacyanoferrate-bound polymer for creatinine determination, Anal. Chim. Acta. 767 (2013) 128–133.

13 R. Matsumoto, M. Mochizuki, K. Kano, T. Ikeda, Unusual response in mediated biosensors with an oxidase/peroxidase bienzyme system, Anal. Chem. 74 (2002) 3297–3303.

14 S. Yoshida, H. Kanno, T. Watanabe, Glutamate sensors carrying glutamate oxidase/peroxidase bienzyme system on tin oxide electrode, Anal. Sci. 11 (1995) 251–256.

15 M. Delvaux, A. Walcarius, S. Demoustier-Champagne, Bienzyme HRP-GOx-modified gold nanoelectrodes for the sensitive amperometric detection of glucose at low overpotentials, Biosens. Bioelectron. 20 (2005) 1587–1594.

16 W. Jia, S. Schwamborn, C. Jin, W. Xia, M. Muhler, W. Schuhmann, L. Stoica, Towards a high potential biocathode based on direct bioelectrochemistry between horseradish peroxidase and hierarchically structured carbon nanotubes, Phys. Chem. Chem. Phys. 12 (2010) 10088–10092.

17 B. Reuillard, A. Le Goff, M. Holzinger, S. Cosnier, Non-covalent functionalization of

carbon nanotubes with boronic acids for the wiring of glycosylated redox enzymes in oxygen-reducing biocathodes, J. Mater. Chem. B 2 (2014) 2228–2232.

18 Y. Sugimoto, R. Takeuchi, Y. Kitazumi, O. Shirai, K. Kano, Significance of mesoporous electrodes for non-catalytic faradaic process of randomly oriented redox proteins, J. Phys. Chem. C 120 (2016) 26270–26277.

19 Y. Sugimoto, Y. Kitazumi, O. Shirai, K. Kano, Effects of mesoporous structures on direct electron transfer-type bioelectrocatalysis: facts and simulation on a three-dimensional model of random orientation of enzymes, Electrochemistry 85 (2017) 82–87.

20 K. Sakai, Y. Sugimoto,Y. Kitazumi, O. Shirai, K. Takagi, K. Kano, Direct electron transfer-type bioelectrocatalytic interconversion of carbon dioxide/formate and NAD^+/NADH redox couples with tungsten-containing formate dehydrogenase, Electrochim. Acta 228 (2017) 537–544.

21 M. Tominaga, M. Ohtani, I. Taniguchi, Gold single-crystal electrode surface modified with self-assembled monolayers for electron tunneling with bilirubin oxidase, Phys. Chem. Chem. Phys. 10 (2008) 6928–6934.

22 Y. Sugimoto, Y. Kitazumi, S. Tsujimura, O. Shirai, M. Yamamoto, K. Kano, Electrostatic interaction between an enzyme and electrodes in the electric double layer examined in a view of direct electron transfer-type bioelectrocatalysis, Biosens. Bioelectron. 63 (2015) 138–144.

23 H. Xia, Y. Kitazumi, O. Shirai, K. Kano, Enhanced direct electron transfer-type bioelectrocatalysis of bilirubin oxidase on negatively charged aromatic compound-modified carbon electrode, J. Electroanal. Chem. 763 (2016) 104–109.

24 H. Xia, K. So, Y. Kitazumi, O. Shirai, K. Nishikawa, Y. Higuchi, K. Kano, Dual gas-diffusion membrane-and mediatorless dihydrogen/air-breathing biofuel cell operating at room temperature, J. Power Sources 335 (2016) 105–112.

25 L. Peng, T. Utesch, A. Yarman, J.H. Jeoung, S. Steinborn, H. Dobbek, F.W. Scheller, Surface-tuned electron transfer and electrocatalysis of hexameric tyrosine-coordinated heme protein, Chem Eur. J. 21 (2015) 7596–7602.

26 K. Monsalve, I. Mazurenko, C. Gutierrez-Sanchez, M. Ilbert, P. Infossi, S. Frielingsdorf, M. T. Giudici-Orticoni, O. Lenz, E. Lojou, Impact of carbon nanotube

surface chemistry on hydrogen oxidation by membrane-bound oxygen-tolerant hydrogenases, ChemElectroChem. 3 (2016) 2179–2188.

27 G. Wilson, Native glucose oxidase does not undergo direct electron transfer, Biosens. Bioelectron. 82 (2016) vii.

28 H. Xia, Y. Hibino, Y. Kitazumi, O. Shirai, K. Kano, Interaction between D-fructose dehydrogenase and methoxy-substituent-functionalized carbon surface to increase productive orientations, Electrochim. Acta 218 (2016) 41–46.

29 B.E.P. Swoboda, V. Massey, On the reaction of the glucose oxidase from *Aspergillus niger* with bisulfite, J. Bio. Chem. 240 (1965) 3409–3416.

30 J.C. Deutsch, Ascorbic acid oxidation by hydrogen peroxide, Anal. Biochem. 255 (1988) 1–7.

31 G. Reach, G.S.Wilson, Can continuous glucose monitoring be used for the treatment of diabetes? Anal. Chem. 64 (1992) 381A–386A.

32 R.D. Milton, F. Giroud, A.E. Thumser, S.D. Minteer, R.C. Slade, Bilirubin oxidase bioelectrocatalytic cathodes: the impact of hydrogen peroxide, Chem. Commun. 50 (2014) 94–96.

33 C. Adam, P. Scodeller, M. Grattieri, M. Villalba, E.J. Calvo, Revisiting direct electron transfer in nanostructured carbon laccase oxygen cathodes, Bioelectrochemistry 109 (2016) 101–107.

1-2 Mesoporous microelectrode for diffusion-controlled amperometric detection of putrescine based on co-immobilization of peroxidase and putrescine oxidase without a mediator

Abstract

A mediator-less amperometric biosensor for putrescine was proposed to obtain a (pseudo) steady-state catalytic current. Putrescine oxidase (PuOD) and peroxidase (POD) were co-immobilized with glutaraldehyde on a Ketjen Black (KB)-based mesoporous electrode. A POD-based direct electron transfer-type bioelectrocatalytic reduction wave of H_2O_2 generated by the reaction of PuOD was observed at a PuOD/POD-immobilized and KB-modified rotating disk glassy carbon electrode with an onset potential of 0.60 V vs. Ag|AgCl. A PuOD/POD-immobilized and KB-modified microdisk electrode produced a spherical diffusion-controlled (pseudo) steady-state catalytic current under quiescent conditions in the presence of putrescine. The bienzyme mesoporous microelectrode exhibited a linear range from 17 μM to 500 μM with a sensitivity of 0.33 ± 0.01 mA mM^{-1} cm^{-2} and a lower detection limit of 5 μM (S/N > 3).

1. Introduction

Putrescine (1,4-diaminobutane), a small aliphatic diamine, is ubiquitous in a wide variety of living cells and plays important roles in many physiological processes.[1–3] In addition, putrescine is often found in several food products due to the decarboxylation of amino acids by microorganisms.[4] A great number of methods have been developed in pursuit of rapid, simple, and sensitive putrescine detection,[5–8] in which redox enzyme-based amperometric biosensors continue to be a topic of interest.

Putrescine oxidase (PuOD) is a flavoenzyme catalyzing the oxidation of putrescine and the concomitant reduction of O_2 to H_2O_2:[9]

$$\text{putrescine} + O_2 + H_2O \rightarrow \text{4-aminobutanal} + H_2O_2 + NH_3 \quad (1)$$

Several oxidases can utilize artificial electron acceptors (or mediators) (M_{Ox}) in place of O_2 (with their dehydrogenase activity), and second generation-type biosensors are often constructed based on mediated electron transfer- (MET-) type bioelectrocatalysis. In the case of PuOD, a similar MET-type electrode was attempted to be constructed based on the reactions shown in Eqs. (2) and (3).[10]

$$\text{putrescine} + 2M_{Ox} + H_2O \rightarrow \text{4-aminobutanal} + 2M_{Red} + NH_3 + 2H^+ \quad (2)$$

$$M_{Red} \rightarrow M_{Ox} + e^- \quad (\text{at } E > \text{the formal potential of the mediator} \quad (3)$$

However, PuOD preferentially and almost exclusively uses O_2 as an electron acceptor, and the second generation-type biosensor showed very low performance due to low dehydrogenase activity. Therefore, the amperometric methods reported to date for putrescine detection are almost all

of the first generation type based on the direct oxidative detection of H_2O_2:[11–13]

$$H_2O_2 \rightarrow O_2 + 2H^+ + 2e^- \quad (\text{at } E > 0.5 \text{ V}) \qquad (4)$$

However, the oxidation of H_2O_2 requires relatively high operation potentials, which are always accompanied by the co-oxidation of other electroactive metabolites in physiological fluids; thus, the oxidative detection of H_2O_2 does not seem to be practical for *in vivo* analysis.

On the other hand, peroxidase (POD)-catalyzed reductive detection of H_2O_2 has often been coupled with several oxidase reactions to construct a variety of biosensors for the detection of biologically related compounds as the substrates of the oxidases.[14–18] POD catalyzes the reduction of H_2O_2 with several artificial mediators (M_{Red}), and the oxidized form of the mediator (M_{Ox}) is reductively detected at electrodes as MET-type bioelectrocatalysis.

$$H_2O_2 + 2M_{Red} + 2H^+ \rightarrow 2H_2O + 2M_{Ox} \qquad (5)$$

$$M_{Ox} \rightarrow M_{Re} \quad (\text{at } E < \text{the formal potential of the mediator}) \qquad (6)$$

Coupling of an oxidase reaction and the MET-type bioelectrocatalysis of H_2O_2 reduction frequently provide bienzyme-type sensors of high sensitivity. However, the system requires a suitable mediator, and more importantly, the coupling often causes a cross reaction in which the M_{Ox} can work as an electron acceptor for the oxidase reaction, leading to disturbance of the quantitative analysis. [14]

Recently, direct electron transfer- (DET-) type bioelectrocatalysis of POD at several suitable electrodes with an onset potential of *ca.* 0.65 V has been reported :[19–21]

$$H_2O_2 + 2H^+ \rightarrow \quad 2H_2O \quad (\text{at } E < \text{the formal potential of POD}) \qquad (7)$$

The DET-type POD-based bioelectrocatalytic system could be coupled with the PuOD reaction (Eq. (1)) for putrescine detection (Scheme 1).

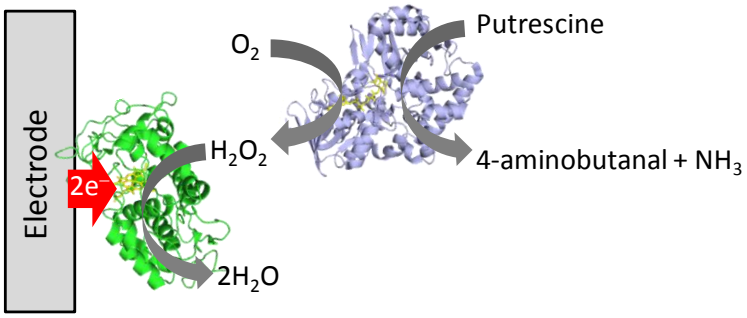

Scheme 1

Proposed cascade reactions at a PuOD/POD bienzyme electrode.

Another important issue to be solved for such biosensors is that the response is liable to be affected by time-dependent characteristics. Rotating disk electrodes or magnetic stirring is often used to minimize the influence of time-dependent mass transfer and to provide steady-state currents.

Such methods always make the system so "fat" that they would not be convenient for *in vivo* detection.

On the other hand, it has been reported that microelectrodes[22] provide steady-state responses under quiescent conditions even in MET-type bioelectrocatalysis under suitable conditions.[23–25] In the case of DET-type biosensors, one may get (pseudo) steady-state diffusion-controlled responses with microdisk electrodes when bioelectrocatalysis proceeds at a very large rate constant. From this viewpoint, a useful strategy is to develop a mesoporous microelectrode for DET-type biosensors; the mesoporous structure suitable for a redox enzyme improves the DET-type bioelectrocatalysis of the enzyme[26,27] and the microdisk electrode provides rapid (pseudo) steady-state amperometric responses proportional to the substrate concentration even in a quiescent electrolyte solution.

In this work, Kejten Black (KB) was utilized to construct a mesoporous carbon platform for co-immobilization of POD and PuOD. Mesoporous structured carbon electrodes are essential for DET of redox enzymes of suitable sizes.[26,27] DET-type bioelectrocatalytic reduction of H_2O_2 by POD (Eq. (7)) and the PuOD reaction (Eq. (1)) were coupled to detect putrescine. In addition, a bienzyme mesoporous microsensor was constructed to obtain spherical diffusion-controlled (pseudo) steady-state currents under quiescent conditions (Scheme 2). The proposed bienzyme microelectrode was capable of putrescine determination under quiescent conditions with a lower detection limit of 10 μM ($S/N > 3$).

2. Experimental

2.1 Materials and reagents

Ketjen Black EC300J (KB) was kindly donated by Lion Co. (Japan). Poly (tetrafluoroethylene) fine powder (PTFE, 6-J) was obtained from DuPont Mitsui Fluorochemicals (Japan). Ascorbic acid, uric acid, glutaraldehyde (20%), putrescine, and H_2O_2 were obtained from Wako Chemicals Co. (Osaka, Japan). Peroxidase from horseradish (POD, EC 1.11.1.7, 282 U mg^{-1}) was purchased from Toyobo Co. (Japan) and used without further purification. Putrescine oxidase from *Rhodococcus erythropolis* (PuOD, EC 1.4.3.10, 9 U mg^{-1}) was expressed from a plasmid pBAD*puo*$_{Rh}$ and purified as described previously.[28] All other chemicals used in this study were of analytical grade. Uric acid solution was prepared with 0.1 M KOH, and all other solutions were prepared with 0.1 M phosphate buffer (pH 7.0).

2.2 Preparation of bienzyme rotating disk electrode

KB-modified glassy carbon rotating disk electrodes (KB/GCE) were constructed as follows. KB (40 mg) and PTFE (10 mg) were distributed in 3.5 mL of 2-propanol and homogenized with an ultrasonic disruptor (Heat Systems GmbH & Co.) for 3 min in an ice bath to prepare a KB slurry. A 3 μL aliquot of the KB slurry was applied onto a GCE surface and dried at room temperature for 10 min. Then, a 20 μL aliquot of an enzyme/reagent mixture containing POD (usually 0.1 mg mL^{-1}), PuOD (2.5 mg mL^{-1}), and glutaraldehyde (5%) was dropped onto the KB/GCE surface and dried at 4 °C for 2 h. Glutaraldehyde was used here as a cross-linker to form a stable enzyme layer for DET-type bioelectrocatalysis. The prepared bienzyme electrode, referred to as PuOD/POD/KB/GCE, was washed with fresh buffer before electrochemical measurements.

2.3 *Preparation of bienzyme mesoporous microelectrode*

Scheme 2 shows the preparation process of a bienzyme mesoporous microelectrode. A polished gold microdisk electrode (AuMDE) was immersed in 4 mL of aqua regia (35% HCl: 70% HNO_3 = 3:1 v:v) for 50 min. The etched AuMDE was washed with and sonicated in distilled water. A 1 μL aliquot of the KB slurry was applied onto the top of the etched AuMDE and dried at room temperature. Any KB particles outside the etched microdisk portion were carefully removed. The KB-modified AuMDE is referred to as KB/AuMDE. Then, a 10 μL aliquot of the enzyme/reagent mixture containing POD, PuOD, and glutaraldehyde was dropped onto the KB/AuMDE surface and dried at 4 °C for 2 h. The bienzyme microporous microelectrode was washed with fresh buffer before electrochemical measurements and is referred to as PuOD/POD/KB/AuMDE. For a long-time storage, the PuOD/POD/KB/AuMDE was immersed in a fresh buffer and stored at 4 °C.

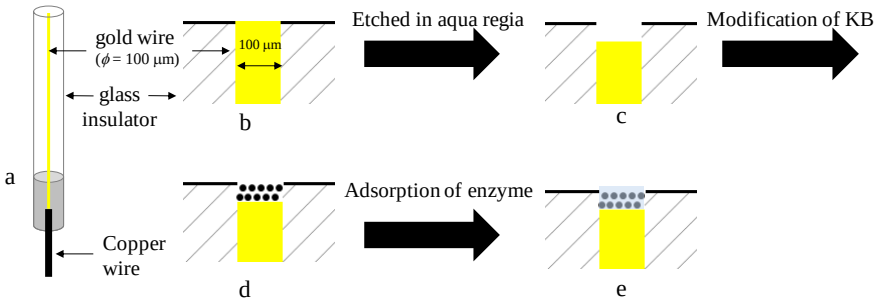

Scheme 2

Illustrative drawing of (a) the structure of an Au microdisk electrode and (b–e) the process of the preparation of a bienzyme mesoporous microelectrode.

2.4 Electrochemical measurements

Cyclic voltammetry and chronoamperometry were performed using an electrochemical

analyzer (ALS 701 E, ALS Co. Ltd., Japan) with either PuOD/POD/KB/GCE or PuOD/POD/KB/AuMDE as the working electrode, a Pt wire as the counter electrode, and an Ag|AgCl|KCl (sat.) electrode as the reference electrode. All potentials were referenced against this reference electrode.

3. Results and discussion

3.1 PuOD/POD modified KB rotating disk electrode

Fig. 1A shows typical rotating-disk cyclic voltammograms (CVs) obtained at the PuOD/POD/KB/GCE in the presence and absence of putrescine. A well-defined reduction wave was observed in the presence of putrescine, whereas no clear wave was observed in the absence of putrescine. Such a reduction wave was also not observed in the absence of POD on the electrode even in the presence of putrescine (Fig. 1B). Therefore, the reduction wave at the PuOD/POD/KB/GCE is ascribed to a DET-type bioelectrocatalytic reduction of H_2O_2 (Eq. (7)) generated during the PuOD-catalyzed two-electron reduction of O_2 with putrescine as an electron donor (Eq. (1)). The steady-state reduction current reached a limiting value at potentials more negative than *ca.* 0.3 V. The onset potential was *ca.* 0.60 V, which is close to the formal potential of POD (the ferric state POD/Compound I redox couple, 0.73 V at pH 7.0),[29] but is a so-called mixed potential determined in this case by the POD-catalyzed reduction of H_2O_2 (at E < 0.7 V) and the non-catalytic direct oxidation of H_2O_2 (at E > 0.5 V, as shown in Fig. 1B).

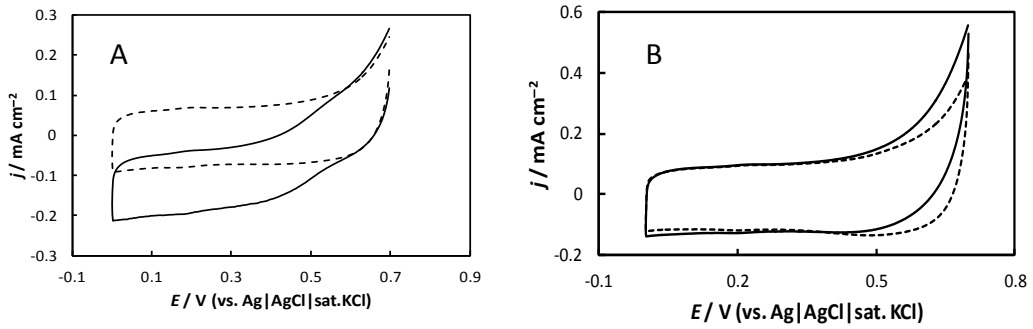

Fig. 1

Rotating disk CVs at (A) PuOD/POD-immobilized KB/GCE and (B) PuOD immobilized KB/GCE in the absence (dashed line) and in the presence (solid line) of 0.5 mM putrescine in 0.1 M phosphate buffer (25 °C, pH 7.0, air-saturated) at υ (scan rate) = 5 mV s^{-1} and ω = 4000 rpm.

For such a co-immobilized bienzyme electrode, the ratio of POD to PuOD is an important

factor balancing the H_2O_2 generation and H_2O_2 reduction, and thus should be optimized.[17,18,21] Fig. 2 shows the effects of the POD/PuOD ratio on the relative current response to 1 mM putrescine (ratios from 0.01 to 0.1 at a constant PuOD amount of 2.5 mg mL^{-1} × 20 μL) in mixed enzyme/reagent solutions for immobilization. The relative response increased with the POD/PuOD ratio and reached the maximum at a POD/PuOD ratio (w/w) of 0.03. The response decreased, however, with a further increase in the POD/PuOD ratio. This might be due to an increase in the thickness of the enzyme layer, which may result in a decrease in the mass transfer of the substrate and O_2.

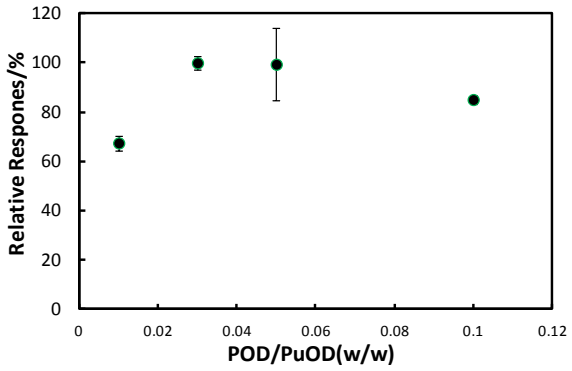

Fig. 2

Dependence of the limiting steady-state current response on the weight ratio of POD to PuOD for the detection of 1 mM putrescine at 0 V and at a rotating rate of 4000 rpm. The currents are depicted as relative values.

The catalytic reduction wave was obtained at the present bienzyme rotating disk electrode without any extra mediator at very high potentials. As shown in Scheme 1, the process at such a bienzyme rotating disk electrode can be given as follows: 1) the mass transfer of substrates (putrescine and O_2) from the bulk solution to the electrode surface; 2) the H_2O_2 generation by the catalytic reaction of PuOD; 3) the mass transfer of H_2O_2 at the electrode surface; 4) the H_2O_2 reduction by the catalytic reaction of POD; and 5) the interfacial electron transfer from POD to the electrode. The processes are complicated, but here, a simple model of a Koutecký-Levich-type equation is used to analyze the rotation rate (ω) dependence of the limiting steady-state catalytic current density (j_{lim}).

$$\frac{1}{j_{lim}} = \frac{1}{j_{cat}} + \frac{1}{j_m} \qquad (8)$$

where j_{cat} and j_m represent the catalytic reaction-controlled current density and the mass-transfer-controlled current density, respectively. Ideal conditions for determination of putrescine should include the mass transfer of putrescine and H_2O_2 generation by the catalytic reaction of PuOD alone as the possible rate-determining processes, and then j_{cat} and j_m are,

respectively, given by:

$$j_{\mathrm{cat}} = n_{\mathrm{S}} F k \Gamma_{\mathrm{E}} c_{\mathrm{S}} \quad (9)$$

$$j_{\mathrm{m}} = 0.62 n_{\mathrm{S}} F {D_{\mathrm{S}}}^{2/3} \omega^{1/2} \nu^{-1/6} c_{\mathrm{S}} \quad (10)$$

where n_s is the number of electrons of putrescine (n_s = 2), F is the Faraday constant, k is the catalytic constant, Γ_s is the surface concentration of PuOD, c_s is the bulk concentration of putrescine, D_s is the diffusion coefficient of putrescine, and ν is the kinematic viscosity of water. Fig. 3 shows Levich plots of the catalytic reaction at the bienzyme rotating disk electrode under air-saturated and O_2-saturated conditions. Only a slight increase in the current density was observed after a fivefold increase in O_2, indicating that the mass transfer of O_2 is not the primary factor controlling the catalytic current density. By fitting Eqs. (8) and (10) to the data, D_s values were evaluated as 5.4 ± 0.3 × 10^{-6} cm^2 s^{-1} under air-saturated conditions and 5.7 ± 0.6 × 10^{-6} cm^2 s^{-1} under O_2-saturated conditions. The curved characteristics in Fig. 3 indicate that the catalytic current density is predominantly controlled by the enzyme kinetics (Eq. (9)) at increased ω, but is controlled by the mass transfer of putrescine (Eq. (10)) at low mass transfer rates (i.e., at low ω). The former situation is not convenient for the analytical purpose, since the amperometric signal is sensitive to the variation in $k\Gamma_E$. In contrast, the latter situation is very convenient and ideal for the determination of putrescine.

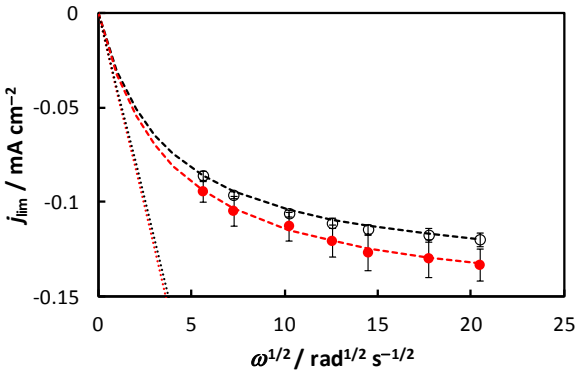

Fig. 3

Levich plots of ω dependence of the limiting steady-state reduction current densities at the PuOD/POD/KB/GCE in the presence of 0.5 mM putrescine under air-saturated condition (open circles) and O_2-saturated condition (closed circles). The broken curves were evaluated by a nonlinear regression analysis with Eq. (8) and the dotted lines represent the ω dependence of the mass transfer-controlled current density (Eq. 10) with the adjusted value of D_s (5.4 ± 0.3 × 10^{-6} cm^2 s^{-1} under air-saturated conditions and 5.7 ± 0.6 × 10^{-6} cm^2 s^{-1} under O_2-saturated conditions.

3.2 PuOD/POD modified mesoporous microdisk electrode

Fig. 4 A compares non-Faradaic waves of bare AuMDE and KB/AuMDE. The drastic increase in the charging current indicates the successful modification of KB on such a microdisk electrode. Fig. 4B shows CVs of PuOD/POD/KB/AuMDE in the presence and absence of 0.5 mM putrescine under quiescent conditions. A clear steady-state wave was observed for the reduction of H_2O_2 generated in the PuOD reaction even under quiescent conditions, and the shape of the catalytic wave is very similar to that at the rotating PuOD/POD/KB/GCE (Fig. 1). The results suggest that spherical diffusion controlled-bioelectrocatalytic reaction occurs at PuOD/POD/KB/AuMDE.

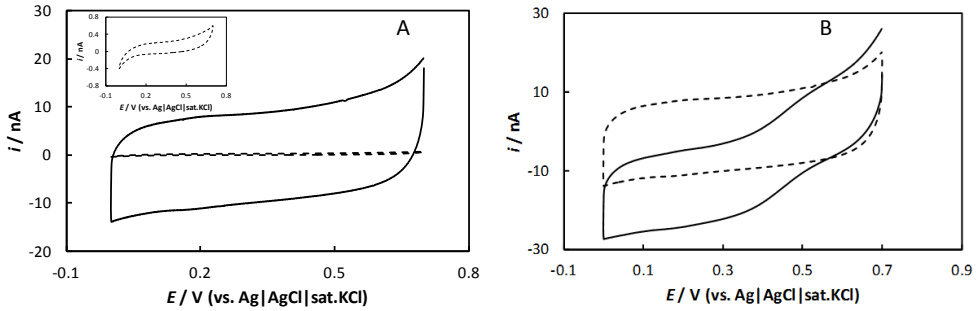

Fig. 4

(A) Non-Faradaic waves of AuMDE before (dashed line) and after (solid line) modified with KB. All measurements were carried out in air-saturated phosphate buffer (0.1 M, pH 7.0, 25 °C) at v = 5 mV s^{-1} under quiescent conditions;

(B) CVs of PuOD/POD/KB/AuMDE in the absence (dotted line) and in the presence (solid line) of 0.5 mM putrescine in 0.1 M phosphate buffer (25 °C, pH 7.0, air-saturated) at v = 5 mV s^{-1} under quiescent conditions.

Fig. 5 shows the time dependence of the currents in potential step chronoamperometry from 0.5 V to 0 V at several values of the total bulk concentrations of putrescine (c_{put}). The charging current disappeared within 5 s after the potential step and the Faradaic response almost reached a steady state after 30 s under quiescent conditions. As shown in the inset of Fig. 5, the (pseudo) steady-state limiting current (at 50 s) increased linearly with c_{put} at low values of c_{put}. When we consider that the steady-state current is controlled by the spherical steady-state mass transfer of an analyte (putrescine in this case) to the microdisk electrode, the current is given by:[30]

$$i_{\mathrm{m\ at\ AuMDE}} = 4n_S FAD_S r c_S \qquad (11)$$

where r is the radius of the microdisk electrode. From the slope of the linear dependence in the inset of Fig. 5, the D_s value was evaluated as $7.8 \pm 0.4 \times 10^{-6}$ cm^2 s^{-1}, which is close to that obtained by rotating disk voltammetry with Eqs. (8) and (10) for the PuOD/POD/KB/GCE. This verifies that the steady-state current at the PuOD/POD/KB/AuMDE is predominantly controlled by the spherical steady-state mass transfer of putrescine, and that the present bienzyme-modified microdisk electrode

can be used successfully for the amperometric determination of putrescine in quiescent solutions.

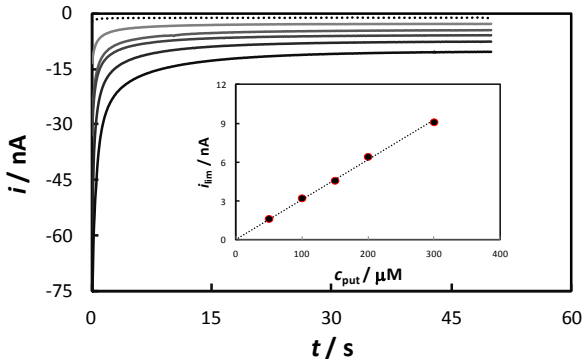

Fig. 5

Potential step chronoamperograms at the PuOD/POD/KB/AuMDE from 0.5 V to 0 V in a quiescent phosphate buffer (pH 7.0, 25 °C) at c_{put} from 50 μM to 300 μM. The inset shows the dependence of i_{lim} on c_{put}.

3.3 Putrescine sensing

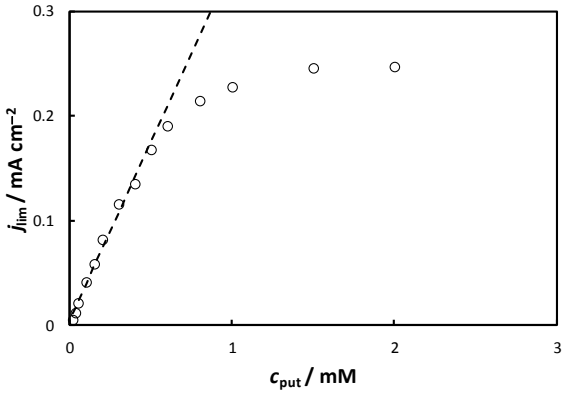

Fig. 6

Dependence of the limiting steady-state current density (j_{lim}) on the concentration of putrescine (c_{put}) at 0 V under quiescent condition. The broken lines is a linear regression curve; current density (mA cm^{-2}) = 0.33 ± 0.01 (mA cm^{-2} mM^{-1}) × [putrescine] (mM) + 6 ± 3(μA cm^{-2}), R^2 = 0.996.

Fig. 6 shows the calibration curve of the proposed microdisk electrode. The data showed a linear dependence of the limiting catalytic current (i_{lim}) on the putrescine concentration (c_{put}) from 17 μM to 500 μM and showed a curved characteristic due to the contribution of the enzyme kinetic factor. The detection limit of putrescine with the POD/PuOD/KB/AuMDE was 5 μM (S/N > 3), and the linear range was from 17 μM to 500 μM with a slope of 0.33 ± 0.01 mA mM^{-1} cm^{-2} (R^2 = 0.996).

The response showed a high reproducibility in the linear range due to the diffusion-controlled characteristics. However, the relative standard deviation increased with increasing c_{put}, which seems to be due to the variation in the enzyme activity at each microdisk electrode (strictly speaking, the variation in $k\Gamma_E$).

The constructed bienzyme mesoporous microdisk electrode is very suitable for *in vivo* putrescine detection with high selectivity under unstirred conditions. However, the response and sensitivity are low in the present situation due to small amounts of adsorbed enzymes on the microdisk electrode. In this viewpoint, in the future, one useful method to improve the response and sensitivity is to construct a microelectrode array.[31]

4. Conclusions

In summary, an amperometric biosensor was developed in this work for detection of putrescine by co-immobilization of POD and PuOD on a mesoporous carbon-modified microdisk electrode. A mesoporous carbon material, KB, is suitable as a platform for DET-type bioelectrocatalysis of POD for two-electron reduction of H_2O_2 even at very positive potentials. On the other hand, an H_2O_2-generating oxidase, PuOD, has very high substrate specificity and can only use O_2 as the electron acceptor. A cascade reaction was proposed to link the H_2O_2-generating reaction and the catalytic H_2O_2 reduction, and to determine the putrescine concentration. The microdisk electrode was constructed to realize a diffusion-controlled bioelectrocatalysis and to obtain a rapid pseudo-steady-state response even in an unstirred solution.

To the best of our knowledge, this is the first case of the amperometric detection of putrescine with such a bienzyme mesoporous microdisk electrode without any redox mediator. This concept can be applied to the detection of substrates of other H_2O_2-generating oxidases by just replacing PuOD with the corresponding H_2O_2-generating oxidase.

5. References

1 D.H. Russel, The roles of the polyamines, putrescine, spermidine, and spermine in normal and malignant tissues, Life Sci. 13 (1973) 1635–1647.

2 C.W. Tabor, H. Tabor, 1,4-Diaminobutane (putrescine), spermidine, and spermine, Annu. Rev. Biochem. 45 (1976) 285–306.

3 T. Thomas, T.J. Thomas, Polyamines in cell growth and cell death: molecular mechanisms and therapeutic applications, Cell. Mol. Life Sci. 58 (2001) 244–258.

4 A. Halász, Á. Baráth, L. Simon-Sarkadi, W. Holzapfel, Biogenic amines and their production by microorganisms in food, Trend. Food Sci. Technol. 51 (1994) 42–49.

5 J.W. Redmond, A. Tseng, High-pressure liquid chromatographic determination of putrescine, cadaverine, spermidine and spermine, J. Chromatogr. A 170 (1979) 479–481.

6 C. Proestos, P. Loukatos, M. Komaitis, Determination of biogenic amines in wines by HPLC with precolumn dansylation and fluorimetric detection, Food Chem. 106 (2008) 1218–1224.

7 A.A.G. Ibarra, K. Wrobel, A.R.C. Escobosa, J.C.T. Elguera, M.E. Garay-Sevilla, K. Wrobel, Determination of putrescine, cadaverine, spermidine and spermine in different chemical matrices by high performance liquid chromatography–electrospray ionization–ion trap tandem mass spectrometry (HPLC–ESI–ITMS/MS), J. Chromatogr. B 1002 (2015) 176–184.

8 P. Chen, H. Sun, X. Wang, Y. Pang, B. Li, A novel chemiluminescence enhanced method for determination of putrescine in shrimp based on the luminol–$[Ag(HIO_6)_2]^{5-}$ reaction, Anal. Methods 8 (2016) 1151–1156.

9 H. Yamada, A. Tanaka, K. Ogata, Putrescine oxidase of Micrococcus rubens, Agric. Biol. Chem. 29 (1965) 260–261.

10 W. Henao-Escobar, L. Del Torno-de Román, O. Domínguez-Renedo, M.A. Alonso-Lomillo, M.J. Arcos-Martínez, Dual enzymatic biosensor for simultaneous amperometric determination of histamine and putrescine, Food Chem. 190 (2016) 818–823.

11 C.X. Xu, S.A.M. Marzouk, V.V. Cosofret, R.P. Buck, M.R. Neuman, R.H. Sprinkle, Development of a diamine biosensor, Talanta 44 (1997) 1625–1632.

12 M.-A. Carsol, M. Mascini, Diamine oxidase and putrescine oxidase immobilized reactors in flow injection analysis: a comparison in substrate specificity, Talanta 50 (1999) 141–148.

13 L. Nagy, G. Nagy, R.E. Gyurcsányi, M.R. Neuman, E. Lindner, Development and study of an amperometric biosensor for the in vitro measurement of low concentration of putrescine in blood, J. Biochem. Biophys. Methods 53 (2002) 165–175.

14 R. Matsumoto, M. Mochizuki, K. Kano, T. Ikeda, Unusual response in mediated biosensors with an oxidase/peroxidase bienzyme system, Anal. Chem. 74 (2002) 3297–3303.

15 B. Bóka, N. Adányi, J. Szamos, D. Virág, A. Kiss, Putrescine biosensor based on putrescine oxidase from *Kocuria rosea*, Enzyme Microb. Technol. 51 (2012) 258–262.

16 J. Castillo, S. Gáspár, I. Sakharov, E. Csöregi, Bienzyme biosensors for glucose, ethanol and putrescine built on oxidase and sweet potato peroxidase, Biosens. Bioelectron. 18 (2003) 705–714.

17 C.H. Nieh, Y. Kitazumi, O. Shirai, K. Kano, Sensitive d-amino acid biosensor based on oxidase/peroxidase system mediated by pentacyanoferrate-bound polymer, Biosens. Bioelectron. 47 (2013) 350–355.

18 C.H. Nieh, S. Tsujimura, O. Shirai, K. Kano, Amperometric biosensor based on reductive H_2O_2 detection using pentacyanoferrate-bound polymer for creatinine determination, Anal. Chim. Acta. 767 (2013) 128–133.

19 W. Jia, S. Schwamborn, C. Jin, W. Xia, M. Muhler, W. Schuhmann, L. Stoica, Towards a high potential biocathode based on direct bioelectrochemistry between horseradish peroxidase and hierarchically structured carbon nanotubes, Phys. Chem. Chem. Phys. 12 (2010) 10088–10092.

20 W. Jia, C. Jin, W. Xia, M. Muhler, W. Schuhmann, L. Stoica, Glucose oxidase/horseradish peroxidase co-immobilized at a CNT-modified graphite electrode: towards potentially implantable biocathodes, Chem. Eur. J. 18 (2012) 2783–2786.

21 H. Xia, Y. Kitazumi, O. Shirai, K. Kano, Direct electron transfer-type bioelectrocatalysis of peroxidase at mesoporous carbon electrodes and its application for glucose determination based on bienzyme system, Anal. Sci. 2017 in press.

22 R.J. Forster, Microelectrodes: new dimensions in electrochemistry, Chem. Soc. Rev. 23 (1994) 289–297.

23 T. Noda, M. Wanibuchi, Y. Kitazumi, S. Tsujimura, O. Shirai, M. Yamamoto, K. Kano, Diffusion-controlled Detection of Glucose with Microelectrodes in Mediated Bioelectrocatalytic Oxidation, Anal. Sci. 29 (2013) 279–281.

24 Y. Kitazumi, T. Noda, O. Shirai, M. Yamamoto, K. Kano, Characteristics of fast mediated bioelectrocatalytic reaction near microelectrodes, Phys. Chem. Chem. Phys. 16 (2014) 8905–8910.

25 Y. Matsui, K. Hamamoto, Y. Kitazumi, O. Shirai, K. Kano, Diffusion-controlled mediated electron transfer-type bioelectrocatalysis using ultrathin-ring and microband electrodes as ultimate amperometric glucose sensors, Anal. Sci. 2017 in press.

26 Y. Sugimoto, Y. Kitazumi, O. Shirai, K. Kano, Effects of mesoporous structures on direct electron transfer-type bioelectrocatalysis: facts and simulation on a three-dimensional model of random orientation of enzymes, Electrochemistry 85 (2017) 82–87.

27 Y. Sugimoto, R. Takeuchi, Y. Kitazumi, O. Shirai, K. Kano, Significance of mesoporous electrodes for non-catalytic faradaic process of randomly oriented redox proteins, J. Phys. Chem. C 120 (2016) 26270–26277.

28 E.W. van Hellemond, M. van Dijk, D.P.H. Heuts, D.B. Janssen, M.W. Fraaije, Discovery and characterization of a putrescine oxidase from *Rhodococcus erythropolis* NCIMB 11540, Appl. Microbiol. Biotechnol. 78 (2008) 455–463.

29 M. Torimura, M. Mochizuki, K. Kano, T. Ikeda, T. Ueda, Mediator-assisted continuous-flow column electrolytic spectroelectrochemical technique for the measurement of protein redox potentials. Application to peroxidase, Anal. Chem. 70 (1998) 4690–4695.

30 Y. Saito, A theoretical study on the diffusion current at the stationary electrodes of circular and narrow band types, Rev. Polagr. (Jpn.) 15 (1968) 177–187.

31 T. Noda, K. Hamamoto, M. Tsutsumi, S. Tsujimura, O. Shirai, K. Kano, Bioelectrocatalytic endpoint assays based on steady-state diffusion current at microelectrode array, Electrochem. Commun. 12 (2010) 839–842.

Chapter 2
Electrostatic interaction between electrode surfaces and enzymes affecting the DET-type bioelectrocatalysis

2-1 Factors affecting the interaction between carbon nanotubes and redox enzymes in direct electron transfer-type bioelectrocatalysis

Abstract

The effects of three types of water-soluble carbon nanotubes (CNTs) of different lengths on the direct electron transfer (DET)-type bioelectrocatalysis of redox enzymes were investigated. Bilirubin oxidase (BOD), copper efflux oxidase (CueO), and a membrane-bound NiFe hydrogenase (H_2ase) were used as model redox enzymes for four-electron dioxygen (O_2) reduction (in the case of BOD and CueO) and two-electron dihydrogen (H_2) oxidation (in the case of H_2ase). As a result, diffusion-controlled O_2 reduction in an O_2-saturated neutral buffer was realized by BOD on CNTs of a length of 1 μm, but the catalytic current densities decreased as the length of CNTs increased. However, almost opposite trends were obtained when CueO and H_2ase were utilized as the biocatalysts. Factors of the CNTs and the enzymes affecting the characteristics of the DET-type bioelectrocatalysis of the three enzymes were investigated and discussed. Finally, the electrostatic interaction between an enzyme (especially the portion near the redox active center) and CNTs is proposed as one of the most important factors governing the performance of DET-type bioelectrocatalysis.

1. Introduction

Direct electron transfer (DET)-type bioelectrocatalysis is an ideal system in which the electron is transferred directly from electrodes to the substrate molecule (or *vice versa*) via the redox active site of an enzyme.[1,2] Since the DET-type system is constructed only with an enzyme and an electrode without any mediator, it is possible to miniaturize devices to extremely small sizes and to minimize the thermodynamic overpotential required in the electron transfer between an enzyme and a mediator, thereby making it very suitable for a variety of bioelectrochemical devices including biofuel cells[3-10] and biosensors[11-13]. However, the redox active sites of enzymes are usually deeply buried in peptides, and the interfacial electron transfer rate constant decreases exponentially with an increase in the distance between the electrode surface and the redox active site of the enzymes.[2] Therefore, the interfacial electron transfer between an enzyme and a solid electrode often has a high kinetic barrier.

Several redox enzymes are capable of direct electrochemical communication with

nanostructural materials, although the number of DET-type enzymes is small.[14-20] Carbon nanotubes (CNTs) are nanowires constituted from one or more layers of seamlessly rolled graphene (single-walled and multi-walled CNTs, respectively) with large specific surface areas (in a precise sense, with large values for surface-to-weight ratio), and are expected to be great platforms for the immobilization of redox enzymes and DET-type bioelectrocatalysis ever since they were discovered in the 1990s.[19-22] CNTs often improve the performance of DET-type bioelectrocatalysis.[23,24] This fact is often accredited to their large specific surface areas, which are responsible for the increased amounts of adsorbed enzymes. However, non-faradaic current will also be proportional to the surface area, and the faradaic vs. non-faradaic current ratio should not increase with an increase in the surface area. Rather, the faradaic vs. non-faradaic current ratio may decrease because of the mass transfer barrier to the nanospace. Actually, some enzymes show poorer catalytic activity when immobilized on CNTs with larger surface areas than those adsorbed onto CNTs with a smaller surface area.[25] On the other hand, when CNTs are modified onto a solid electrode surface, hydrophobic interactions between CNTs may converge to form three-dimensional nanostructures with different pore sizes.[26] Furthermore, the carboxy group (–COOH) on the surface of CNTs may be dissociated to provide a negatively charged surface. To the best of the authors' knowledge, both the pore size[27,28] and the surface charge of the electrode[10,29-32] may affect DET-type bioelectrocatalysis.

In this work, three kinds of multi-walled CNTs of different lengths (referred to as CNT1, CNT2, and CNT3) were utilized as platforms for the adsorption of bilirubin oxidase (BOD), copper efflux oxidase (CueO), and a membrane-bound NiFe hydrogenase (H_2ase), respectively. All three enzymes are reported as DET-type enzymes at suitable electrodes.[15-17] Both BOD and CueO belong to the family of multicopper oxidases that contain four copper atoms in the active site and catalyze a four-electron reduction of dioxygen (O_2).[33] One of the four copper atoms (known as the "blue" type I (T1) copper atom) is responsible for accepting electrons directly from an electrode and then donating the electrons to the other three copper atoms (in the T2/T3 cluster) wherein O_2 is reduced to water.[15,16] On the other hand, H_2ase contains Ni and Fe atoms in the catalytic center for the bidirectional reaction of H_2 oxidation and evolution and a series of FeS clusters for the electron transfer directly from or to an electrode.[34] We investigated and discussed several factors of the CNTs and the enzymes affecting the interaction between the CNTs and the redox enzymes in the DET-type bioelectrocatalysis.

2. Experimental

2.1 Materials, enzymes, and reagents

Three types of water-dispersed multi-walled CNTs (0.1%, w/w) (an average length of CNT1 (L) = 1 μm), CNT2 (L = 3 μm), and CNT3 (L = 10 μm)) were obtained from Nitta Corp. (Japan) (Fig. 1). BOD (EC 1.3.3.5) from *Myrothecium verrucaria* was donated by Amano Enzyme Inc. (Japan) and used without further purification. CueO from *Escherichia coli* was expressed and purified as previously described.[35] O_2-sensitive hydrogenase (H_2ase, EC 1.12.2.1) from *Desulfovibrio vulgaris* Miyazaki F was purified according to the literature.[36] All other chemicals were of analytical grade, unless otherwise specified, and all solutions were prepared with distilled water.

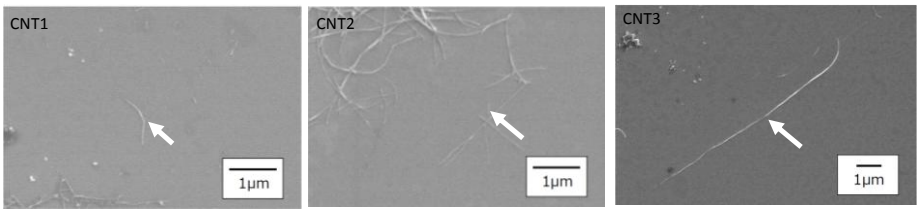

Fig. 1

SEM images of the three types of CNTs; CNT1, CNT2, and CNT3 from left to right. The narrows indicate individual CNTs.

2.2 Preparation of enzyme–CNT-modified electrodes

A glassy carbon disk electrode (GCE; diameter, 3 mm) was utilized as a working electrode and was polished and washed before modification. A 10 μL aliquot of a water-dispersed CNT suspension was applied onto the GCE surface and dried at 60 °C for 10 min. This operation was repeated six times and the final amount of CNTs was about 60 μg without any binder. The prepared CNT-modified GCE is referred to as CNT/GCE and was cooled down to room temperature. A 30 μL aliquot of a BOD solution (10 mg mL^{-1}) was dropped onto the CNT/GCEs and dried at 4 °C for 2 h. The BOD-adsorbed CNT/GCE was referred to as BOD/CNT/GCE and washed with a fresh buffer solution before electrochemical measurements were carried out. CueO/CNT/GCEs and H_2ase/CNT/GCEs were similarly prepared.

2.3 Electrochemical measurements

All electrochemical measurements were performed using an electrochemical analyzer (ALS 701E, ALS Co. Ltd., Japan) with the prepared CNT/GCE as a working electrode, a Pt wire as a counter electrode, and an Ag|AgCl|sat. KCl electrode as a reference electrode. All potentials were referred against the reference electrode in this study.

2.4 Zeta potential measurements

Scanning electron microscopy (SEM) was performed using a Hitachi S-4300 instrument. Average zeta potentials (ζ) of the three kinds of CNTs were measured at 25 °C using a Zeta-potential and Particle size Analyzer (ELS-Z2, Otsuka Electronics Co. Ltd., Japan). It should be noted that all dispersions were sonicated before measurements in order to work with fully dispersed CNT samples.

3. Results and discussions

3.1 Four-electron reduction of O_2 at BOD/CNT/GCEs and CueO/CNT/GCEs

Fig. 2A shows rotating disk linear scan voltammograms (LSVs) of the three kinds of BOD/CNT/GCEs under an O_2-saturated phosphate buffer (0.1 M, pH 7.0, and 25 °C) at a rotating rate (ω) of 4000 rpm and a scan rate (υ) of 5 mV s^{-1}. Well-defined reduction waves were observed with an onset potential of ~0.55 V for all of the BOD/CNT/GCEs examined. No obvious catalytic reduction current was detected in the absence of BOD. These catalytic waves are ascribed to the DET-type bioelectrocatalytic reduction of O_2 by BOD on the electrodes.[25,30]

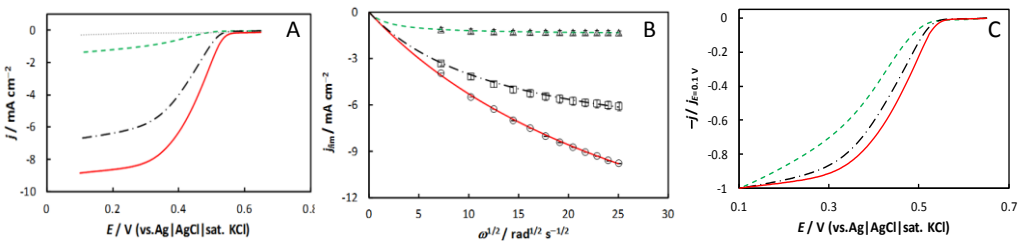

Fig. 2

(A) LSVs of O_2 reduction for BOD/CNT1/GCE (solid line), BOD/CNT2/GCE (dashed-dotted line), and BOD/CNT3/GCE (broken line). The dotted line represents an LSV on a CNT1/GCE without BOD.

(B) Levich plots of ω dependence of the steady-state reduction current densities (0.1 V) of O_2 for the BOD/CNT1/KB/GCE (circle), BOD/CNT2/GCE (square) and BOD/CNT3/GCE (triangle).

(C) Normalized LSVs of O_2 reduction for BOD/CNT1/GCE (solid line), BOD/CNT2/GCE (dashed-dotted line), and BOD/CNT3/GCE (broken line). All measurements were carried out in O_2-saturated phosphate buffer (0.1 M, pH 7.0, 25 °C).

However, the limiting catalytic current densities (at 0.1 V) were dependent on the CNTs used; the density reached as high as 8.6 ± 0.3 mA cm^{-2} for BOD/CNT1/GCE and 6.3 ± 0.5 mA cm^{-2}

for BOD/CNT2/GCE, while only 1.6 ± 0.4 mA cm^{-2} was achieved for BOD/CNT3/GCE. The total amount of CNTs used was almost the same for the three electrodes. Fig. 2B shows Levich plots of the catalytic reduction of O_2 for the three kinds of BOD/CNT/GCEs. The plot for BOD/CNT1/GCE was almost linear. Note here that, according to the Levich equation,[37] the diffusion-controlled current density under O_2-saturated conditions at 25 °C and at ω = 4000 rpm is expected to be 8.1 mA cm^{-2} with a diffusion coefficient of 1.7 × 10^{-5} cm^2 s^{-1}.[25] The detected O_2 reduction current density for BOD/CNT1/GCE was close to, or somewhat larger than, the theoretical value. Therefore, it can be concluded that BOD/CNT1/GCE can almost realize a diffusion-controlled O_2 reduction in the O_2-saturated pH 7.0 buffer. Furthermore, compared to BOD/CNT2/GCE and BOD/CNT3/GCE, BOD/CNT1/GCE provided a much sharper sigmoidal curve (Fig. 2C), indicating a significantly better performance in the interfacial electron transfer kinetics for CNT1/GCE than those for CNT2/GCE and CNT3/GCE.

Fig. 3A shows rotating disk LSVs of the catalytic O_2 reduction for the three kinds of CueO/CNT/GCEs under O_2-saturated phosphate buffer (0.1 M, pH 7.0, and 25 °C). As shown in Fig. 3A, clear reduction waves were observed for all of the CueO/CNT/GCEs with an onset potential of ~0.35 V. The waves are ascribed to the DET-type bioelectrocatalytic reduction of O_2 by CueO. However, in contrast to BOD/CNT/GCE, the catalytic current density for CueO/CNT1/GCE was much smaller than those for CueO/CNT2/GCE and CueO/CNT3/GCE. In addition, the sharper sigmoidal curve (Fig. 3B) of CueO/CNT3/GCE indicated a better interfacial electron transfer kinetic performance for CNT3/GCE than for CNT2/GCE and CNT1/GCE. The effects of CNTs on the DET-type catalysis of CueO seem to show an opposite trend compared to those for BOD.

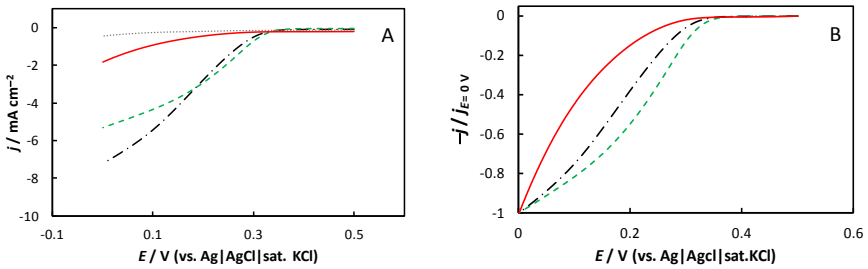

Fig. 3

Rotating disk LSVs (A) and normalized LSVs (B) of O_2 reduction for CueO/CNT1/GCE (solid line), CueO/CNT2/GCE (dashed–dotted line), and CueO/CNT3/GCE (broken line). The dotted line represents an LSV for CNT1/GCE without CueO. All measurements were carried out in O_2-saturated phosphate buffer (0.1 M, pH 7.0, and 25 °C) at ω = 4000 rpm and υ = 5 mV s^{-1}.

3.2 Two-electron oxidation of H_2 at H_2ase/CNT/GCEs

Fig. 4 shows rotating disk cyclic voltammograms (CVs) obtained for the three kinds of H_2ase/CNT/GCEs in an H_2-saturated buffer solution (pH 7.0 and 25 °C). Clear oxidation and reduction waves were observed for H_2ase/CNT3/GCE with a zero-current potential of –0.61 V. The oxidation and reduction waves correspond to the reversible and bidirectional oxidation of H_2 and reduction of H^+ catalyzed by H_2ase, and the zero-current potential corresponds to the formal potential of the H^+/H_2 redox couple at pH 7.0 and 25 °C (0.610 V).[9,10] The H_2 oxidation current decreased at electrode potentials more positive than –0.4 V, which was ascribed to a reversible oxidative-inactivation of H_2ase. Similar catalytic waves were observed for H_2ase/CNT2/GCE, although the current density was much smaller than for H_2ase/CNT3/GCE (Fig. 4C).

In contrast, such a bidirectional catalytic reaction, as well as reversible inactivation, was not observed for H_2ase/CNT1/GCE, as shown in Fig. 4A. The effects of CNTs on the DET-type catalysis of H_2ase showed an opposite trend compared to those for BOD. The H_2 oxidation current density increased with increasing the CNT length, as shown in Fig. 4D, which compares the background-current-corrected maximum current densities of the catalytic H_2 oxidation (at an electrode potential of –0.4 V).

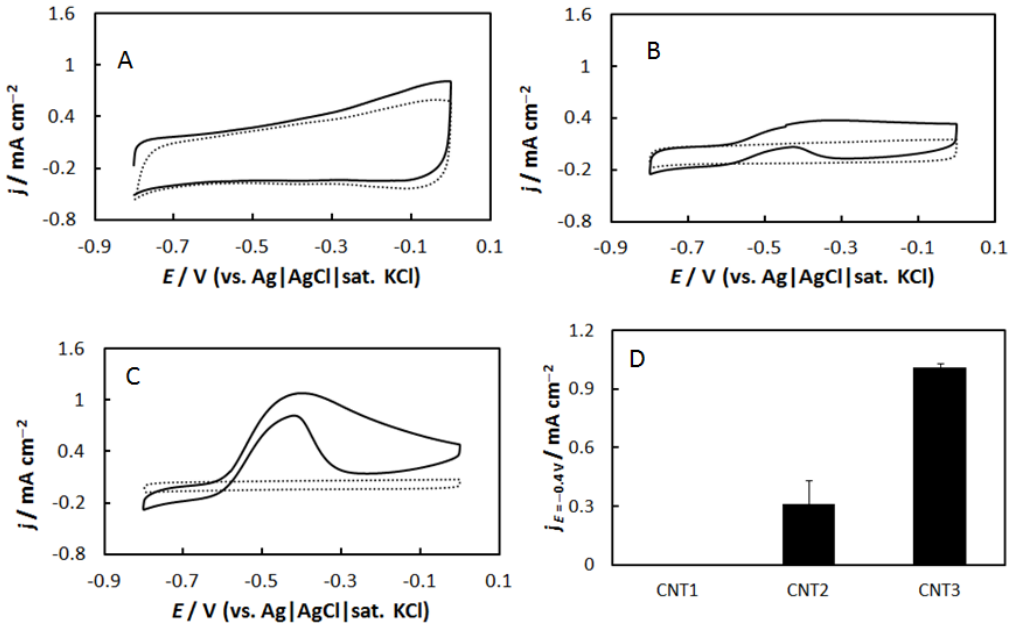

Fig. 4

Rotating disk CVs of (A) H_2ase/CNT1/GCE, (B) H_2ase/CNT2/GCE, and (C) H_2ase/CNT3/GCE. The dotted lines in A–C represent CVs for the corresponding CNT/GCEs without H_2ase.

(D) Comparison of the background-current-corrected current density at –0.4 V of the H_2 oxidation for the H_2ase/CNT/GCEs. All measurements were carried out in H_2-saturated phosphate buffer (0.1 M, pH 7.0, and 25 °C) at ω = 4000 rpm and υ = 5 mV s^{-1}.

3.3 Factors affecting the adsorption of redox enzymes

Table 1 summarizes several characteristics of the three types of CNTs as well as the catalytic performances of BOD, CueO, and H_2ase with these CNTs. As described above, BOD has a preference for shorter CNTs whereas CueO and H_2ase have a preference for longer CNTs. The size of the three-dimensional nanostructures was a very important factor governing the performance of the DET-type communication between an enzyme and the electrode.[27,28] CNTs of different *L* would provide different sizes of three-dimensional nanostructures. However, the sizes of the three enzymes are similar to each other: the diameter of BOD and CueO are 5–6 nm[38,39] and that of H_2ase is ~7 nm[36]. Therefore, the parameter *L* does not seem to be a primary factor for causing the difference in the DET-type performance of the enzymes.

In an intuitive consideration, ζ seems to reflect the averaged density of the carboxy group on the surface of CNTs since ζ is strongly related to the surface charge. However, the catalytic current density does not seem to depend on ζ. The isoelectric points (p*I*) of BOD and CueO are calculated to be 4.1 and 6.1 (http://web.expasy.org/compute_pi/), respectively, indicating that both BOD and CueO have a negative net charge under neutral conditions. Therefore, the net charge of the enzyme also does not seem to be a significant factor for causing the difference in the DET-type bioelectrocatalytic performance of BOD and CueO.

Table 1 Summaries of CNT characteristics and the catalytic performances of the redox enzymes adsorbed onto the CNTs

	Characters of CNTs			$j_{steady\text{-}state}$/ mA cm^{-2}***		
	L / μm	A_r*	ζ / mV**	BOD	CueO	H_2ase
CNT1	1	1	–42 ±1	–8.6 ± 0.3	–1.4 ± 0.5	0
CNT2	3	0.5	–49 ±1	–6.3 ± 0.5	–6.8 ± 0.4	0.3 ± 0.1
CNT3	10	0.3	–14 ± 7	–1.6 ± 0.4	–5.0 ± 0.2	1.0 ± 0.1

*The relative electroactive surface area (A_r) was roughly evaluated from the charging current at 0.4 V.

**The zeta potential (ζ) of CNTs in the solution.

***The steady-state catalytic current densities ($j_{steady\text{-}state}$) were obtained from background-current-corrected catalytic current densities for different CNT/GCEs with an electrode potential of 0.1 V (BOD), 0 V (CueO), and –0.4 V (H_2ase). All measurements were carried out in O_2-saturated (in the case of BOD and CueO) or H_2-saturated (in the case of H_2ase) phosphate buffer (0.1 M, pH 7.0, and 25 °C) and at ω = 4000 rpm.

The relative electroactive surface area (A_r) of the CNTs was roughly estimated from the non-faradic charging current at a potential of 0.4 V where faradic processes were minimal.[40] The surface area itself does not seem to be a primary factor causing the difference in the performance of the DET-type bioelectrocatalysis, as described above. However, by considering the fact that A_r increases with a decrease in L, we can expect that the open-end part increases with a decrease in L. The density of the carboxy group at the open end is expected to be larger than at a side surface. A part of the carboxy groups is dissociated to provide a highly negatively charged surface.

On the other hand, in the case of BOD, the region close to the T1 copper site (where electrons are transferred from the electrodes) is positively charged under neutral conditions (Fig. 5, left).[10,30] Thus, the attractive electrostatic interaction between the positively charged T1 region and the negatively charged CNT surface may induce a productive orientation for the DET-type bioelectrocatalysis. The surface concentration of BOD molecules with convenient orientations for the DET-type bioelectrocatalysis must increase with the number of the carboxy groups on the CNTs (especially at the open-end part). This scenario can explain the L (or A_r) dependence of the current density for the DET-type bioelectrocatalysis of BOD.

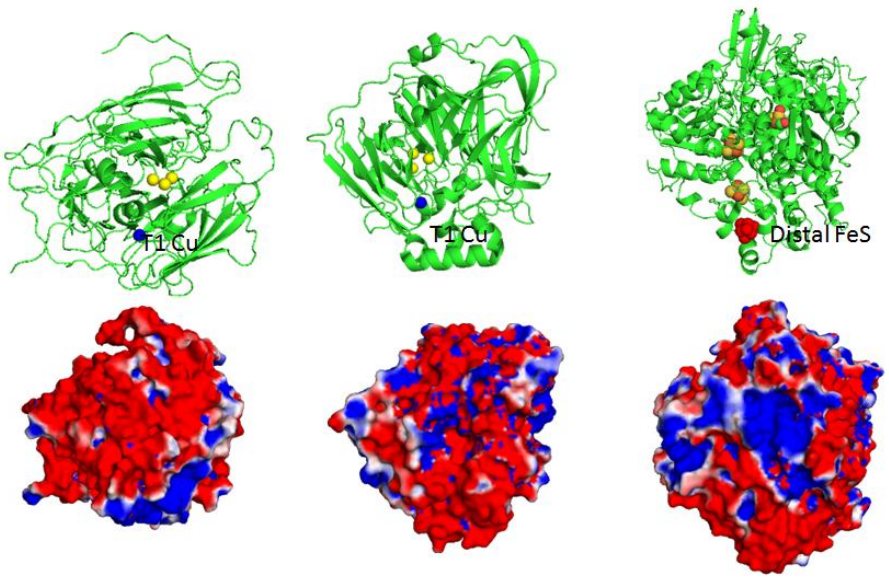

Fig. 5

Three-dimensional structures (top) and the surface electrostatic potential distributions (bottom) of BOD (left, PDB code: 3ABG), CueO (middle, PDB code: 1KV7), and H_2ase (right, PDB code: 1H2A). The color of blue and red represent positive and negative surface electrostatic potential regions, respectively, which were generated using PyMOL at pH 7 (25 °C).

In contrast, the region near the T1 site of CueO is negatively charged under neutral conditions (Fig. 5, middle).[30] Thus, in the case of CNT1, the high density of the carboxy groups

seems to cause strong repulsive electrostatic interactions with the T1 site of CueO. This situation leads to a poor performance of the DET-type bioelectrocatalysis for shorter CNTs. For CueO/CNT2/GCE and CueO/CNT3/GCE, the catalytic wave rose sharply with the electrode potential and the onset potential shifted to the positive side compared with CueO/CNT1/GCE (Fig. 3). CueO/CNT2/GCE and CueO/CNT3/GCE provided much sharper sigmoidal curves than CueO/CNT2/GCE (Fig. 3), indicating better performance in the DET-type bioelectrocatalysis. All these characteristics seem to be due to a decrease in the carboxy group density on CNTs (especially at the side surfaces). The limiting current density for CueO/CNT3/GCE was somewhat smaller than that for CueO/CNT2/GCE. This may be ascribed to the increased hydrophobicity of CNT3, leading to a decrease in the total amount of adsorbed CueO.

Thus, we can propose here that the electrostatic interaction between the CNT/GCE surface and the region near the active (redox) center of an enzyme is one of the main factors controlling the orientation of the enzyme on the electrode for the DET-type bioelectrocatalysis.

Further experimental evidence was obtained in favor of the electrostatic repulsion between CueO and CNT1. We attempted to reduce the electrostatic repulsion by the addition of Ca^{2+}. Fig. 6 A shows the effects of $Ca(NO_3)_2$ on the rotating disk catalytic reduction waves for CueO/CNT/GCE in an acetate buffer (0.1 M and pH 5.0). Acetate buffer was used instead of phosphate buffer to prevent precipitation of $CaHPO_4$. The limiting catalytic current density increased and the curve became sharper with the addition of Ca^{2+}. It can be considered that Ca^{2+} ions bridge the negatively charged T1 site of CueO with the negatively charged CNT surface.

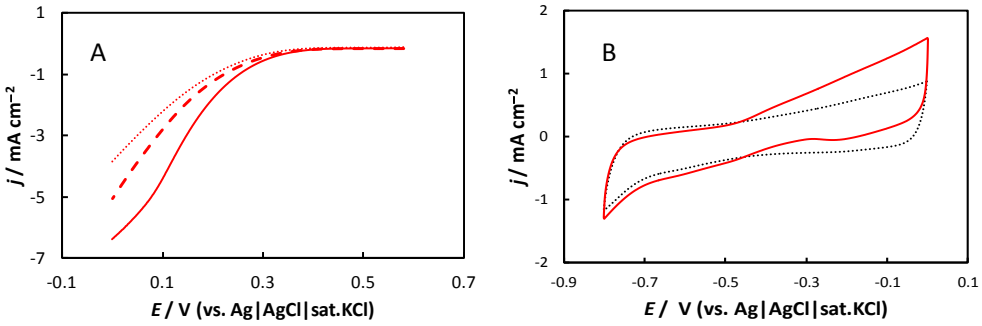

Fig. 6

(A) Rotating disk LSVs of O_2 reduction for CueO/CNT1/GCE at 0 M (dotted line), 0.1 M (broken line), and 0.5 M (solid line) $Ca(NO_3)_2$. (B) Rotating disk CVs of H_2 oxidation for H_2ase/CNT1/GCE at 0 M (dotted line) and 0.1 M (solid line) $Ca(NO_3)_2$. All measurements were carried out in O_2- (or H_2-) saturated acetate buffer (0.1 M, pH 5.0, 25 °C) at ω = 4000 rpm and υ = 5 mV s^{-1}.

In the case of H_2ase, the region near the distal FeS cluster (where electrons are directly

shuttled to an electrode) is negatively charged under neutral conditions (Fig. 5, right).[10] Therefore, the repulsive electrostatic interaction between the negatively charged distal FeS cluster area and the negatively charged CNT surface leads to inconvenient orientations of H_2ase that cause poor characteristics in the interfacial electron transfer, especially in the case of CNT1. By the addition of Ca^{2+} into the electrolyte, an increase in the catalytic current density as well as the reversible inactivation was observed. The results indicate great improvement of heterogeneous electron transfer kinetics between H_2ase and CNT1 (Fig. 6B). The improvement should be ascribed to the reduced electrostatic repulsion between H_2ase and CNT1, as discussed above in the case of CueO. All of these results support our proposal quite well.

4. Conclusions

We constructed nanostructured carbon electrodes with water-soluble CNTs of different lengths without any binder, and examined the effects of three types of CNTs of different lengths on the performance of the DET-type bioelectrocatalysis of three kinds of redox enzymes. In the case of BOD, the O_2 reduction current increased with decreasing the CNT length and almost diffusion-controlled bioelectrocatalytic reduction of O_2 was realized with CNTs of an average length (L) of 1 μm at pH 7.0, 25 °C, and a rotating rate of 4000 rpm. In contrast, the almost opposite tendency was obtained when CueO was utilized as a biocatalyst despite both BOD and CueO having similar sizes and a net negative charge in neutral solutions. On the other hand, the region near the T1 copper atom in BOD is positively charged, while that in CueO is negatively charged in neutral solutions. Furthermore, the CNT surface will be negatively charged in neutral solutions due to the dissociation of the carboxy group on the CNT surface, and the number of the carboxy groups increases with the decrease of L. Therefore, the electrostatic interaction between the CNT and the region near the redox active site of an enzyme is proposed to be one of the most important factors controlling the adsorption of the enzyme for DET-type bioelectrocatalysis. This assumption was reinforced using H_2ase as the model enzyme.

5. References

1 A.L. Ghindilis, P. Atanasov, E. Wilkins, Enzyme-catalyzed direct electron transfer: Fundamentals and analytical applications, Electroanalysis 9 (1997) 661–674.

2 C. Léger, P. Bertrand, Direct electrochemistry of redox enzymes as a tool for mechanistic studies, Chem. Rev. 108 (2008) 2379−2438.

3 M. Falk, Z. Blum, S. Shleev, Direct electron transfer based enzymatic fuel cells, Electrochim. Acta 82 (2012) 191−202.

4 A. Ramanavicius, A. Kausaite, A. Ramanaviciene, Biofuel cell based on direct bioelectrocatalysis, Biosens. Bioelectron. 20 (2005) 1962−1967.

5 Y. Kamitaka, S. Tsujimura, N. Seyoyama, T. Kajino, K. Kano, Fructose/dioxygen biofuel cell based on direct electron transfer-type bioelectrocatalysis, Phys. Chem. Chem. Phys. 9 (2007) 1793−1801.

6 K. So, S. Kawai, Y. Hamano, Y. Kitazumi, O. Shirai, O. Hibi, J. Ogawa, K. Kano, Improvement of a direct electron transfer-type fructose/dioxygen biofuel cell with a substrate-modified biocathode, Phys. Chem. Chem. Phys. 16 (2014) 4823−4829.

7 A. de Poulpiquet, A. Ciaccafava, R. Gadiou, S. Gounel, M.T. Giudici-Orticoni, N. Mano, E. Lojou, Design of a H_2/O_2 biofuel cell based on thermostable enzymes, Electrochem. Commun. 42 (2014) 72−74.

8 N. Lalaoui, A. de Poulpiquet, R. Haddad, A. Le Goff, M. Holzinger, S. Gounel, M. Mermoux, P. Infossi, N. Mano, E. Lojou, S. Cosnier, A membraneless air-breathing hydrogen biofuel cell based on direct wiring of thermostable enzymes on carbon nanotube electrodes, Chem. Commun. 51 (2015) 7447−7450.

9 K. So, Y. Kitazumi, O. Shirai, K. Nishikawa, Y. Higuchi, K. Kano, Direct electron transfer-type dual gas diffusion H_2/O_2 biofuel cells, J. Mater. Chem. A 4 (2016) 8742−8749.

10 H. Xia, K. So, Y. Kitazumi, O. Shirai, K. Nishikawa, Y. Higuchi, K. Kano, Dual gas-diffusion membrane-and mediatorless dihydrogen/air-breathing biofuel cell operating at room temperature, J. Power Sources 335 (2016) 105−112.

11 W. Zhang, G. Li, Third-generation biosensors based on the direct electron transfer of proteins, Anal. Sci. 20 (2004) 603−609.

12 S. Tsujimura, A. Nishina, Y. Kamitaka, K. Kano, Coulometric d-fructose biosensor based on direct electron transfer using d-fructose dehydrogenase, Anal. Chem. 81 (2009) 9383−9387.

13 H. Xia, Y. Kitazumi, O. Shirai, K. Kano, Direct electron transfer-type bioelectrocatalysis of peroxidise at mersoporous carbon electrodes and its application for glucose dectection, Anal. Sci. in press

14 K. Sakai, Y. Sugimoto, Y. Kitazumi, O. Shirai, K. Takagi, K. Kano, Direct electron transfer-type bioelectrocatalytic interconversion of carbon dioxide/formate and NAD+/NADH redox couples with tungsten-containing formate dehydrogenase, Electrochim. Acta 228 (2017) 537–544.

15 S. Tsujimura, K. Kano, T. Ikeda, Bilirubin oxidase in multiple layers catalyzes four-electron reduction of dioxygen to water without redox mediators, J. Electroanal. Chem. 576 (2005) 113–120.

16 M.A. Alonso-Lomillo, O. Rüdiger, A. Maroto-Valiente, M. Velez, I. Rodríguez-Ramos, F.J. Muñoz, V.M. Fernández, A.L. de Lacey, Hydrogenase-coated carbon nanotubes for efficient H2 oxidation, Nano Lett. 7 (2007) 1603–1608.

17 S. Tsujimura, Y. Miura, K. Kano, CueO-immobilized porous carbon electrode exhibiting improved performance of electrochemical reduction of dioxygen to water, Electrochim. Acta 53 (2008) 5716–5720.

18 C. Xiang, Y. Zou, L.X. Sun, F. Xu, F. Direct electron transfer of cytochrome c and its biosensor based on gold nanoparticles/room temperature ionic liquid/carbon nanotubes composite film, Electrochem. Commun. 10 (2008) 38–41.

19 J. Wang, M. Li, Z. Shi, N.Li, Z. Gu, Direct electrochemistry of cytochrome c at a glassy carbon electrode modified with single-wall carbon nanotubes, Anal. Chem. 74 (2002) 1993–1997.

20 W. Zheng, Q. Li, L. Su, Y. Yan, J. Zhang, L. Mao, Direct Electrochemistry of Multi-Copper Oxidases at Carbon Nanotubes Noncovalently Functionalized with Cellulose Derivatives, Electroanalysis 18 (2006) 587–594.

21 G. Göbel, F. Lisdat,Organic interlayers for oxygen reducing electrodes based on bilirubin oxidase and MWCNT modified gold, Electrochem. Commun. 10 (2008) 1691–1694.

22 M. Tominaga, S. Nomura, I. Taniguchi, d-Fructose detection based on the direct heterogeneous electron transfer reaction of fructose dehydrogenase adsorbed onto multi-walled carbon nanotubes synthesized on platinum electrode, Biosens. Bioelectron. 24 (2009) 1184–1188.

23 K. Gong, Y. Yan, M. Zhang, L. Su, S. Xiong, L. Mao, Electrochemistry and electroanalytical applications of carbon nanotubes: a review, Anal. Sci. 21 (2005) 1383–1393.

24 B. Reuillard, A.L. Goff, C. Agnès, A. Zebda, M. Holzinger, S. Cosnier, Direct electron transfer between tyrosinase and multi-walled carbon nanotubes for bioelectrocatalytic oxygen reduction, Electrochem. Commun. 20 (2012) 19–22.

25 K. So, M. Onizuka, T. Komukai, Y. Kitazumi, O. Shirai, K. Kano, Significance of the Length of Carbon Nanotubes on the Bioelectrocatalytic Activity of Bilirubin Oxidase for Dioxygen Reduction, Electrochem. Acta 192 (2016) 133–138.

26 W. Feng, P. Ji, Enzymes immobilized on carbon nanotubes, *Biotechnol. Advances* 29 (2011) 889–895.

27 Y. Sugimoto, Y. Kitazumi, O. Shirai, K. Kano, Effects of mesoporous structures on direct electron transfer-type bioelectrocatalysis: facts and simulation on a three-dimensional model of random orientation of enzymes, Electrochemistry 85 (2017) 82-87.

28 Y. Sugimoto, R. Takeuchi,Y. Kitazumi, O. Shirai, and K. Kano, Significance of Mesoporous Electrodes for Noncatalytic Faradaic Process of Randomly Oriented Redox Proteins, J. Phys. Chem. C. 120 (2016) 26270–26277.

29 Y. Sugimoto, Y. Kitazumi, S. Tsujimura, O. Shirai, M. Yamamoto, K. Kano, Electrostatic interaction between an enzyme and electrodes in the electric double layer examined in a view of direct electron transfer-type bioelectrocatalysis, Biosens. Bioelectron. 63 (2015) 138–144.

30 H. Xia, Y. Kitazumi, O. Shirai, K. Kano, Enhanced direct electron transfer-type bioelectrocatalysis of bilirubin oxidase on negatively charged aromatic compound-modified carbon electrode, J. Electroanal. Chem. 763 (2016) 104–109.

31 F. Oteri, A. Ciaccafava, A. De Poulpiquet, M. Baaden, E. Lojou, S. Sacquin-Mora, The weak, fluctuating, dipole moment of membrane-bound hydrogenase from Aquifex aeolicus accounts for its adaptability to charged electrodes, Phys. Chem. Chem. Phys. 16 (2014) 11318–11322.

32 I. Mazurenko, K. Monsalve, J. Rouhana, P. Parent, C. Laffon, A.L.Goff, E. Lojou, How the intricate interactions between carbon nanotubes and two bilirubin oxidases control direct and mediated O_2 reduction, ACS Appl. Material. Interfaces 8 (2016) 23074–23085.

33 T. Sakurai, K. Kataoka, Basic and applied features of multicopper oxidases, CueO, bilirubin oxidase, and laccase, Chem. Rec. 7 (2007) 220–229.

34 H.S. Shafaat, O. Rüdiger, H. Ogata, W. Lubitz, [NiFe] hydrogenases: a common active site for hydrogen metabolism under diverse conditions, Biochim. Biophys. Acta (BBA)-Bioenerg. 1827 (2013) 986–1002.

35 Y. Ueki, M. Inoue, S. Kurose, K. Kataoka, T. Sakurai, Mutations at Asp112 adjacent to the trinuclear Cu center in CueO as the proton donor in the four-electron reduction of dioxygen, FEBS Lett. 580 (2006) 4069–4072.

36 Y. Higuchi, N. Yasuoka, M. Kakudo, Y. Katsube, T. Yagi, H. Inokuchi, Single crystals of hydrogenase from *Desulfovibrio vulgaris* Miyazaki F, J. Biol. Chem. 262 (1987) 2823–2825.

37 A.J. Bard, L.R. Faulkner, Electrochemical methods: fundamentals and applications (2nd ed.) Wiley, New York (2016) 335.

38 S.A. Roberts, A. Weichsel, G. Grass, K. Thakali, J.T. Hazzard, G. Tollin, C. Rensing, W.R. Montfort, Crystal structure and electron transfer kinetics of CueO, a multicopper oxidase required for copper homeostasis in Escherichia coli, Proc. Natl. Acad. Sci. 99 (2002) 2766–2771.

39 K. Mizutai, M. Toyoda, K. Sagara, N. Takahashi, A. Sato, Y. Kamitaka, S. Tsujimura, Y. Nakanishi, T. Sugiura, S. Yamaguchi, K. Kano, B. Mikami, X-ray analysis of bilirubin oxidase from *Myrothecium verrucaria* at 2.3 Å resolution using a twinned crystal, Acta Crystallogr. F 66 (2010) 765–770.

40 G.M. Swain, T. Kuwana, Electrochemical formation of high surface area carbon fibers, Anal. Chem. 63 (1991) 517–519.

Chapter 3
Oriented immobilization of enzymes at functionalized electrode surface

3-1 Enhanced direct electron transfer-type bioelectrocatalysis of bilirubin oxidase on negatively charged aromatic compound-modified carbon electrode

Abstract

Effects of chemical modification of mesoporous Ketjen Black (KB) electrodes on direct electron transfer (DET)-type bioelectrocatalytic reduction of dioxygen by bilirubin oxidase (BOD) were investigated under air-saturated neutral conditions. Several amines were electrochemically oxidized at KB-modified electrode to generate nitrogen-carbon bond. The modification with negatively charged aromatic amines such as 4-aminobenzoic acid (4-ABA) drastically increased the catalytic current density compared with that by positively charged and non-charged aromatic compounds and negatively charged non-aromatic compound. Considering the basic amino acid residues around the type I site of BOD, it can be concluded that weakly negative charge on electrode surface induces a favorable orientation of BOD for the DET-type catalysis via the electrostatic interaction, while the π-π interaction is also essential for effective orientation of BOD on the electrode surface. The 4-ABA-modification leads to an increase in the heterogeneous electron transfer rate constant and a decrease in the randomness of the orientation as well as a slight increase in the surface concentration of BOD.

1. Introduction

Direct electron transfer (DET)-type bioelectrocatalysis has attracted increasing attention in the past decades due to its advantages such as simple construction, the absence of energy loss concerning mediators, and the absence of the problem on the stability of mediators.[1-5] Unfortunately, most of enzymes have been found to be difficult or limited to directly communicate with electrodes, because the active center of enzymes is often embedded deeply in the polypeptides. Therefore, some novel materials and methods have been developed to improve the activity of the DET-type bioelectrocatalysis. Good performance of DET-type reaction can be achieved by using nano-materials, such as carbon nano-materials,[6,7] Fe_3O_4magnetic nanoparticle,[8] and Au nanoparticle,[9] thanks to increased specific surface areas and high conductivity.

On the other hand, the electron-transfer rate is governed by the potential difference, the reorganization energy, and most importantly the distance between the active center of enzymes and the electrode surface, as described in Marcus theory.[10] Therefore, it is important to control the orientation of enzymes on the electrode surface to shorten the distance from the active center of

enzymes to the electrode surface. Several immobilization methods of enzymes on the electrode surface have been reported to control the orientation of enzymes for DET-type bioelectrocatalysis via covalent amide bond and Au-S bond.[11-13]

Recently, modification of electrodes with substrate or 'substrate-like linker' with structurally similar to natural substrate has been reported to induce a favorable orientation of the enzyme for the DET-type bioelectrocatalysis.[14-20] The linker is expected to be inserted into the active center 'pocket' of the enzyme and improves the coverage, the orientation, and the stability of the enzyme on the electrode. More recently, the characteristics of the electrode surface, such as positively/negatively charged property, hydrophilic or hydrophobic property, are considered to affect the orientation of enzymes.[21,22]

Bilirubin oxidase (BOD) is in a family of multi-copper oxidase (MCO) and our group has first found that BOD can work as a good DET-type bioelectrocatalyst for four-electron reduction of dioxygen in neutral solution.[23,24] The active site of BOD contains four copper atoms which can be divided into three types according to their spectroscopic and magnetic properties: type I (T1), type II (T2), and type III (T3) coppers.[25,26] The T1 copper oxidizes bilirubin to biliverdin and transfers the electron to the trinuclear center composed of one T2 copper and two T3 copper atoms where O2 is reduced to H2O. In a DET-type reaction, the T1 site accepts electron from electrodes.[27,28] Recently, higher DET-type bioelectrocatalytic activity of BOD on electrodes modified with several compounds have been reported.[14,28-31] Although the accurate information about the interaction between BOD and the modified electrode surface remains still unclear, DET-type BOD-based biocathodes have been developed for biofuel cells in the past decades.[4,13,14,32-37]

In this work, we focus on effects of chemical modification of carbon electrode surface on the DET-type bioelectrocatalytic activity of BOD. Several amines were linked to Ketjen Black (KB) through an electrochemically generated nitrogen-carbon bond. The modification provides charged/non-charged characteristics and aromatic/aliphatic characteristics on the KB surface. We may show that the electrostatic interaction between the active site of BOD and negatively charged aromatic compounds on the modified surface leads to a favorable orientation of BOD.

2. Experimental

2.1 Materials and regents

Ketjen Black EC300J (KB) was kindly donated from Lion Co. (Japan). Poly (tetrafluoroethylene) fine powder (PTFE, 6-J) was obtained from DuPont Mitsui Fluorochemicals (Japan). 4-Aminobenzoic acid (4-ABA), 2-aminobenzoic acid (2-ABA), 4-aminophthalic acid (4-APA), 4-aminobenzenesulfonic acid (4-ABS), 3-aminobenzenesulfonic acid (3-ABS),

2-aminobenzenesulfonic acid (2-ABS), *p*-phenylenediamine (*p*-PDA), methyl 4-aminobenzoate (MABA), and 6-aminohexanoic acid (6-AHA) were purchased from Tokyo Chemical Industry Co. (Japan). Bilirubin oxidase (BOD; EC 1.3.3.5) from *Myrothecium verrucaria* was donated from Amano Enzyme Inc. (Japan) (3.04 unit mg^{-1}) and used without further purification. Copper efflux oxidase (CueO) from *Escherichiacoli* was prepared as described previously (187 unit mg^{-1}).[38,39] All other chemicals used in this study were of analytical grade, and all solutions were prepared with distilled water.

2.2 Electrochemical measurements

All of electrochemical measurements were performed on an electrochemical analyzer ALS 701E with a rotating disk glassy carbon electrode (GCE, 3 mm in diameter, BAS) as a working electrode, a Pt wire as a counter electrode, and an Ag|AgCl|sat. KCl electrode as a reference electrode, respectively. All potentials are referred to the reference electrode in this work. The bioelectrocatalytic activity of BOD for the dioxygen reduction was evaluated by linear scan and cyclic rotating disk voltammetry at a scan rate (v) of 20 mV s^{-1} at 25 °C in 0.1 M air-saturated phosphate buffer (pH 7.0) at a rotating rate (ω) of 2000 rpm to get steady-state voltammograms (1 M = 1 mol dm^{-3}).

2.3 Electrochemical modification of carbon electrodes with amines

GCE was polished with alumina slurry (3μm and 0.5μm, in turn), sonicated, and washed with distilled water. The GCEs were chemically modified with several amines according to the literature.[40] In brief, amine was dissolved in 0.1 M KCl at a final concentration of 5 mM. In preliminary experiments, the amine solution was electrolyzed by 5-cycle potential scan in the potential range from 0.5 to 1.4 V at v =20 mV s^{-1}. A large oxidation peak of the amino group of 4-ABA was observed at around 0.95 V in the first cycle, but the current decreased drastically in the subsequent scans (Fig. 1 A). The oxidation of the amine on carbon electrodes generates a nitrogen-carbon bond and the carbon electrodes were chemically modified with the amine.[40] In the following, one-step electrochemical oxidation was done at 0.8 V for 40 s to simplify the procedure. The modified electrode was washed with distilled water to remove physically absorbed amines. The expected structure of the covalently bound amines is given in Fig. 1B. For example, the modification with 4-ABA povides negatively charged aromatic platform, since the carboxy group is dissociated under neutral pH and the amino group is oxidized and covalently linked to the electrode. The chemical modification of the amines were electrochemically checked with $[Fe(CN)_6]^{3-/4-}$ and $[Ru(NH_3)_6]^{2+/3+}$ as redox probes (Fig. 1C and Fig 1 D).[40] As shown in Fig. 1, $[Fe(CN)_6]^{3-/4-}$ redox

was inhibited at negatively charged 4-ABA/GCE, while $[Ru(NH_3)_6]^{2+/3+}$ redox was inhibited at positively charged *p*-PDA/GCE.

KB-modified GCE (KB/GCE) was prepared according to the literature.[14] Briefly, KB and PTFE (4:1, w:w) were distributed in 2-propanol and homogenized by ultrasonic disruptor (Heat Systems GmbH & Co.) for 3 min in an ice bath to prepare KB slurry. One μL of the KB slurry was dropped on a GCE surface and dried at room temperature (about 25°C) for 10 min to make a KB/GCE (1 L = 1 dm^{-3}). The oxidation peak of 4-ABA at KB/GCE was observed at around 0.85 V (data not shown). The KB/GCEs were chemically modified with the amines in a manner identical

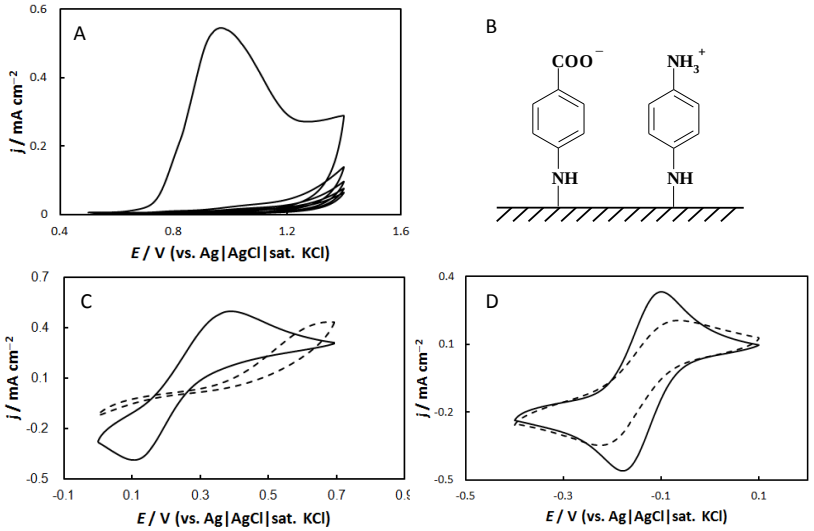

Fig. 1

(A) Cyclic voltammograms of 4-ABA at GCE at v = 20 mV s^{-1} in 0.1 M KCl.

(B) The expected structures of the covalently bound amines that are electrochemically oxidized on carbon electrodes. The original amines are 4-aminobenzoic acid (4-ABA, left) and *p*-phenylenediamine (*p*-PDA, right).

(C) Cyclic voltammograms of $Fe(CN)_6^{3-/4-}$ (10 mM) on (solid line) bare GCE and (dashedline) 4-ABA/GCE in air-saturated phosphate buffer (pH 7).

(D) Cyclic voltammograms of $Ru(NH_3)_6^{2+/3+}$ (5 mM) on (solid line) bare GCE, (dashed line) *p*-PDA/GCE in air-saturated phosphate buffer(pH 4.5).

with that in the case of GCE described above. In the following, the chemically modified KB/GCE is called amine/KB/GCE. The surface area of the modified electrode was roughly estimated from the charging current at a potential where faradic processes are minimal.[41] The surface area of KB/GCE was calculated as 6.9 cm^2, which is about 100 times larger than bare GCE (0.07 cm^2). The chemical modification of KB/GCE described here caused practically no change in the surface area.

2.4 Adsorption of BOD on KB/GCEs and amine/KB/GCEs

BOD solution was prepared by dissolving the enzyme into 0.1 M phosphate buffer (pH 7.0) at a concentration of 10 mg mL^{-1}. Ten μL of the BOD solution was dropped on KB/GCEs or amine/KB/GCEs and dried at room temperature for 1.5 h. The electrode was washed with distilled water and used for electrochemical experiments. In the following, the electrodes are called BOD/KB/GCE and BOD/amine/KB/GCE, respectively. For long time storage, BOD/amine/KB/GCEs were kept in water-saturated atmosphere at 4 °C.

3. Results and discussion

3.1 Effects of the chemical modification of KB/GCE with amines on the bioelectrocatalytic activity of BOD

Fig. 2 shows rotating disk cyclic voltammograms at several BOD/amine/KB/GCEs at ω = 2000 rpm under air-staturated conditions. Well-difined sigmoidal catalytic waves were observed at all of the BOD/amine/KB/GCEs examined. Such catalytic waves were not obeserved in the absence of BOD or dioxygen (data not shown). Thus, the catalytic current is ascribed to the DET-type bioelectrocatalytic reduction of dioxygen by BOD on the electrode.

As comparison, the broken line in Fig. 2 indicates the rotaing disk voltammetric response at a BOD/KB/GCE without amine-modification. As judged from Fig. 2, BOD/4-ABA/KB/GCE (panel D) gave much larger density of the limitting current (1.2 ± 0.1 mA cm^{-2} at 0V) compared with the other electrodes modified with *p*-PDA, MABA, and 6-AHA. In addition, the onset potential of the catalytic wave at the BOD/4-ABA/KB/GCE was about 0.58 V, which is more positive than that at BOD/KB/GCE without amine-modification (0.52 V). Two pair of peaks at around 0.1 and 0.3 V are surface-confined redox species (most probably quinone species) generated as by-products during the oxidation of 4-ABA, as judged from voltammogram in the absence of BOD (data not shown). Since the redox waves do not change after adsorption of BOD, the by-products on the electrode surface do not affect the BOD activity. Therefore, we can conclude that the aromatic carboxy group generated on the carbon electrode (Fig. 1 B) enhances the BOD activity.

Improvement of the DET-type bioelectrocatalytic activity of BOD has been reported at negatively charged SAM modified Au,[30] pyrolytic graphite edge (PGE),[28] and carbon nanotubes (CNTs),[29,31] while the reason has not been given in the literature. 4-ABA modification generates a negatively charged aromatic platform due to the dissociation of the carboxy group. The surface of PGE and CNT is also negatively charged. On the other hand, *p*-PDA and MABA give (partially) positively charged and neutral aromatic platforms, respectively, and these amines were not effective

to improve the DET-type bioelectrocatalytic activity of BOD (Fig. 2). Therefore, the negative charge is essential to improve the catalytic activity of BOD.

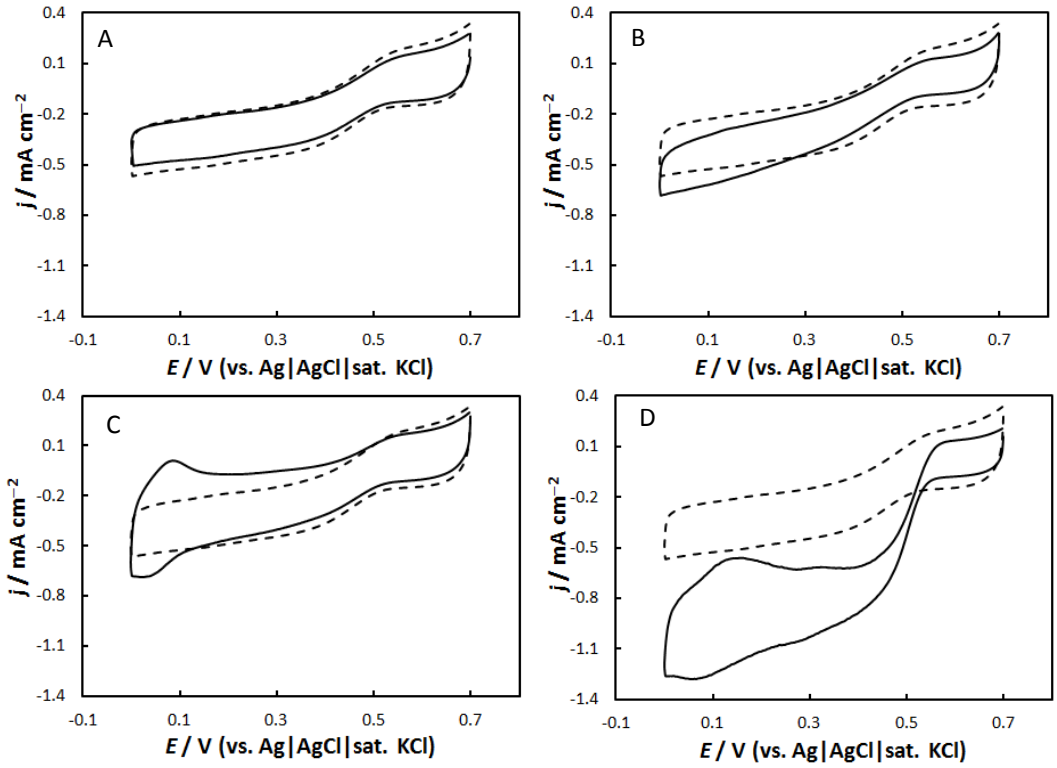

Fig. 2

Rotating disk cyclic voltammograms of catalytic dioxygen reduction at (A) BOD/6-AHA/KB/GCE, (B) BOD/MABA/KB/GCE, (C) BOD/*p*-PDA/KB/GCE, and (D) BOD/4-ABA/KB/GCE at ω = 2000 rpm and v = 20 mV s^{-1} in air-saturated phosphate buffer (pH 7). Dashed lines represent a rotating disk cyclic voltammogram at BOD/KB/GCE taken under the same conditions for comparison.

6-AHA-modification to give negative but non-aromatic propety was not effective to improve the bioelectrocatalytic activity of BOD. Therefore, the π-π interaction with BOD seems to also be improtant to lead BOD to an orientation convient for the DET-type bioelectrocatalysis.[13,28] Finally, we conclude a hypothesis that the negative charged aromatic characteristics are the key factor to improve the catalytic activity.

In order to confirm our conclusions, we examined the characteristics of the other KB/GCEs modified with negatively charged aromatic amines (2-ABA, 4-APA, 4-ABS, 3-ABS and 2-ABS). The limiting current density at these electrodes is depicted in Fig. 3. All of negatively charged aromatic amines provide nice platforms for BOD as in the case of 4-ABA. The result supports our conclusion.

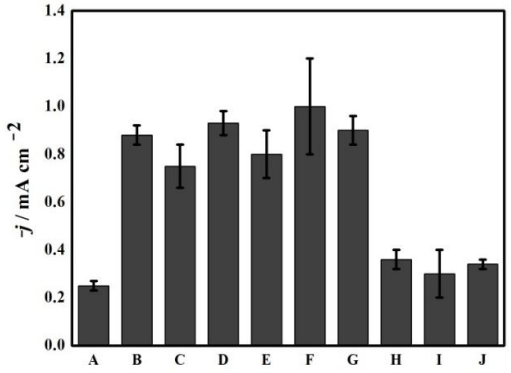

Fig. 3

The background current-corrected limiting current density of the O_2 reduction at several BOD-adsorbed KB/GCEs (0.3 V). (A) unmodified KB, (B)-(J) KB modified with (B) 4-ABA, (C) 4-APA, (D) 2-ABA, (E) 4-ABS, (F) 3-ABS, (G) 2-ABS, (H) *p*-PDA, (I) MABA, (J) 6-AHA.

3.2 Kinetic analysis of the improved performance of BOD/4-ABA/KB/GCE

The behavior of BOD on 4-ABA/KB/GCE was kinetically examined by rotating disk voltammetry with KB/GCE as a reference platform. As shown in Fig. 4 (A), the limiting current density increased with an increase in ω both at BOD/4-ABA/KB/GCE and BOD/KB/GCE, but BOD/4-ABA/KB/GCE yielded larger current density than BOD/KB/GCE at increased ω. The observed density of the steady-state catalytic limiting current (j_{lim}) at rotating disk electrode can be given by Koutecký-Levich equation as:

$$\frac{1}{j_{\mathrm{lim}}} = \frac{1}{j_{\mathrm{d,lim}}} + \frac{1}{j_{\mathrm{cat,lim}}} \tag{1}$$

$$j_{\mathrm{d,lim}} = 0.62 n_{\mathrm{O_2}} F D_{\mathrm{O_2}}{}^{2/3} \nu^{-1/6} c_{\mathrm{O_2}} \omega^{1/2} \tag{2}$$

$$j_{\mathrm{cat,lim}} = n_{\mathrm{E}} F k_{\mathrm{cat}} \Gamma \tag{3}$$

Where $j_{\mathrm{d,lim}}$ and $j_{\mathrm{cat,lim}}$ are the diffusion-limiting current density and the catalytic limiting current density, respectively. Other symbols mean, respectively: $n_{\mathrm{O_2}}$, the number of electrons of dioxygen (= 4); F, Faraday constant; $D_{\mathrm{O_2}}$, the diffusion constant of dioxygen (2.0×10^{-5} cm s^{-1});[42] ν, the kinematic viscosity of buffer (0.908×10^{-6} m^2 s^{-1} in 25 °C);[42] $c_{\mathrm{O_2}}$, the bulk concentration of dioxygen (0.25 mM in air-saturated solution at 25 °C); k_{cat}, the catalytic constant (250 s^{-1});[23] n_{E}, the number of electrons of enzyme in one catalytic turnover (= $n_{\mathrm{O_2}}$ in this case); and Γ, the surface concentration of the effective enzyme immobilized on the electrode.

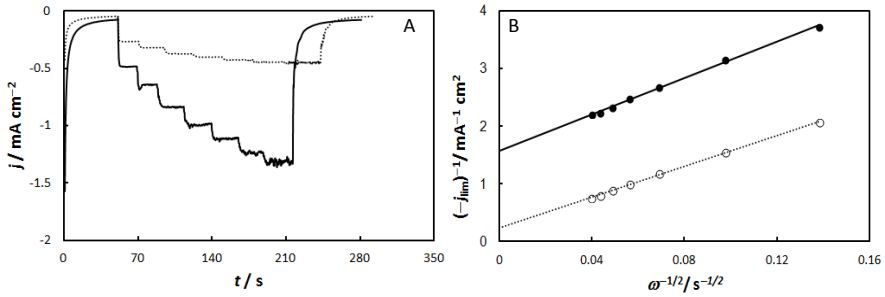

Fig. 4

(A): Amperometric *i-t* curves of catalytic reduction of dioxygen at (a) BOD/KB/GCE and (b) BOD/4-ABA-KB/GCE at ω = 0, 500, 1000, 2000, 3000, 4000, 5000 and 6000 rpm and at 0 V in air-saturated phosphate buffer (pH 7);

(B): Koutecký-Levich plot of the data given in (A).

Koutecký-Levich plots (j_{lim}^{-1} vs. $\omega^{-1/2}$ plots) for BOD/4-ABA/KB/GCE and BOD/KB/GCE are given in Fig.4 (B). The slopes of the linear fit are 16.5 ± 0.3 $\mathrm{mA^{-1}\ cm^2\ s^{-1/2}}$ for BOD/4-ABA/KB/GCE and 15.7 ± 0.1 $\mathrm{mA^{-1}\ cm^2\ s^{-1/2}}$ for BOD/KB/GCE, and are almost identical with each other, as expected by Eq. (2) (the theoretical value being 10.6 $\mathrm{mA^{-1}\ cm^2\ s^{-1/2}}$). Note here that we performed non-linear regression of the non-linear j_{lim} vs. $\omega^{1/2}$ relation using Excel® to avoid the change in the weight of the data in reciprocal plots. The catalytic contribution $j_{\mathrm{cat,lim}}$ was evaluated as 3.0 ± 0.3 $\mathrm{mA\ cm^{-2}}$ for BOD/4-ABA/KB/GCE, which is more than 4.6 times larger than that of BOD/KB/GCE (0.640 ± 0.003 $\mathrm{mA\ cm^{-2}}$). Based on Eq. (3), $k_{\mathrm{cat}}\Gamma$ was evaluated as (7.7 ± 0.8) $\times 10^{-9}$ mol $\mathrm{cm^{-2}\ s^{-1}}$ for BOD/4-ABA/KB/GCE, while (1.66 ± 0.01) × 10^{-9} mol $\mathrm{cm^{-2}\ s^{-1}}$ for BOD/KB/GCE. The data suggest that slight increase in Γ by the 4-ABA modification.

Next, the interfacial electron transfer rate constant was also evaluated from the steady-state currentdensity (*j*) vs. the electrode potential (*E*) in linear-scan rotating disk linear scan voltammetry. We use a steady-state model without the concentration polarization of the substrate by considering the randum orientation.[43] For the model, the $j/j_{\mathrm{cat,lim}}$ vs. *E* relationship is given by thefollowing equation(Appendix):

$$\frac{j}{j_{\mathrm{cat,lim}}} = \frac{1}{\beta\Delta d\left(1+\exp\left\{\frac{n'_{\mathrm{E}}F}{RT}\left(E-E^{\circ\prime}{}_{\mathrm{E}}\right)\right\}\right)}\ln\left|\frac{k_{0,\max}\left(1+\exp\left\{\frac{n'_{\mathrm{E}}F}{RT}\left(E-E^{\circ\prime}{}_{\mathrm{E}}\right)\right\}\right)+k_{\mathrm{c}}\exp\left\{\frac{\alpha n'_{\mathrm{E}}F}{RT}\left(E-E^{\circ\prime}{}_{\mathrm{E}}\right)\right\}}{k_{0,\max}\exp\left(-\beta\Delta d\left(1+\exp\left\{\frac{n'_{\mathrm{E}}F}{RT}\left(E-E^{\circ\prime}{}_{\mathrm{E}}\right)\right\}\right)\right)+k_{\mathrm{c}}\exp\left\{\frac{\alpha n'_{\mathrm{E}}F}{RT}\left(E-E^{\circ\prime}{}_{\mathrm{E}}\right)\right\}}\right| \quad (4)$$

where n'_{E} is the number of the electron in the rate determining step of the interfacial electron transfer (= 1 in this case as the number of the electron for the T1site in BOD); *R*, the gas constant; *T*, the absolute temperature; $k_{0,\max}$, the standard rate constant at the distance of the closest approach in the best orientation of enzyme; Δd, the distance between the closest and farthest approach of enzyme; α, the transfer coefficient; β, the coefficient in the long range electron transfer; $E^{\circ\prime}{}_{\mathrm{E}}$, the formal

potential of the redox center of enzyme for electrochemical communication with electrode.

Using $k_{0,max}$, $\beta\Delta d$, and $k_{cat}\Gamma$ as adjustable parameters, Eq. (3) was fitted to the rotating disk voltammogram using a non-linear regression analysis by Excel© (Fig.5). The value of $j_{cat,lim}$ (and then $k_{cat}\Gamma$) may be set to be identical with that obtained in the above Koutecký-Levich analysis. However, strictly speaking, the rotating disk voltammogram at ω = 2000 rpm in Fig. 5 is not completely controlled by enzyme kinetics, but is affected in part by the steady-state mass transfer of dioxygen to the electrode (see Eq. (1)). This is the reason why we set $k_{cat}\Gamma$ as an adjustable parameter. α was assumed to be 0.3.

The experimental voltammograms are well reproduced as shown by the broken lines in Fig. 5. The evaluated values of $k_{cat}\Gamma$ are $(8.4 \pm 0.8) \times 10^{-9}$ mol cm^{-2} s^{-1} and $(7.6 \pm 0.1) \times 10^{-9}$ mol cm^{-2} s^{-1} for BOD/4-ABA/KB/GC and BOD/KB/GC, respectively. These values are slightly larger than those obtained in the above Koutecký-Levich analysis. The discrepancy between the values obtained by two methods is due to the situation that the voltammogram in Fig. 5 is not completely in kinetic control.

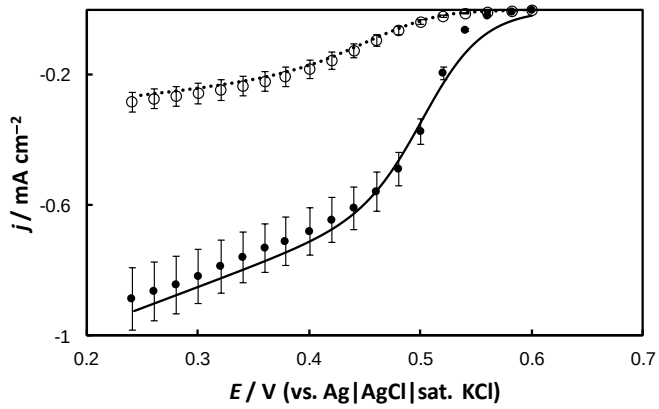

Fig. 5

Background current-corrected rotating disk linear sweep voltammograms of catalytic reduction of O_2 at (open circles) BOD/KB/GCE and (closed circles) BOD/4-ABA/KB/GCE and at v = 20 mV s^{-1} in air-saturated phosphate buffer (pH 7). The lines represent the best fitted curves obtained by non-linear least square method.

On the other hand, the evaluated values of $k_{0,max}$ is 6.0×10^3 s^{-1} for BOD/4-ABA/KB/GC and is three times larger than that of BOD/KB/GC (2.0×10^3 s^{-1}). Therefore, the negatively charged aromatic platform is convenient in the heterogeneous electron transfer between the electrochemically active site of BOD and the electrode. Finally, the $\beta\Delta d$ is evaluated as 3.6 ± 0.3 for BOD/4-ABA/KB/GC electrode, while 12 ± 1 for BOD/KB/GC electrode. By using the reported value of β for proteins (approximately 1.4 Å^{-1}),[44] Δd can be calculated as 2.6 ± 0.2Å and 8.2 ± 0.8Å for BOD/4-ABA/KB/GCE and BOD/KB/GCE, respectively. Considering the size of BOD (4~6

nm), the T1 site of the most of the adsorbed BOD faces to the negatively charged aromatic part on 4-ABA/KB/GCE, as shown in Fig. 4S (A). On the other hand, BOD at KB/GCE seems to be randomly oriented on the electrode. The increase in $k_{0,max}$ and decrease in Δd are responsible for the positive shift of the onset potential (Fig. 2 (D)).

3.3 Interaction between BOD and negatively charged surface

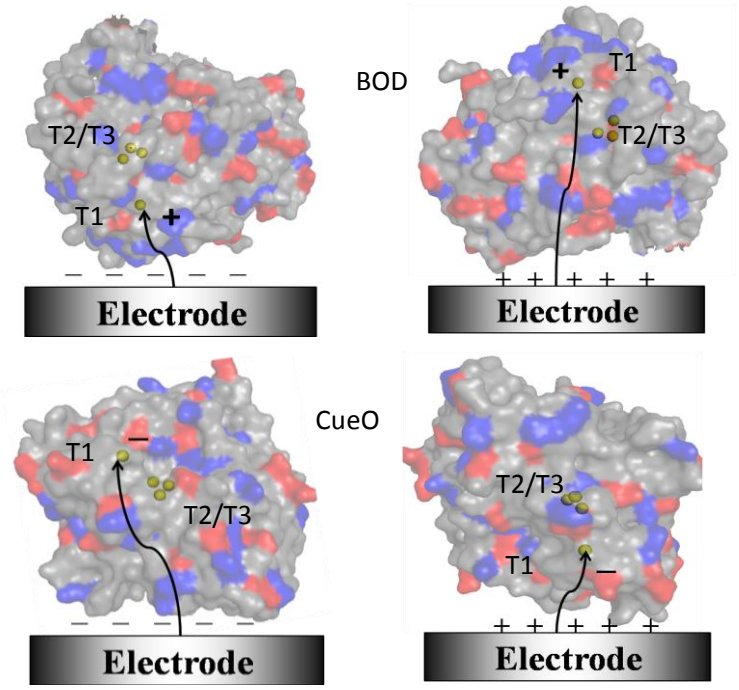

Fig. 6

Presumable orientation of (top) BOD and (bottom) CueO on (left) negatively charged or (right) positively charged surfaces. Red color represent the acidic amino acid residues (Glu and Asp), and blue color represents the basic amino acid residues (Lys, Arg and His). Yellow spheres represent T1, T2, and T3 copper, respectively. The signs + and – located in the enzymes indicate the charge of amino acid residues around the T1 site under neutral conditions. Arrows indicate the tentative electron transfer route from electrode to the T1 sites.

BOD contains 572 amino residues with a molar mass of 64 kDa, the number of the acidic and basic amino acid residues being 65(Asp 35, Glu 30) and 60 (Arg 29, Lys 13, His 18), respectively. [45] The isoelectric point (p*I*) of BOD is calculated to be 4.1 on an ExPASy-Compute p*I*/Mw tool (http://web.expasy.org/compute_pi/), indicating that BOD seems to have totally negative net charge when dissolved in neutral phosphate buffer. The distribution of amino acid residues on BOD surface is given in Fig. 6. As shown in Fig. 6, the T1 region of BOD is surrounded by the basic amino acid residues. The residues seem to be positively charged under neutral conditions. Thus,

when electrode surface is negatively charged, the attractive electrostatic interaction between the T1 region and the electrode surface induces a favorable orientation of BOD for the DET-type bioelectrocatalytic reaction with the T1 site facing to the electrode surface.

Copper efflux oxidase (CueO) is also in a family of multi-copper oxidase, but the T1 site is surrounded by the acidic amino acid residues (Fig. 6 bottom). Therefore, based on the our model of the interaction, we can expect that the chemical modification of 4-ABA will not so effective for CueO under neutral conditions due to the repulsive electrostatic interaction between negatively charged electrode surface and the negatively charged T1 region. This expectation was experimentally verified: any improvement in the bioelectrocatalytic activity was not observed and the onset potential shifted to the negative direction resulting in an increase in the overpotential (Fig. 7A). In contrast, we tried to generate positive charge on the electrode to induce the attractive electrostatic interaction between the T1 site of CueO and the electrode by modifying the KB/GCE with *o*-phenylenediamine (pK_b = 9.523). Slight but clear improvement was observed as shown in Fig. 7B.

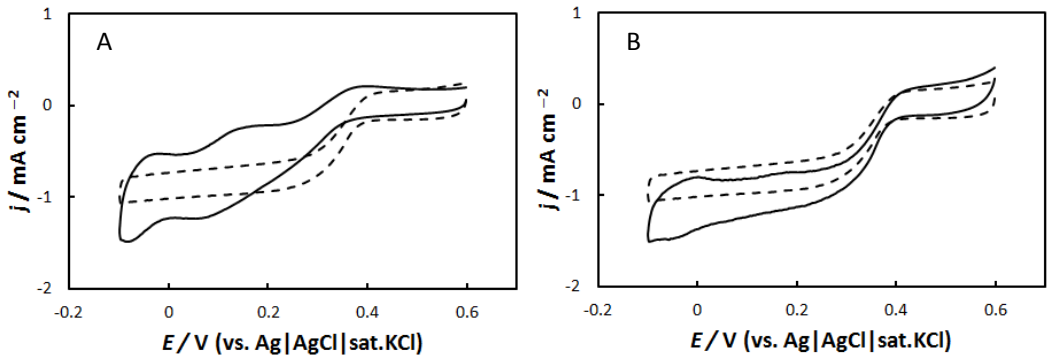

Fig. 7

Rotating disk cyclic voltammogram (A) CueO/4-ABA-KB/GCE and (B) CueO/*o*-PDA-KB/GCE in air-saturated phosphate buffer (pH 7) atω = 2000 rpm and v = 20 mV s^{-1}. Dashed lines represent a rotating disk cyclic voltammogram at CueO/KB/GCE taken under the same conditions for comparison.

The stability of the DET-type bioelectrocatalytic activity was investigated by time dependence of the catalytic current of BOD adsorbed on the amine/KB/GCE after storage at 4 °C. The catalytic activity remained more than 60% when BOD/4-ABA/KB/GC electrodes was stored for 4 d, while that was less than 40% when BOD/KB/GC electrode was stored for only 3 d (Fig. 8). This implies that the KB surface modified with 4-ABA not only improves the catalytic performance of BOD for the dioxygen reduction but also provides a stable state for BOD on the electrode surface.

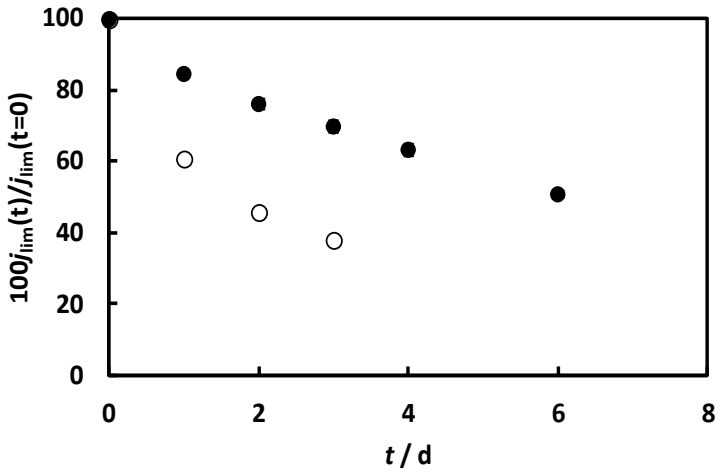

Fig. 8

The long-term stability of BOD/4-ABA/KB/GCE (closed circles) and BOD/KB/GCE (open circles). The activity was measured from the steady-state limiting catalytic current at 0 V and 60 s after the potential step at ω = 2000 rpm in air-saturated phosphate buffer (pH 7).

4. Conclusion

In summary, in this paper we have reported that negatively charged aromatic characteristics are a key factor to enhance the DET-type bioelectrocatalytic activity of BOD towards the dioxygen reduction. Here, we consider that the negative charge on the electrode surface is essential for a favorable orientation of BOD by attractive electrostatic interaction, since the T1 site of BOD are surrounded mainly by the basic amino acids which will be positively charged under neutral conditions. The aromatic structure is also essential for an effective orientation of BOD on the electrode surface with π-π interaction. The situation leads to an increase in the heterogeneous electron transfer rate constant and a decrease in the randomness of the orientation as well as a slight increase in the surface concentration of BOD.

5. Appendix

The steady-state current density (j) caused by the DET-type bioelectrocatalysis is written as Eq. (A.1)[46,23,]

$$j = \frac{j_{\mathrm{cat,lim}}}{1 + k_{\mathrm{cat}}/k_{\mathrm{f}} + k_{\mathrm{b}}/k_{\mathrm{f}}} \qquad \text{(A.1)}$$

where k_f, k_b are the forward and reverse rate constants for the electrode reaction, respectively, k_{cat} is the catalytic constant for the DET reaction, and $j_{cat,lim}$ is the current density under kinetically-controlled limiting current conditions (without substrate concentration polarization). The electrode reaction is expressed as the Butler-Volmer equations as follows,

$$k_f = k_0 \exp\left\{-\frac{\alpha n'_E F}{RT}\left(E - E^{\circ\prime}{}_E\right)\right\} = k_0 e_f \tag{A.2}$$

and

$$k_b = k_0 \exp\left\{\frac{(1-\alpha) n'_E F}{RT}\left(E - E^{\circ\prime}{}_E\right)\right\} = k_0 e_b \tag{A.3}$$

where k_0 is the standard rate constant for the electrode reaction of one of the redox centers of the enzyme.

The value of k_0 will depend on the distance (d) between the redox center in the enzyme and electrode and changes from $k_{0,min}$ (at $d = d_{max}$) to $k_{0,max}$ (at $d = d_{min}$). Here, we assume the exponential distribution of k_0, $f(k_0)$. The both ends of the distribution are constrained by:

$$k_{0,min} = k_{0,max} \exp(-\beta \Delta d) \tag{A.4}$$

In this model, the enzyme redox center homogeneously distributes in d, that is, the probability of d is $1/\Delta d$ between d_{min} and $d_{max=}\ d_{min}+ \Delta$d. Therefore, the probability of k_0 is written as follows [43]

$$p_{k_0}(k_0) = 1 \Big/ \beta k_0 \Delta d \tag{A.5}$$

When the randomly adsorbed enzymes have the distributed values of k_0, j is written as follows.

$$j = \int_{k_{0,min}}^{k_{0,max}} j(k_0)\, p_{k_0}(k_0) \mathrm{d}k_0 , \tag{A.6}$$

where $j(k_0)$ is the current density caused by the enzyme having the standard rate constant of k_0. Substitution of Eq. (A.1) to (A.5) into Eq. (A.6) provides the following equation.

$$\frac{j}{j_{cat,lim}} = \int_{k_{0,min}}^{k_{0,max}} \frac{1}{1 + \dfrac{k_c}{k_0 e_f} + \dfrac{e_b}{e_f}} \frac{1}{\beta k_0 \Delta d} dk_0 \tag{A.7}$$

The integration in Eq. (A.6) gives the following equation:

$$\frac{j}{j_{cat,lim}} = \frac{1}{\beta \Delta d \left(1 + \dfrac{e_b}{e_f}\right)} \ln \left| \frac{k_{0,max} + \dfrac{k_c}{(e_f + e_b)}}{k_{0,min} + \dfrac{k_c}{(e_f + e_b)}} \right| \tag{A.8}$$

Therefore, the DET reaction with randomly adsorbed enzyme has varied conformation provides the current as follows.

$$\frac{j}{j_{\mathrm{cat,lim}}}=\frac{1}{\beta\Delta d\left(1+\exp\left\{\frac{n'_{\mathrm{E}}F}{RT}\left(E-E^{\circ\prime}{}_{\mathrm{E}}\right)\right\}\right)}\ln\left|\frac{k_{0,\max}\left(1+\exp\left\{\frac{n'_{\mathrm{E}}F}{RT}\left(E-E^{\circ\prime}{}_{\mathrm{E}}\right)\right\}\right)+k_{\mathrm{c}}\exp\left\{\frac{\alpha n'_{\mathrm{E}}F}{RT}\left(E-E^{\circ\prime}{}_{\mathrm{E}}\right)\right\}}{k_{0,\max}\exp\left(-\beta\Delta d\right)\left(1+\exp\left\{\frac{n'_{\mathrm{E}}F}{RT}\left(E-E^{\circ\prime}{}_{\mathrm{E}}\right)\right\}\right)+k_{\mathrm{c}}\exp\left\{\frac{\alpha n'_{\mathrm{E}}F}{RT}\left(E-E^{\circ\prime}{}_{\mathrm{E}}\right)\right\}}\right| \tag{A.9}$$

When the adsorbed enzyme has unique conformation, that is, when $\Delta d\rightarrow 0$, the current converges to eq. (A.1).

6. References

1 J.E. Frew, H.A.O. Hill, Direct and indirect electron transfer between electrodes and redox proteins, Eur. J. Biochem. 172 (1988) 261–269.

2 A.L. Ghindilis, P. Atanasov, E. Wilkins, Enzyme-catalyzed direct electron transfer: Fundamentals and analytical applications, Electroanalysis 9 (1997) 661–674.

3 R.S. Freire, C.A. Pessoa, L.D. Mello, L.T. Kubota, Direct electron transfer: an approach for electrochemical biosensors with higher selectivity and sensitivity, J. Brazilian Chem. Soc. 14 (2003) 230–243.

4 Y. Kamitaka, S. Tsujimura, N. Setoyama, T. Kajino, K. Kano, Fructose/dioxygen biofuel cell based on direct electron transfer-type bioelectrocatalysis, Phys. Chem. Chem. Phys. 9 (2007) 1793–1801.

5 S. Tsujimura, A. Nishina, Y. Kamitaka, K. Kano, Coulometric d-fructose biosensor based on direct electron transfer using d-fructose dehydrogenase, Anal. Chem. 81 (2009) 9383–9387.

6 M. Zhao, Y. Gao, J. Sun, F.Gao, Mediatorless glucose biosensor and direct electron transfer type glucose/air biofuel cell enabled with carbon nanodots, Anal. Chem. 87 (2015) 2615–2622.

7 G. Sanzó, C. Tortolini, R. Antiochia, G. Favero, F. Mazzei, Development of carbon-based nano-composite materials for direct electron transfer based biosensors, J. Nanosci. Nanotechnol. 15 (2015) 3423–3428.

8 T. Gu, J. Wang, H. Xia, S. Wang, X. Yu, Direct electrochemistry and electrocatalysis of horseradish peroxidase immobilized in a DNA/chitosan-Fe_3O_4 magnetic nanoparticle bio-complex film, Materials 7 (2014) 1069–1083.

9 V. Krikstolaityte, A. Barrantes, A. Ramanavicius, T. Arnebrant, S. Shleev, T. Ruzgas, Bioelectrocatalytic reduction of oxygen at gold nanoparticles modified with laccase, Bioelectrochemistry 95 (2014) 1–6.

10 R.A. Marcus, N. Sutin, Electron transfers in chemistry and biology, Biochim. Biophys. Acta Rev. Bioenergetics 811 (1985) 265–322.

11 O. Rüdiger, J.M. Abad, E.C. Hatchikian, V.M. Fernandez, A.L. De Lacey, Oriented immobilization of *Desulfovibrio gigas* hydrogenase onto carbon electrodes by covalent bonds for nonmediated oxidation of H_2, J. Am. Chem. Soc. 127 (2005) 16008–16009.

12 M. Pita, C. Gutierrez-Sanchez, D. Olea, M. Velez, C. Garcia-Diego, S. Shleev, A.L. De Lacey, High redox potential cathode based on laccase covalently attached to gold electrode, J. Phys. Chem. C 115 (2011) 13420−13428.

13 I.W. Schubart, G. Gero, F. Lisdat, A pyrroloquinolinequinone-dependent glucose dehydrogenase (PQQ-GDH)-electrode with direct electron transfer based on polyaniline modified carbon nanotubes for biofuel cell application, Electrochim. Acta 82 (2012) 224–232.

14 K. So, S. Kawai, Y. Hamano, Y. Kitazumi, O. Shirai, M. Hibi, K. Kano, Improvement of a direct electron transfer-type fructose/dioxygen biofuel cell with a substrate-modified biocathode, Phys. Chem. Chem. Phys. 16 (2014) 4823–4829.

15 R.J. Lopez, S. Babanova, Y. Ulyanova, S. Singhal, P. Atanassov, ChemElectroChem. Improved interfacial electron transfer in modified bilirubin oxidase biocathodes, 1 (2014) 241–248.

16 C.F. Blanford, R.S. Heath, F.A. Armstrong, A stable electrode for high-potential, electrocatalytic O_2 reduction based on rational attachment of a blue copper oxidase to a graphite surface, Chem. Commun. 17 (2007) 1710−1712.

17 M. Bourourou, K. Elouarzaki, N. Lalaoui, C. Agnès, A. Le Goff, M. Holzinger, S. Cosnier, Supramolecular immobilization of laccase on carbon nanotube electrodes functionalized with (methylpyrenylaminomethyl) anthraquinone for direct electron reduction of oxygen, Chem. Eur. J. 19 (2013) 9371−9375.

18 N. Lalaoui, K. Elouarzaki, A. Le Goff, M. Holzinger, S. Cosnier, Efficient direct oxygen reduction by laccases attached and oriented on pyrene-functionalized polypyrrole/carbon nanotube electrodes, Chem. Commun. 49 (2013) 9281–9283.

19 A.A. Arrocha, U. Cano-Castillo, S.A. Aguila, R. Vazquez-Duhalt, Enzyme orientation for direct electron transfer in an enzymatic fuel cell with alcohol oxidase and laccase electrodes, Biosens. Bioelectron. 61 (2014) 569–574.

20 N. Lalaoui, A. Le Goff, M. Holzinger, M. Mermoux, S. Cosnier, Wiring laccase on covalently modified graphene: carbon nanotube assemblies for the direct bioelectrocatalytic reduction of oxygen, Chem. Eur. J. 21 (2015) 3198–3201.

21 R. Kontani, S. Tsujimura, K. Kano, Air diffusion biocathode with CueO as electrocatalyst adsorbed on carbon particle-modified electrodes, Bioelectrochemistry 76 (2009) 10–13.

22 Y. Sugimoto, Y. Kitazumi, S. Tsujimura, O. Shirai, M. Yamamoto, K. Kano, Electrostatic interaction between an enzyme and electrodes in the electric double layer examined in a view of direct electron transfer-type bioelectrocatalysis, Biosens. Bioelectron. 63 (2015) 138–144.

23 S. Tsujimura, T. Nakagawa, K. Kano, T. Ikeda, Kinetic study of direct bioelectrocatalysis of dioxygen reduction with bilirubin oxidase at carbon electrodes, Electrochemistry 72 (2004) 437–439.

24 S. Tsujimura, K. Kano, T. Ikeda, Bilirubin oxidase in multiple layers catalyzes four-electron reduction of dioxygen to water without redox mediators, J. Electroanal. Chem. 576 (2005) 113–120.

25 E.I. Solomon, U.M. Sundaram, T.E. Machonkin, Multicopper oxidases and oxygenases, Chem. Rev. 96 (1996) 2563–2606.

26 A. Shimizu, J.H. Kwon, T. Sasaki, T. Satoh, N. Sakurai, T. Sakurai, T. Samejima, *Myrothecium verrucaria* bilirubin oxidase and its mutants for potential copper ligands, Biochemistry 38 (1999) 3034–3042.

27 Y. Kamitaka, S. Tsujimura, K. Kataoka, T. Sakurai, T. Ikeda, K. Kano. Effects of axial ligand mutation of the type I copper site in bilirubin oxidase on direct electron transfer-type bioelectrocatalytic reduction of dioxygen, J. Electroanal. Chem. 601 (2007) 119–124.

28 L. Dos Santos, V. Climent, C.F. Blanford, F.A. Armstrong, Mechanistic studies of the 'blue'Cu enzyme, bilirubin oxidase, as a highly efficient electrocatalyst for the oxygen reduction reaction, Phys. Chem. Chem. Phys. 12 (2010) 13962–13974.

29 G. Göbel, F. Lisdat, Organic interlayers for oxygen reducing electrodes based on bilirubin oxidase and MWCNT modified gold, Electrochem. Commun. 10 (2008) 1691–1694.

30 M. Tominaga, M. Ohtani, I. Taniguchi, Gold single-crystal electrode surface modified with self-assembled monolayers for electron tunneling with bilirubin oxidase, Phys. Chem. Chem. Phys. 10 (2008) 6928–6934.

31 Y. Ogawa, S. Yoshino, T. Miyake, M. Nishizawa, Surfactant-assisted direct electron transfer between multi-copper oxidases and carbon nanotube-based porous electrodes, Phys. Chem. Chem. Phys. 16 (2014) 13059–13062.

32 A. De Poulpiquet, A. Ciaccafava, R. Gadiou, S. Gounel, M.T. Giudici-Orticoni, N. Mano, E. Lojou, Design of a H_2/O_2 biofuel cell based on thermostable enzymes, Electrochem. Commun. 42 (2014) 72–74.

33 V. Scherbahn, M.T. Putze, B. Dietzel, T. Heinlein, J.J. Schneider, F. Lisdat, Biofuel cells based on direct enzyme–electrode contacts using PQQ-dependent glucose dehydrogenase/bilirubin oxidase and modified carbon nanotube materials, Biosens. Bioelectro. 61 (2014) 631–638.

34 J. Filip, J. Šefčovičová, P. Gemeiner, J. Tkac, Electrochemistry of bilirubin oxidase and its use in preparation of a low cost enzymatic biofuel cell based on a renewable composite binder chitosan, Electrochim. Acta 87 (2013) 366–374.

35 K. Monsalve, M. Roger, C. Gutierrez-Sanchez, M. Ilbert, S. Nitsche, D. Byrne-Kodjabachian, E. Lojou, Hydrogen bioelectrooxidation on gold nanoparticle-based electrodes modified by *Aquifex aeolicus* hydrogenase: Application to hydrogen/oxygen enzymatic biofuel cells, Bioelectrochemistry 106 (2015) 47–55.

36 C. Santoro, S. Babanova, P. Atanassov, B. Li, I. Ieropoulos, P. Cristiani, High power generation by a membraneless single chamber microbial fuel cell (SCMFC) using enzymatic bilirubin oxidase (BOx) air-breathing cathode, J. Electrochem. Soc. 160 (2013) H720–H726.

37 N. Lalaoui, A. De Poulpiquet, R. Haddad, A. Le Goff, M. Holzinger, S. Gounel, S. Cosnier, A membraneless air-breathing hydrogen biofuel cell based on direct wiring

of thermostable enzymes on carbon nanotube electrodes, Chem. Commun. 51 (2015) 7447–7450.

38 Y. Ueki, M. Inoue, S. Kurose, K. Kataoka, T. Sakurai, Mutations at Asp112 adjacent to the trinuclear Cu center in CueO as the proton donor in the four - electron reduction of dioxygen, FEBS Lett. 580 (2006) 4069–4072.

39 Y. Miura, S. Tsujimura, Y. Kamitaka, S. Kurose, K. Kataoka, T. Sakurai, K. Kano, Bioelectrocatalytic reduction of O2 catalyzed by CueO from Escherichia coli adsorbed on a highly oriented pyrolytic graphite electrode, Chem. Lett. 36 (2007) 132–133.

40 G. Yang, Y. Shen, M. Wang, H. Chen, B. Liu, S. Dong, Copper hexacyanoferrate multilayer films on glassy carbon electrode modified with 4-aminobenzoic acid in aqueous solution, Talanta 68 (2006) 741–747.

41 G.M. Swain, T. Kuwana. Electrochemical formation of high surface area carbon fibers, Anal. Chem. 63 (1991) 517–519.

42 S.B. Hall, E.A. Khudaish, A.L. Hart, Electrochemical oxidation of hydrogen peroxide at platinum electrodes. Part III: Effect of temperature, Electrochim. Acta 44 (1999) 2455–2462.

43 C. Léger, A.K. Jones, S.P. Albracht, F.A. Armstrong, Effect of a dispersion of interfacial electron transfer rates on steady state catalytic electron transport in [NiFe]-hydrogenase and other enzymes, J. Phys. Chem. B 106 (2002) 13058–13063.

44 C.C. Moser, J.M. Keske, K. Warncke, R.S. Farid, P.L. Dutton, Nature of biological electron transfer, Nature 355 (1992) 796-802.

45 K. Mizutani, M. Toyoda, K. Sagara, N. Takahashi, A. Sato, Y. Kamitaka, S. Tsujimura, Y. Nakanishi, T. Sugiura, S. Yamaguchi, K. Kano, B. Mikami, X-ray analysis of bilirubin oxidase from Myrothecium verrucaria at 2.3 Å resolution using a twinned crystal, Acta Crystallogr. F 66 (2010) 765–770.

46 T. Ikeda, D. Kobayashi, F. Matsushita, T. Sagara, K. Niki, Bioelectrocatalysis at electrodes coated with alcohol dehydrogenase, a quinohemoprotein with heme c serving as a built-in mediator, J. Electroanal. Chem. 361 (1993) 221–228.

Chapter 3-2

Dual gas-diffusion membrane- and mediatorless dihydrogen/air-breathing biofuel cell operating at room temperature

Abstract

A membraneless direct electron transfer (DET)-type dihydrogen (H_2)/air-breathing biofuel cell without any mediator was constructed wherein bilirubin oxidase from *Myrothecium verrucaria* (BOD) and membrane-bound [NiFe] hydrogenase from *Desulfovibrio vulgaris* Miyazaki F (MBH) were used as biocatalysts for the cathode and the anode, respectively, and Ketjen black-modified water proof carbon paper (KB/WPCC) was used as an electrode material. The KB/WPCC surface was modified with 2-aminobenzoic acid and *p*-phenylenediamine, respectively, to face the positively charged electron-accepting site of BOD and the negatively charged electron-donating site of MBH to the electrode surface. A gas-diffusion system was employed for the electrodes to realize high-speed substrate supply. As result, great improvement in the current density of O_2 reduction with BOD and H_2 reduction with MBH were realized at negatively and postively charged surfaces, repectively. Gas diffusion system also supressed the oxidative inactivation of MBH at high electrode potentials. Finally, based on the impoved bioanode and biocathode, a dual gas-diffusion membrane- and mediatorless H_2/air-breathing biofuel cell was constructed. The maximum power density reached 6.1 mW cm^{-2} (at 0.72 V), and the open circuit voltage was 1.12 V using 1 atm of H_2 gas as a fuel at room temperature and under passive and quiescent conditions.

1. Introduction

Enzymatic biofuel cells (EBFCs) are devices for converting chemical energy into electrical energy that utilize enzymes as electrocatalysts for the oxidation of fuels at the anode and the reduction of dioxygen (O_2) or hydrogen peroxide at the cathode.[1–4] In principle, a variety of compounds, such as sugar,[5–13] alcohol,[14–17] formate[18,19] and dihydrogen (H_2),[20–31] can be utilized as fuels of EBFCs. Thanks to substrate specificity and high catalytic efficiency under mild conditions (e.g., room temperature, around neutral pH), EBFCs are expected to be one of the next-generation energy conversion systems, comparable to conventional fuel cells, such as polymer electrolyte fuel cell;[32] however, the low power densities of EBFCs hinder technological applications.[1–4] The main factor limiting the performance of EBFCs has been reported to be relatively slow interfacial electron transfer between the enzyme and electrode.[1–4]

The first step to construct an EBFC is the immobilization of a redox enzyme onto a solid electrode for bioelectrocatalysis that couples the enzymatic and electrode processes;[1–4] however, for mediatorless direct electron transfer (DET)-type bioelectrocatalysis, the electrochemical

communication between the enzyme and electrode is mainly limited due to the long-distance electron transfer from the active center of the enzyme to the electrode surface, and when enzymes are adsorbed in random orientation on electrode surface, the apparent interfacial electron-transfer kinetics decrease.[1–4,33] In addition, details of the interaction between the enzyme and electrode remain to be elucidated, unlike the well understood interaction between the enzyme and its natural substrate.[1–4] Although some suitable redox mediators may assist electron transfer,[34,35] several drawbacks arise:[1–4,10,34,35] (a) the toxicity of the mediator, (b) leakage of the mediator, and (c) cell voltage loss to set up the driving force in the electron transfer between the enzyme and mediator. Therefore, multiple studies, such as creating novel electrode materials,[36–42] functionalizing electrode surface,[9,43–51] and protein engineering,[52–54] to improve DET-type bioelectrocatalysis have been reported.

H_2/O_2 biofuel cells wherein H_2 is oxidized by hydrogenase at the bioanode and O_2 is typically reduced by multi-copper oxidases (MCOs) at the biocathode are known as clean and highly efficient energy conversion devices that have attracted increasing attention for establishing a "hydrogen economy".[20–31]

Bilirubin oxidase from *Myrothecium verrucaria* (BOD, EC 1.3.3.5) is a member of the MCOs, which catalyzes a four-electron reduction of O_2 to water under mild conditions with low overpotentials. The active site of BOD contains four copper atoms, which can be divided into three classes according to their spectroscopic and magnetic properties:[56,57] type I (T1), type II (T2), and type III (T3) coppers. T2/T3 is responsible forO_2 reduction, and T1 is the electron-accepting site from a donor or electrode.[58,59] In our previous study, enhanced DET-type bioelectrocatalysis using BOD was accomplished at a negatively charged surface, constructed by modifying 4-aminobenzoic acid on a carbon electrode.[49] The electrostatic and π–π interactions between BOD and the modified electrode surface are responsible for the improvement in DET-type bioelectrocatalysis.[49]

Hydrogenase catalyzes the reversible reaction of H_2 oxidation and proton (H^+) reduction and can be classified according to the metal ion composition of their active sites into [NiFe], [FeFe], and [Fe] hydrogenases.[60–65] Among them, [NiFe] hydrogenases are the most widely investigated.[62,66–71] Membrane-bound [NiFe] hydrogenase from *Desulfovibrio Vulgaris* Miyazaki F (MBH) comprises a heterodimer with a total molecular mass of 91 kDa (α: 62.5 kDa and β: 28.8 kDa).[67] The larger subunit hosts the [NiFe] center while the smaller subunit contains three ion–sulfur (FeS) clusters called the proximal, medial, and distal clusters, relative to the [NiFe] center.[67] The distal FeS cluster has been reported to be responsible for the electronic communication between the enzyme and electrode.[67,71] From this viewpoint, it appears to be important for MBH to face the distal FeS toward the electrode surface to improve the performance of DET-type bioelectrocatalysis.[67] There are multiple reports focusing on the improvements of the DET-type bioelectrocatalytic performance of several [NiFe] hydrogenases with modified electrodes,[72–75] but not for MBH to the

best of our knowledge.

Other important issues for H_2/O_2 biofuel cells are the low-saturated concentrations of the gases in solution, the gas supply system, and risk of explosion.[29,31,76] Rotating disk electrodes (RDE) or stir bars are usually utilized to minimize the concentration depression near the electrode surface. These methods require external power to drive the RDEs or stir bars. More importantly, it may result in a biofuel cell that is too "fat" to improve the power density (power at a unit of surface area or volume). Recent findings have reported that MCOs[9,29,31,77–79] and several MBHs[76] could efficiently operate in a gas-diffusion system. In addition, a gas-diffusion system is useful for suppressing the oxidative inactivation that occurs at positive electrode potentials and competitively with the catalytic cycle, and is another important issue in hydrogenase applications.[76] On the other hand, to avoid the risk of explosion, the compartmentalization of fuel cells[20,21,23,25,27,31] and operation at low concentrations of $H_2$and/or O_2 [22,24,26,28–30] are frequently explored. The former requires sophisticated cell construction and the latter results in low power density.

In this study, we attempt to construct a safe H_2/air-breathing biofuel cell operating at room temperature with a high power density using BOD and MBH on the functionalized mesoporous carbon electrodes. This is the first attempt to fabricate a membrane- and mediatorless H_2/air-breathing biofuel at room temperature.

2. Experimental

2.1 Biocatalysts, materials, and reagents

BOD (EC 1.3.3.5) from *Myrothecium verrucaria* was donated by Amano Enzyme Inc. (Japan) (3.04 unit mg^{-1}) and used without further purification. O_2-sensitive MBH from *Desulfovibrio vulgaris* Miyazaki F was purified according to the literature.[80] Ketjen black EC300J (KB) was kindly donated by Lion Co. (Japan). Waterproof carbon cloth (WPCC; EC-CC1-060T) was purchased from Toyo Co. (Japan), and polytetrafluoroethylene fine power (PTFE, 6-J) was obtained from DuPont Mitsui Fluorochemicals (Japan). 4-Aminobenzoic acid (4-ABA), 4-aminobenzenesulfonic acid (4-ABS), methyl-4-aminobenzoate (MABA), 2-aminobenzoic acid (2-ABA), and *p*-phenylenediamine chloride (*p*-PDA) were purchased from Tokyo Chemical Industry Co. (Japan). All other chemicals used in this study were of analytical grade unless otherwise specified, and all solutions were prepared with distilled water.

2.2 Electrochemical measurement

Cyclic voltammetry and chronoamperometry were performed using an electrochemical

analyzer ALS 701 E with a glassy carbon (GC) electrode as a working electrode, Pt wire as a counter electrode, and an Ag|AgCl|KCl (sat.) electrode as a reference electrode. For a gas-diffusion-type bioelectrode, WPCC and Pt mesh were used as a working electrode and a counter electrode, respectively. All potentials were referenced against the reference electrode.

2.3 Preparation of functionalized biocathodes

The gas-diffusion-type biocathode was prepared according to a previously reported method.[31] In brief, 40 mg of KB powder was mixed with PTFE and homogenized in 3.5-mL 2-propanol for 3 min in ice to prepare a KB slurry (L = dm^3). The slurry (approximately 100 mL) was applied to one side of a WPCC sheet and dried at room temperature to prepare the KB-modified WPCC electrode (KB/WPCC, 0.95 cm^2). The functionalization of the KB/WPCC electrode was conducted by one-step electrochemical oxidation at 0.8 V in a 2-ABA solution (5 mM, 0.1 M KCl) for 40 s (M= mol dm^{-3}) wherein the amino group of 2-ABA was oxidized at the carbon electrode to form a N–C bond to immobilize 2-ABA.[49,81] The electrode was washed with distilled water and dried at room temperature. The 2-ABA-modified electrode is called 2-ABA/KB/WPCC. A 300-μL BOD solution (20 mg mL^{-1}, pH 7 phosphate buffer) was applied on the 2-ABA/KB/WPCC surface and dried for 2 h under reduced pressure at room temperature. The electrode is called BOD/2-ABA/KB/WPCC. As a control, BOD was adsorbed on pristine KB/WPCC, and the electrode is called BOD/KB/WPCC.

2.4 Adsorption of MBH on functionalized carbon surface

KB-modified GC electrode (KB/GCE) was prepared according to a previously described method.[49] In brief, 3 μL of a KB slurry (PTFE:KB=1:4, w/w) was dropped on a rotating disk GCE surface (diameter: 3 mm) and dried at room temperature. Amine-functionalized KB/GCE (amine/KB/GCE) was prepared by one-step electrochemical oxidation at 0.8 V in an aniline derivative solution (5 mM, 0.1 M KCl) for 40 s and washed with distilled water.[49,81] Subsequently, a 10-μL MBH solution (0.02 mM, pH 7.4 Tris-HCl) was applied on the KB/GCE or amine/KB/GCE and dried at room temperature for 2 h. The electrode was washed with a McIlvaine buffer (pH 5) and used for electrochemical measurements.

For the gas-diffusion system, KB/WPCC and *p*-PDA/KB/WPCC were prepared with the methods similar to those described above. A 250-μL MBH solution (0.02 mM, pH 7.4 Tris-HCl) was applied on KB/WPCC or *p*-PDA/KB/WPCC surface and dried for 2 h under reduced pressure at room temperature.

2.5 DET-type biofuel cell

A DET-type membraneless one-compartment biofuel cell was constructed combining the gas-diffusion biocathode and bioanode, as shown in Fig.1. The projected surface area of the cathode and anode was adjusted to be 0.95 cm^2 by covering the electrodes with a cell vessel, and the total volume of the electrolysis solution in the vessel was 2.0 mL. Titanium mesh was used as a current collector. The cathode and anode of the cell were connected through a variable resistor (Type 2786 Decade Resistance Box, Yokogawa Hokushin Electric, Japan). The cell voltage and potentials of the cathode and anode were measured with an electrometer (HE-106, Hokuto Denko, Japan) at the given values of resistance in the range from 100 kΩ to 10 Ω.[5,6,9] The current and power densities were calculated based on the projected surface area of the electrodes. Measurements were performed in 1.5 M citrate buffer (pH 5.0) at room temperature (25 ± 2 °C).

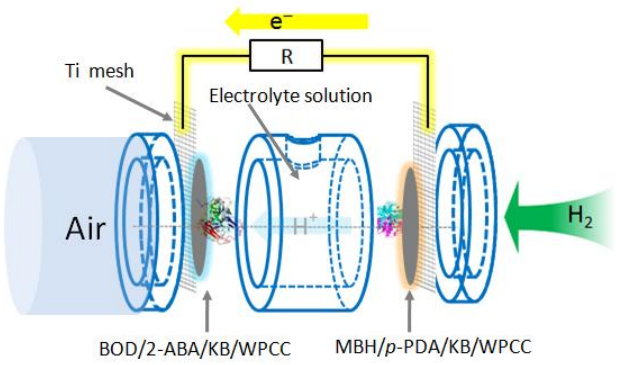

Fig. 1

Schematic illustration of a gas-diffusion type H_2/air-breathing biofuel cell.

3. Results and discussion

3.1 Optimization of gas-diffusion biocathode with a negatively charged surface

Fig. 2(A) shows cyclic voltammograms (CVs) of O_2 reduction at a scan rate (v) of 5 mV s^{-1} with BOD/2-ABA/KB/WPCC (solid line) and BOD/KB/WPCC (dash line) in a quiescent citrate buffer (pH 5, 1.5 M) under an atmosphere of air or argon (dotted line) (25 ± 2 °C). The O_2 was passively supplied from the air to the electrode. The ratio of PTFE:KB was set to be 1:1according to a previously described method.[31] The onset potential was approximately 0.6 V at both BOD-adsorbed electrodes. As shown in Fig. 2(A), compared to BOD/KB/WPCC, a much sharper sigmoidal curve was observed at BOD/2-ABA/KB/WPCC. This means kinetic improvement in DET-type bioelectrocatalysis using BOD at the negatively charged 2-ABA-modified KB

surface.[9,31,49] The electron-accepting site (T1) in BOD is located in the positively charged region of the protein surface.[82] Thus, it can be considered that the electrostatic interaction between the positively charged T1 of BOD and the negatively charged electrode surface produced by the carboxy substituent of 2-ABA induces a productive orientation for DET-type bioelectrocatalysis. In addition, the π–π interaction between BOD and the benzene ring of 2-ABA may assist the productive orientation[49] that improves the kinetic performance in the interfacial electron transfer.

Fig. 3 (B) shows chronoamperograms (CAs) of BOD/KB/WPCC and BOD/2-ABA/KB/WPCC at 0 V. A steady-state catalytic current density was recorded as 7.0 ± 0.3 mA cm^{-2} at BOD/KB/WPCC. At BOD/2-ABA/KB/WPCC, the catalytic current density reached about 30 mA cm^{-2} until about 5 s, but decreased quickly down to 8.0 ± 0.1 mA cm^{-2} at 60 s. Since similar behavior was observed in repeated experiments with the same electrode (data not shown), the current decrease after 5 s at BOD/2-ABA/KB/WPCC is not ascribed to a decrease in the enzyme activity but to some change in the bio-three-phase circumstance around the electrode surface during the bioelectrocatalysis at high current densities.[31,77]

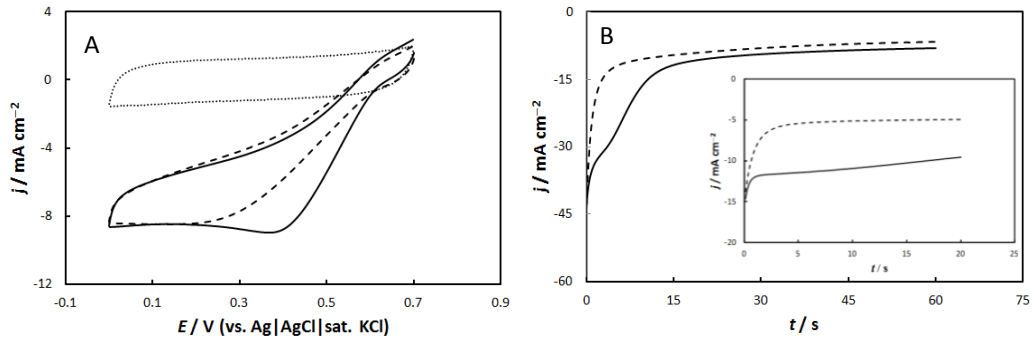

Fig. 2

(A) CVs of BOD/KB/WPCC (broken line) and BOD/2-ABA/KB/WPCC (solid line) at v = 5 mV s^{-1}.

(B) CAs of BOD/KB/WPCC (broken line) and BOD/2-ABA/KB/WPCC (solid line) at 0 V. The inset shows the CAs at 0.4 V. Measurements were carried out in 1.5 M citrate buffer (pH 5.0) at room temperature (25 ± 2°C) under quiescent and air atmospheric conditions. The ratio of PTFE to KB was 1:1. The dotted line in panel A shows the CV of BOD/KB/WPCC under argon atmospheric conditions.

In order to check the effect of time on the current density, CAs were measured at 0.4 V. As shown in the inset of Fig. 2 (B), relatively stable steady-state catalytic current was recorded at both of the electrodes and the current density at 20 s was 8.9 ± 0.8 and 5.3 ± 0.3 mA cm^{-2} at BOD/2-ABA/KB/WPCC and BOD/KB/WPCC, respectively. The data verify the significance of the 2-ABAmodification at moderate current densities.

On the other hand, the hydrophobic property of the electrode surface is an important factor for improving the performance of gas-diffusion biocathodes.[31,77] Although the optimum ratio of PTFE to KB was reported to be 2:3 for copper efflux oxidase[77] and 1:1 for BOD[31] in a gas-diffusion system, we re-optimized the ratio of PTFE to KB for BOD/2-ABA/KB/WPCC.

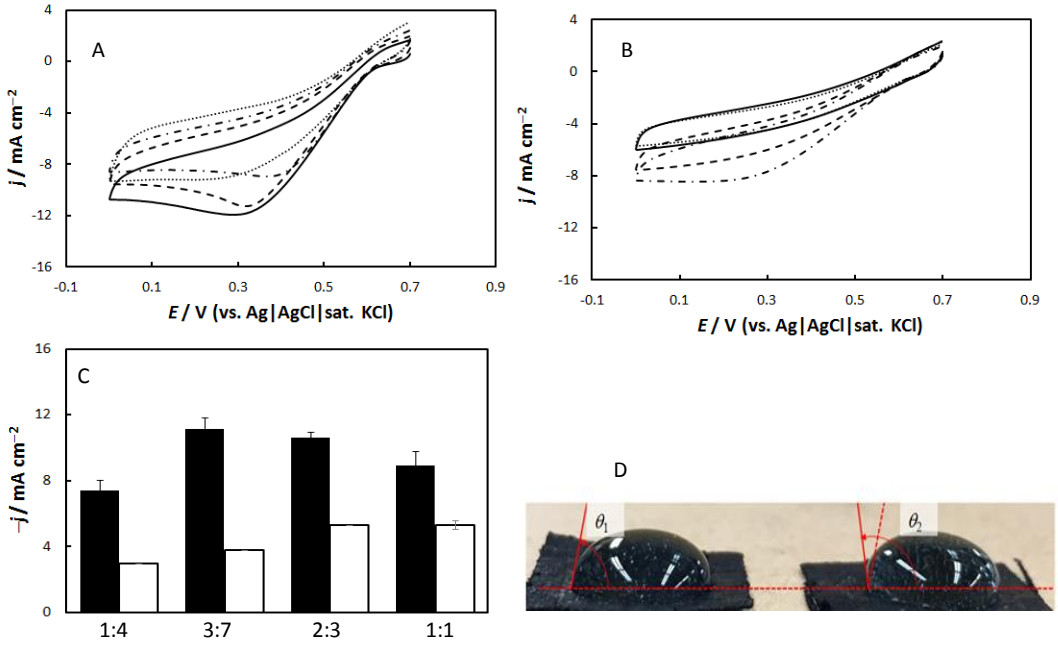

Fig. 3

CVs of the catalytic O_2 reduction at (A) BOD/2-ABA/KB/WPCC and (B) BOD/KB/WPCC at ratios of PTFE to KB of (dotted line) 1:4, (solid line)3:7, (broken line) 2:3 and (dashed-dotted line) 1:1. Measurements were carried out in 1.5 M citrate buffer (pH 5.0) at room temperature (25 ±2°C) under quiescent and air atmospheric conditions at v= 5 mV s^{-1}.

(C) Effects of the ratio of PTFE to KB on the catalytic current densities at BOD/2-ABA/KB/WPCC (filled bar) and BOD/KB/WPCC (unfilled bar).The current densities were obtained at 0.4 V after 20 s. Measurements were carried out in 1.5 M citrate buffer (pH 5.0) at room temperature (25 ± 2°C) under quiescent and air atmospheric conditions.

(D) Photographs to show the contact angle of the enzyme solution on KB/WPCC (θ_1) and 2-ABA/KB/WPCC (θ_2). The ratio of PTFE to KB was 1:1 in this experiment.

CVs of the O_2 reduction were recorded with BOD/2-ABA/KB/WPCC and BOD/KB/WPCC at various weight ratios of PTFE to KB in a range from 1:4 to 1:1 (Fig. 3). The ratio of 3:7 was found to be better for BOD/2-ABA/KB/WPCC. The effects of the ratio of PTFE to KB were also examined by chronoamperometry. The result is summarized in Fig. 3(C). At

BOD/2-ABA/KB/WPCC, the best ratio was 3:7 and the catalytic current density reached 11.2 ± 0.7 mA cm^{-2} at 0.4 V, while the best ratio at BOD/KB/WPCC was 5:5, in accordance with a previous report.[31] We hypothesize that modification with 2-ABA increased the hydrophobicity of the KB-modified electrode surface. The hydrophobic properties of KB/WPCC and 2-ABA/KB/WPCC surfaces were roughly estimated by measuring the contact angles of the enzyme solution on the electrode surface. As shown in Fig. 3 (D), a larger contact angle was observed on the 2-ABA-modified KB/WPCC surface compared to a pristine KB/WPCC surface. These results support our hypothesis. In this study, we set the weight ratio of PTFE to KB as 3:7 for the gas-diffusion system used in further studies.

3.2 DET-type bioelectrocatalysis of MBH at amine-modified electrode

Fig. 4 shows rotating disk CVs of H_2 oxidation (in the potential region from −0.45 to +0.2 V) and H^+ reduction(in the potential region from −0.5 to −0.7 V) catalyzed by MBH on *p*-PDA/KB/GCE, KB/GCE and 4-ABS/KB/GCE. No catalytic current was observed in the absence of MBH. The zero-current potential in the catalytic waves was −0.49V, which corresponds to the formal potential of the $H_2/2H^+$ redox couple at pH 5.0 due to the reversible and bi-directional catalytic properties of MBH.[60]

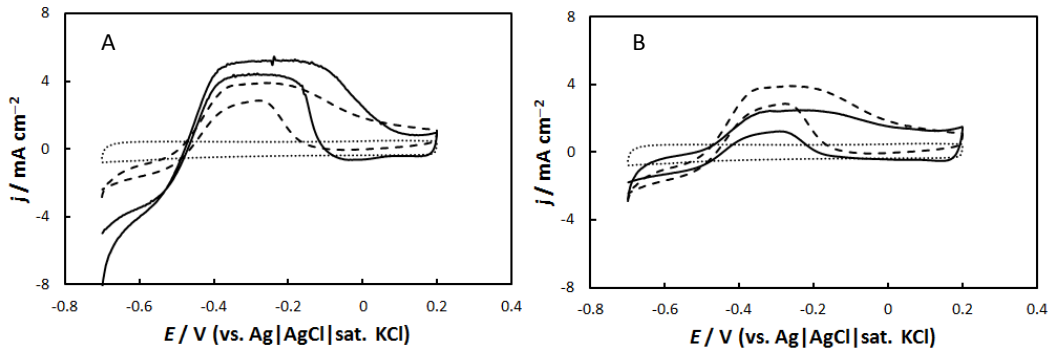

Fig. 4

Rotating disk CVs at (A) MBH/*p*-PDA/KB/GCE, (B) MBH/4-ABS/KB/GC. All measurements were carried out in an H_2-saturated McIlvaine buffer (pH 5.0, 40 °C) at ω = 2000 rpm and v = 20 mV s^{-1}. The dotted lines and broken lines show the CV of MBH/KB/WPCC and KB/WPCC taken under the same condition.

Interestingly, the H^+-reduction and H_2-oxidation currents increased with modification using *p*-PDA on KB/GCE, but decreased with modification using 4-ABS, as compared to unmodified KB/GCE. *p*-PDA/KB/GCE is expected to produce a positively charged surface, while 4-ABS/KB/GCE produces a negatively charged surface, according to our previous study.[49,81] On the

other hand, as shown in Fig. 5, the distal FeS cluster (that works as the electron-donating site for the H_2 oxidation and the electron-accepting site for the H^+ reduction) is located in the negatively charged region of the protein surface. Therefore, the attractive electrostatic interaction between the negatively charged FeS cluster region and the positively charged electrode surface seems to induce MBH to face the distal FeS to the electrode surface. In contrast, at a negatively charged electrode surface produced by modification with 4-ABS, a repulsive electrostatic interaction occurs with the distal FeS cluster region and leads to orientations detrimental for DET-type bioelectrocatalysis of MBH.[49]

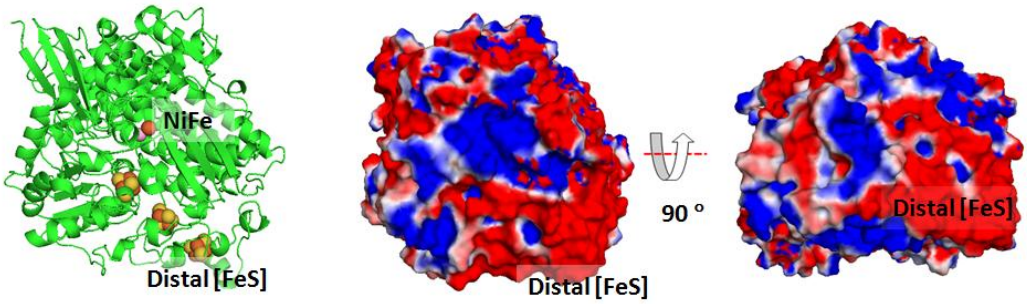

Fig. 5

Three-dimensional structures and the surface electrostatic potential distributions of MBH (PDB code: 1H2A). The colour of blue and red represent positive and negative surface electrostatic potential regions were generated using PyMOL in pH 7 (25 °C), respectively.

Further experimental evidence was obtained in favor of the electrostatic interaction between MBH and modified electrode surfaces. The steady-stateH_2-oxidation current was measured at –0.3 V with MBH-adsorbed electrodes that were modified with several aniline derivatives. The results are summarized in Fig. 6A. Modification with non-charged MABA caused practically no change in the current density compared to pristine KB/GCE. Modification with 4-ABA slightly decreased the current density due to the electrostatic repulsion between the partially deprotonated carboxy substituent of 4-ABA and the distal FeS cluster region.

We also tried to weaken the electrostatic attractive interaction between the positively charged *p*-PDA/KB/GCE and the distal FeS cluster region by increasing the ionic strength (and then by screening the ionic atmosphere). As shown in Fig. 6B, the catalytic density decreased to the level of MBH/KB/GCE when MBH was adsorbed on *p*-PDA/KB/GCE in the presence of 1 M KCl. All these results support our hypothesis.

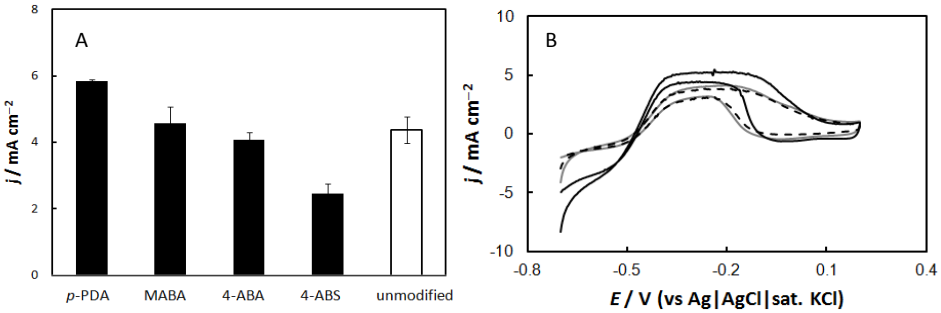

Fig. 6

(A) Comparison of the limiting current density of the H_2 oxidation (at −0.3 V) at pristine and modified KB/GCEs. The abbreviated name of the amines used for the modification are given in the below.

(B) CVs at MBH/*p*-PDA/KB/GCEs prepared in the absence (black solid line) and presence (gray solid line) of 1 M KCl. CV at MBH/KB/GCE (broken line) is shown here as a comparison. All measurements were carried out in an H_2-saturated McIlvaine (pH 5.0, 40 °C) at ω = 2000 rpm and v = 20 mV s^{-1}.

The catalytic turnover of MBH is sufficiently fast and the saturated concentration of H_2 is low. Therefore, the mass transport of H_2 strongly influences the bioelectrocatalytic density.[69] In order to adequately assess the effect of *p*-PDA modification on the catalytic activity of MBH, rotating disk voltammetry was carried out. The observed density of steady-state limiting catalytic current density (j) at a rotating disk electrode can be given by Koutecký–Levich equation as

$$\frac{1}{j} = \frac{1}{j_{\mathrm{d}}} + \frac{1}{j_{\mathrm{cat}}}, \tag{1}$$

$$j_{\mathrm{d}} = 0.62nFD^{2/3}v^{-1/6}c\omega^{1/2}, \tag{2}$$

$$j_{\mathrm{cat}} = (n/n_{\mathrm{E}})Fk_{\mathrm{cat}}\Gamma_{\mathrm{e}}, \tag{3}$$

where j_{d} and j_{cat} are the diffusion-limiting and catalytic limiting current densities, respectively. Additionally, n is the number of electrons for H_2 (= 2); F is Faraday's constant; D is the diffusion constant of H_2 in a buffer; v is the kinematic viscosity of the buffer (0.0066 cm^2 s^{-1} in 40 °C);[83] c is the bulk concentration of H_2 (0.74 mM in H_2-saturated solution at 40 °C and 1 atm);[84] k_{cat} is the catalytic rate constant; n_{E} is the number of electrons of for enzyme in the electron-donating FeS site (=1 in this case); and Γ_{e} is the surface concentration of effective enzymes oriented conveniently for DET-type bioelectrocatalysis on the electrode. The steady-state limiting current of H_2oxidation was measured at various values of the rotating speed (ω) with MBH/*p*-PDA/KB/GCE and MBH/KB/GCE (Fig. 7A). The Levich plot is shown in Fig. 7B. The data were analyzed by Gnuplot©

5.0 based on Eq. (1). The refined values of j_{cat} are 20 ± 2 mA cm^{-2} at *p*-PDA-KB/GCE and 8.4 ± 0.4 mA cm^{-2} at unmodified KB/GCE with a *D* of (7 ± 1) × 10^{-5} cm^2 s^{-1}. The $k_{cat}\Gamma_e$ are calculated as (1.0 ± 0.1) × 10^{-7} mol cm^{-2} s^{-1} for MBH/*p*-PDA/KB/GCE, which is 2.5 times larger than that of MBH/KB/GCE ((4.3 ± 0.2) × 10^{-8} mol cm^{-2} s^{-1}). Thus, we conclude that modification with *p*-PDA to produce a positive charge on the KB electrode surface increases Γ_e of MBH.

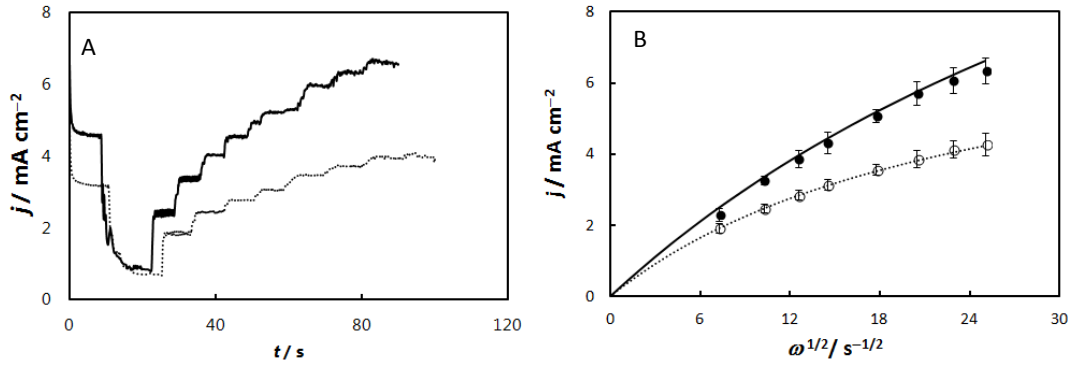

Fig.7

(A) As of MBH/*p*-PDA/KB/GCE (red line) and MBH/KB/GCE (black line) for the H_2 oxidation at –0.3 V and 40 °C, ω = 500, 1000, 1500, 2000, 2500, 3000, 4000, 5000, 6000 rpm in turn.

(B) Levich plots of ω dependence of the steady-state H_2 oxidation current densities at the MBH/*p*-PDA/KB/GCE (closed circle) and MBH/KB/GCE (open circle). The lines were evaluated by a nonlinear regression analysis with Eq. (1).

Similar analysis was also carried out for H^+ reduction at –0.7 V (data not shown); however, H^+ reduction was almost independent of ω. The limited current densities reached –5.8 ± 0.4 mA cm^{-2} at MBH/*p*-PDA/KB/GCE and are about 1.5 times larger than that at MBH/KB/GCE (–3.8 ± 0.3 mA cm^{-2}). The activity ratio is close but somewhat smaller than that ofH_2 oxidation. At increased current densities of H^+ reduction, the dissociation kinetics of the weak acid (as a buffer component) may affect the overall kinetics (and decrease the current density).[85–87] In addition, the H^+-reduction catalytic activity of MBH may be inhibited by H_2 generated near the electrode surface.[60, 88–90]

On the other hand, as shown in Fig. 4, the H_2-oxidation current at the MBH-adsorbed electrodes decrease to zero at potentials over −0.2 V. This is ascribed to oxidative inactivation (formation of Ni-B) of MBH at high potentials.[31,65] In this study, a gas-diffusion system was employed to protect from oxidative inactivation according to the method described in our previous papers,[31,76] Fig. 8 shows CVs of MBH/*p*-PDA/KB/WPCC and MBH/KB/WPCC in the gas-diffusion system. Note here that the ratio of PTFE to KB was set as 3:7 according to optimization of the *p*-PDA/KB/WPCC-based gas-diffusion system as described above. Clear H_2-oxidation waves were observed at both MBH-adsorbed electrodes. The current density (at 0.2 V) for H_2 oxidation reached

15.8 mA cm^{-2} at MBH/*p*-PDA/KB/WPCC and 5.8 mA cm^{-2} at MBH/KB/WPCC. These values are much larger than those at the corresponding GCEs (MBH/*p*-PDA/KB/GCE and MBH/KB/GCE), respectively. In addition, the effects of oxidative inhibition at high potentials were successfully suppressed.[76] These results support the conclusion that H_2 gas is passively supplied at high speeds to the electrodes from the gas phase.

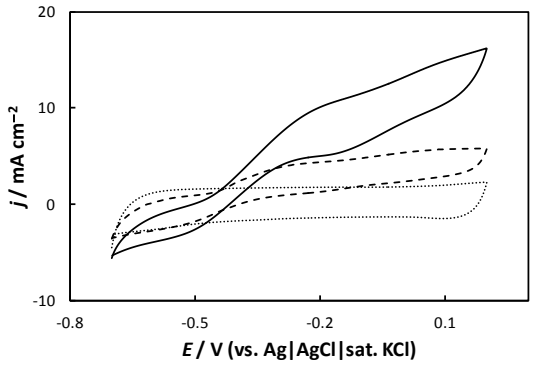

Fig. 8

CVs of MBH/*p*-PDA/KB/WPCC (solid line), MBH/KB/WPCC (broken line) and KB/WPCC (dotted line) at v = 10 mV s^{-1}. Measurements were carried out in 1.5 M citrate buffer (pH 5.0) at room temperature (25 ± 2 °C) under quiescent and H_2-atmospheric conditions. The ratio of PTFE to KB was 3:7.

3.3 DET-type H_2/air biofuel cell

Finally, a dual gas-diffusion-type H_2/air-breathing biofuel cell was fabricated by combining BOD/2-ABA/KB/WPCC as a biocathode and MBH/*p*-PDA/KB/WPCC as a bioanode, as shown in Fig. 1. In most H_2/O_2 biofuel cells in the literature, pure O_2 and H_2 gasses are separately pumped to the biocathode and bioanode, respectively,[20,21,23,25,27,31] and the cells are operated at high temperatures[25, 28,29,31] to improve their performance; however, such situations risk explosion and are not convenient for practical applications. Therefore, in this study, only H_2 gas was supplied to the bioanode, while the biocathode was open to air at room temperature (25 ± 2 °C). The biofuel cell was operated in a 1.5 M citrate buffer (pH 5.0) under passive and quiescent conditions. The cell voltage, cathode potential, and anode potential were measured at (quasi)-steady state and at given values of resistance. The values were decreased stepwise and the potentials were recorded about 15 s after the change in the resistance.

Fig. 9(A) summarizes the results. The open circuit voltage was 1.12 ± 0.03V, close to the standard driving force of an ideal H_2/O_2 cell (1.23 V at 25 °C).[20,31] The current density increased with a decrease in the voltage, and the maximum current density reached about 11 ± 1 mA cm^{-2};

however, the current density decreases suddenly after reaching the maximum. The decrease may be caused by oxidative inactivation of MBH due to fast H_2-comsumption near the electrode surface at increased current densities and at positive potentials.[31] The power density is given in Fig. 9 (B) and the maximum power density reached 6.1 ± 0.4 mW cm^{-2} at a 0.72 V cell voltage, much higher than that of other H_2 biofuel cells in the literature.[20–30]

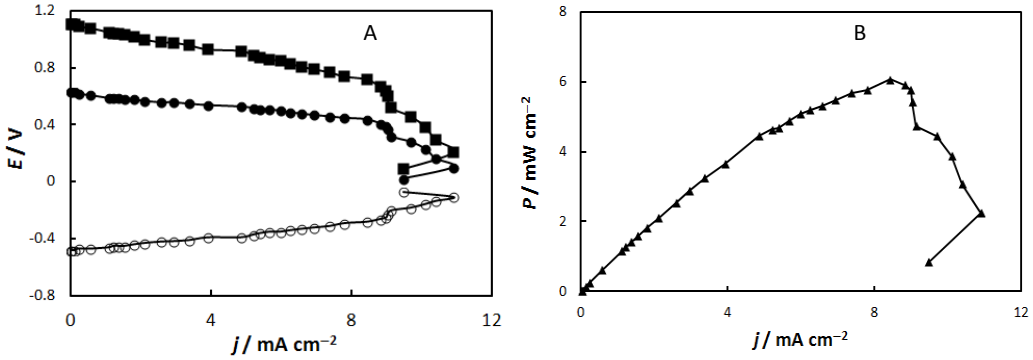

Fig.9

(A) Polarization curves of the biofuel cell. The cell voltage (closed square) and the cathode (closed circle) and anode potentials (open circle) (vs. Ag|AgCl|KCl (sat.)) are plotted as functions of the current density (*j*). The measurements were performed in 1.5 M citrate buffer (pH 5.0) under quiescent conditions. H_2 gas (1 atm) was supplied to the outside of the bioanode, while the biocathode was opened to air atmosphere (in a passive mode) at room temperature (25 ± 2 °C).

(B) The power density (*P*) as a function of the current density (*j*) of the biofuel cell.

4. Conclusions

To the best of our knowledge, this is the first report of a membrane- and mediatorless dual gas-diffusion-type H_2/air-breathing biofuel cell. The orientation of BOD and MBH was successfully controlled by the electrostatic attractive-interaction between the enzymes and electrodes. Aniline derivatives were utilized to control the surface charge in which the amino group of the aniline derivatives was electrochemically oxidized at the carbon electrodes to form N-C bonds to immobilize the derivatives. For BOD with positively charged electron-accepting sites (T1), 2-ABA was modified on KB-modified electrodes and the deprotonated carboxy group of 2-ABA is responsible for the negative charge on the electrode surface. In contrast, for MBH with negatively charged electron-donating sites (distal FeS), *p*-PDA was modified on KB-modified electrodes and the protonated amino group of *p*-PDA is responsible for the positive charge of the electrode surface at pH 5.0.

A gas-diffusion system was employed using KB/WPCC and the hydrophobicity required for gas permeation through the electrode was controlled by adjusting the ratio of PTFE:KB. The combination of BOD/2-ABA/KB/WPCC as a biocathode and MBH/*p*-PDA/KB/WPCC as a bioanode realizes a dual gas-diffusion membrane- and mediatorless H_2/air-breathing biofuel cell. The maximum power density reached 6.1 mW cm^{-2} at a 0.72 V cell voltage at room temperature (25 ± 2°C) and under quiescent conditions. The performance is comparable to that of a dual gas-diffusion type virtual biofuel cell at 40 °C with pure H_2 and O_2 gases (8.4 mW cm^{-2}),[31] and is better than those of real biofuel cells in the literature (0.56 mW cm^{-2} at 25 °C with 78% H_2 + 22% air under bubbling,[26] 0.72 mW cm^{-2} at 45 °C with pure H_2 and air under gas-diffusion,[29] 1.5 mW cm^{-2} at 60 °C with pure H_2 and O_2 gases and with a membrane as separator[27]). The air-breathing BOD biocathode with improved performance can be utilized for a variety of biofuel cells with fuels other than H_2.

5. References

1 J.A. Cracknell, K.A. Vincent, F.A. Armstrong, Enzymes as working or inspirational electrocatalysts for fuel cells and electrolysis, Chem. Rev. 108 (2008) 2439–2461.

2 D. Leech, P. Kavanagh, W. Schuhmann, Enzymatic fuel cells: Recent progress, Electrochim. Acta 84 (2012) 223–234.

3 R.A.S. Luz, A.R. Pereira, J.C.P. de Souza, F.C.P.F. Sales, F.N. Crespilho, Enzyme biofuel cells: thermodynamics, kinetics and challenges in applicability, ChemElectroChem 1 (2014) 1751–1777.

4 M. Rasmussen, S. Abdellaoui, S.D. Minteer, Enzymatic biofuel cells: 30 years of critical advancements, Biosens. Bioelectron. 76 (2016) 91–102.

5 Y. Kamitaka, S. Tsujimura, N. Seyoyama, T. Kajino, K. Kano, Fructose/dioxygen biofuel cell based on direct electron transfer-type bioelectrocatalysis, Phys. Chem. Chem. Phys. 9 (2007) 1793–1801.

6 H. Sakai, T. Nakagawa, Y. Tokita, T. Hatazawa, T. Ikeda, S. Tsujimura, K. Kano, A high-power glucose/oxygen biofuel cell operating under quiescent conditions, Energy Environ. Sci. 2 (2009) 133–138.

7 B. Reuillard, A. Le Goff, C. Agnès, M. Holzinger, A. Zebda, C Gondran, S. Cosnier, High power enzymatic biofuel cell based on naphthoquinone-mediated oxidation of glucose by

glucose oxidase in a carbon nanotube 3D matrix, Phys. Chem. Chem. Phys. 15 (2013) 4892–4896.

8 L. Stoica, N. Dimcheva, Y. Ackermann,K. Karnicka, D.A. Guschin, P.J. Kulesza, J. Rogalski, D. Haltrich, R. Ludwig,L. Gorton, W. Schuhmann, Membrane-less Biofuel Cell Based on Cellobiose Dehydrogenase (Anode)/Laccase (Cathode) Wired via Specific Os - Redox Polymers, Fuel cell 9 (2009) 53–62.

9 K. So, Y. Kawai, Y. Hamano, Y. Kitazumi, O. Shirai, O. Hibi, J. Ogawa, K. Kano, Improvement of a direct electron transfer-type fructose/dioxygen biofuel cell with a substrate-modified biocathode, Phys. Chem. Chem. Phys. 16 (2014) 4823–4829.

10 S. Fujita, S.Yamanoi, K. Murata, H. Mita, T. Samukawa, T. Nakagawa, H. Saikai, Y. Tokita, A repeatedly refuelable mediated biofuel cell based on a hierarchical porous carbon electrode, Sci. Rep. 4 (2014) 4937.

11 M. Karaśkiewicz, E. Nazaruk, K. Żelechowska, J.F. Biernat, J. Rogalski, R. Bilewicz, Fully enzymatic mediatorless fuel cell with efficient naphthylated carbon nanotube–laccase composite cathodes, Electrochem. Commun. 20 (2012) 124–127.

12 B. Reuillard, C. Abreu, N. Lalaoui, A. Le Goff, M. Holzinger, O. Ondel, F. Buret, S. Cosnier, One-year stability for a glucose/oxygen biofuel cell combined with pH reactivation of the laccase/carbon nanotube biocathode, Bioelectrochemistry 106 (2015) 73–76.

13 Y. Zhang, M.A. Arugula, S.T. Williams, S.D. Minteer, A.L. Simonian, Layer-by-Layer Assembly of Carbon Nanotubes Modified with Invertase/Glucose Dehydrogenase Cascade for Sucrose/O_2 Biofuel Cell, J. Electrochem. Soc. 163 (2016) F449–F454.

14 S.A. Neto, E.L. Suda, S. Xu, M.T. Meredith, A.R. De Andrade, S.D. Minteer, Direct electron transfer-based bioanodes for ethanol biofuel cells using PQQ-dependent alcohol and aldehyde dehydrogenases, Electrochim. Acta 87 (2013) 323–329.

15 Y.M. Yan, I. Baravik, R. Tel-Vered, I. Willner, An Ethanol/O2 Biofuel Cell Based on an Electropolymerized Bilirubin Oxidase/Pt Nanoparticle Bioelectrocatalytic O_2-Reduction Cathode, Adv. Materal. 21 (2009) 4275–4279.

16 L. Deng, L. Shang, D. Wen, J. Zhai, S. Dong, A membraneless biofuel cell powered by ethanol and alcoholic beverage, Biosens. Bioelectron. 26 (2010) 70–73.

17 S.A. Neto, R.D. Milton, D.P. Hickey, A.R. De Andrade, S.D. Minteer, Membraneless enzymatic ethanol/O_2 fuel cell: Transitioning from an air-breathing Pt-based cathode to a bilirubin oxidase-based biocathode, J. Power Sources 324 (2016) 208–214.

18 P. Gai, Y. Ji, Y. Chen, C. Zhu, J. Zhang, J.J. Zhu, A nitrogen-doped graphene/gold nanoparticle/formate dehydrogenase bioanode for high power output membrane-less formic acid/O_2 biofuel cells, Analyst 140 (2015) 1822–1826.

19 K. Sakai, Y. Kitazumi, O. Shirai, K. Kano, Bioelectrocatalytic formate oxidation and carbon dioxide reduction at high current density and low overpotential with tungsten-containing formate dehydrogenase and mediators, Electrochem. Commun. 65 (2016) 31–34.

20 S. Tsujimura, M. Fujita, H. Tatsumi, K. Kano, T. Ikeda, Bioelectrocatalysis-based dihydrogen/dioxygen fuel cell operating at physiological pH, Phys. Chem. Chem. Phys. 3 (2001) 1331–1335.

21 M.R. Tarasevich, V.A. Bogdanovskaya, N.M. Zagudaeva, A.V Kapustin, Composite materials for direct bioelectrocatalysis of the hydrogen and oxygen reactions in biofuel cells, Russ. J. Electrochem. 38 (2002) 335.

22 K.A. Vincent, J.A.Cracknell, J.R. Clark, M. Ludwig, O. Lenz, B. Friedrich, F.A. Armstrong, Electricity from low-level H_2 in still air–an ultimate test for an oxygen tolerant hydrogenase, Chem. Commun. 48 (2006) 5033–5035.

23 A.F. Wait, A. Parkin, G.M. Morley, L. dos Santos, F.A. Armstrong, Characteristics of enzyme-based hydrogen fuel cells using an oxygen-tolerant hydrogenase as the anodic catalyst, J. Phys. Chem. C 114 (2010) 12003–12009.

24 S. Krishnan, F.A. Armstrong, Order-of-magnitude enhancement of an enzymatic hydrogen-air fuel cell based on pyrenyl carbon nanostructures, Chem. Sci. 3 (2012) 1015–1023.

25 A. Ciaccafava, A. de Poulpiquet, V. Techer, M.T. Giudici-Orticoni, S. Tingry, C. Innocent, E. Lojou, An innovative powerful and mediatorless H_2/O_2 biofuel cell based on an outstanding bioanode, Electrochem. Commun. 23 (2012) 25–28.

26 L. Xu, F.A. Armstrong, Optimizing the power of enzyme-based membrane-less hydrogen fuel cells for hydrogen-rich H_2–air mixtures, Energy Environ. Sci. 6 (2013) 2166–2171.

27 A. de Poulpiquet, A. Ciaccafava, R. Gadiou, S.Gounel, M.T. Giudici-Orticoni, N. Mano, E. Lojou, Design of a H_2/O_2 biofuel cell based on thermostable enzymes, Electrochem. Commun. 42 (2014) 72–74.

28 N. Plumeré, O. Rüdiger, A.A. Oughli, R. Williams, J. Vivekananthan, S. Pöller, W. Schuhmann, W. Lubitz, A redox hydrogel protects hydrogenase from high-potential deactivation and oxygen damage, Nat. Chem. 6 (2014) 822–827.

29 N. Lalaoui, A. dePoulpiquet, R. Haddad, A. Le Goff, M.Holzinger, S. Gounel, M. Mermoux, P. Infossi, N. Mano, E. Lojou, S. Cosnier, A membraneless air-breathing hydrogen biofuel cell based on direct wiring of thermostable enzymes on carbon nanotube electrodes, Chem. Commun. 51 (2015) 7447–7450.

30 Y. Wang, T.F. Esterle, F.A. Armstrong, Electrocatalysis by H2–O2 membrane-free fuel cell enzymes in aqueous microenvironments confined by an ionic liquid, RSC Advances 6 (2016) 44129–44134.

31 K. So, Y. Kitazumi, O. Shirai, K. Nishikawa, Y. Higuchi, K. Kano, Direct electron transfer-type dual gas diffusion H_2/O_2 biofuel cells, J. Mater. Chem. A 4 (2016) 8742–8749.

32 X. Cheng, Z. Shi, N. Glass, L. Zhang, J. Zhang, D. Song, Z.-S. Liu, H. Wang, J. Shen, A review of PEM hydrogen fuel cell contamination: Impacts, mechanisms, and mitigation, J. Power Sources 165 (2007) 739–756.

33 C. Léger, P. Bertrand, Direct electrochemistry of redox enzymes as a tool for mechanistic studies. Chem. Rev. 108 (2008) 2379–2438.

34 K. Kano, T. Ikeda, Fundamentals and Practices of Mediated Bioelectrocatalysis, Anal. Sci., 16 (2000) 1013–1021.

35 T. Ikeda, K. Kano, An electrochemical approach to the studies of biological redox reactions and their applications to biosensors, bioreactors, and biofuel cells, J. Biosci. Bioeng. 92 (2001) 9–18.

36 S.Tsujimura, Y. Miura, K. Kano, CueO-immobilized porous carbon electrode exhibiting improved performance of electrochemical reduction of dioxygen to water, Electrochim. Acta 53 (2008) 5716–5720.

37 K. Murata, K. Kajiya, N. Nakamura, H. Ohno, Direct electrochemistry of bilirubin oxidase on three-dimensional gold nanoparticle electrodes and its application in a biofuel cell, Energy Environ. Sci. 2 (2009) 1280–1285.

38 T. Gu, J. Wang, H. Xia, S. Wang, X. Yu, Direct electrochemistry and electrocatalysis of horseradish peroxidase immobilized in a DNA/chitosan-Fe_3O_4 magnetic nanoparticle bio-complex film, Materials 7 (2014) 1069–1083.

39 V. Krikstolaityte, A. Barrantes, A. Ramanavicius, T. Arnebrant, S. Shleev, T. Ruzgas, Bioelectrocatalytic reduction of oxygen at gold nanoparticles modified with laccase, Bioelectrochemistry 95 (2014) 1–6.

40 M. Zhao, Y. Gao, J. Sun, F. Gao, Mediatorless glucose biosensor and direct electron transfer type glucose/air biofuel cell enabled with carbon nanodots, Anal. Chem. 87 (2015) 2615–2622.

41 G. Sanzó, C. Tortolini, R. Antiochia, G. Favero, F. Mazzei, Development of Carbon-Based Nano-Composite Materials for Direct Electron Transfer Based Biosensors, J. Nanosci. Nanotechnol. 15 (2015) 3423–3428.

42 K. So, M. Onizuka, T. Komukai, Y. Kitazumi, O. Shirai, K. Kano, Significance of the Length of Carbon Nanotubes on the Bioelectrocatalytic Activity of Bilirubin Oxidase for Dioxygen Reduction, Electrochem. Acta 192 (2016) 133–138.

43 C.F. Blanford, R.S. Heath, F.A. Armstrong, A stable electrode for high-potential, electrocatalytic O2 reduction based on rational attachment of a blue copper oxidase to a graphite surface, Chem. Commun. 17 (2007) 1710–1712.

44 F. Tasca, W. Harreither, R. Ludwig, J.J. Gooding, L. Gorton, Cellobiose dehydrogenase aryl diazonium modified single walled carbon nanotubes: enhanced direct electron transfer through a positively charged surface, Anal. Chem. 83 (2011) 3042–3049.

45 N. Lalaoui, A. Le Goff, M. Holzinger, S. Cosnier, Fully Oriented Bilirubin Oxidase on Porphyrin-Functionalized Carbon Nanotube Electrodes for Electrocatalytic Oxygen Reduction, Chem- Eur. J. 21 (2015) 16868–16873.

46 P. Olejnik, B. Palys, A. Kowalczyk , A.M. Nowicka, Orientation of laccase on charged surfaces. Mediatorless oxygen reduction on amino-and carboxyl-ended ethylphenyl groups, J. Phys. Chem. C 116 (2012) 25911–25918.

47 F. Giroud, S.D. Minteer, Anthracene-modified pyrenes immobilized on carbon nanotubes for direct electroreduction of O_2 by laccase, Electrochem. Commun. 34 (2013) 157–160.

48 L. Peng, T.Utesch, A.Yarman, J.-H.Jeoung, S. Steinborn, H. Dobbek, M.A. Mroginski, J. Tanne, U. Wollenberger, F.W. Scheller, Surface-Tuned Electron Transfer and Electrocatalysis of Hexameric Tyrosine-Coordinated Heme Protein, Chem-Eur. J. 21 (2015) 7596–7602.

49 H. Xia, Y. Kitazumi, O. Shirai, K. Kano, Enhanced direct electron transfer-type bioelectrocatalysis of bilirubin oxidase on negatively charged aromatic compound-modified carbon electrode, J. Electroanal. Chem. 763 (2016) 104–109.

50 J.A. Cracknell, T.P. McNamara, E.D. Lowe, C.F. Blanford, Bilirubin oxidase from Myrothecium verrucaria: X-ray determination of the complete crystal structure and a rational surface modification for enhanced electrocatalytic O_2 reduction, Dalton Trans. 40 (2011) 6668–6675.

51 M. Tominaga, A. Sasaki, M. Togami, Laccase bioelectrocatalyst at a steroid-type biosurfactant-modified carbon nanotube interface, Anal. Chem. 87 (2015) 5417–5421.

52 T.S. Wong, U. Schwaneberg, Protein engineering in bioelectrocatalysis, Curr. Opin. Biotechnol. 14 (2003) 590–596.

53 R. Ortiz, H. Matsumura, F. Tasca, K. Zahma, M. Samejima, K. Igarashi, R. Ludwig, L. Gorton. Effect of deglycosylation of cellobiose dehydrogenases on the enhancement of direct electron transfer with electrodes, Anal. Chem. 84 (2012) 10315–10323.

54 Y. Hibino, S. Kawai, Y. Kitazumi, O. Shirai, K. Kano, Mutation of heme c axial ligands in d-fructose dehydrogenase for investigation of electron transfer pathways and reduction of overpotential in direct electron transfer-type bioelectrocatalysis, Electrochem. Commun. 67 (2016) 43–46.

55 M. Falk, Z. Blum, S. Shleev, Direct electron transfer based enzymatic fuel cells, Electrochim. Acta 82 (2012) 191–202.

56 S. Shleev, J. Tkac, A. Christenson, T. Ruzgas, A.I. Yaropolov, J.W. Whittaker, L. Gorton, Direct electron transfer between copper-containing proteins and electrodes, Biosens. Bioelectron. 20 (2005) 2517–2554.

57 S. Tsujimura, K. Kano, T. Ikeda, Bilirubin oxidase in multiple layers catalyzes four-electron reduction of dioxygen to water without redox mediators, J. Electroanal. Chem. 576 (2005) 113–120.

58 A. Volbeda, E. Garcin, C. Piras, A.L. de Lacey, V.M. Fernandez, E.C. Hatchikian, J.C. Fontecilla-Camps, Structure of the [NiFe] Hydrogenase Active Site: Evidence for Biologically Uncommon Fe Ligands, J. Am. Chem. Soc. 118 (1996) 12989–12996.

59 Y. Kamitaka, S. Tsujimura, K. Kataoka, T. Sakurai, T. Ikeda, K. Kano, Effects of axial ligand mutation of the type I copper site in bilirubin oxidase on direct electron transfer-type bioelectrocatalytic reduction of dioxygen, J. Electroanal. Chem. 601 (2007) 119–124.

60 K.A. Vincent, A. Parkin, F.A. Armstrong, Investigating and exploiting the electrocatalytic properties of hydrogenases, Chem. Rev. 107 (2007) 4366–4413.

61 C. Tard, C.J. Pickett, Structural and functional analogues of the active sites of the [Fe]-,[NiFe]-, and [FeFe]-hydrogenases, Chem. Rev. 109 (2009) 2245–2274.

62 W. Lubitz, H. Ogata, O. Rüdiger, E. Reijerse, Hydrogenase, Chem. Rev. 114 (2014) 4081–4148.

63 H. Ogata, W. Lubitz, Y. Higuchi, [NiFe] hydrogenases: structural and spectroscopic studies of the reaction mechanism, Dalton Trans. 37 (2009) 7577–7587.

64 Y. Nicolet, J.K. Rubach, M.C. Posewitz, P. Amara, C. Mathevon, M. Atta, J.C. Fontecilla-Camps, X-ray structure of the [FeFe]-hydrogenase maturase HydE from Thermotoga maritime, J. Biol. Chem. 283 (2008) 18861–18872.

65 X. Liu, S.K. Ibrahim, C. Tard, C.J. Pickett, Iron-only hydrogenase: Synthetic, structural and reactivity studies of model compounds, Coord. Chem. Rev. 249 (2005) 1641–1652.

66 S.V. Morozov, P.M. Vignais, L. Cournac, N.A. Zorin, E.E. Karyakina, A.A. Karyakin, S. Cosnier, Bioelectrocatalytic hydrogen production by hydrogenase electrodes, Int. J. Hydrogen. Energy, 27 (2002) 1501–1505.

67 H. Ogata, Y. Mizoguchi, N. Mizuno, K. Miki, S. Adachi, N. Yasuoka, T. Yagi, O. Yamauchi, S. Hirota, Y. Higuchi. Structural studies of the carbon monoxide complex of [NiFe] hydrogenase from *Desulfovibrio vulgaris* Miyazaki F: suggestion for the initial activation site for dihydrogen, J. Am. Chem. Soc. 124 (2002) 11628–11635.

68 H.S. Shafaat, O. Rüdiger, H. Ogata, W. Lubitz, [NiFe] hydrogenases: a common active site for hydrogen metabolism under diverse conditions, Biochim. Biophys. Acta (BBA)-Bioenerg. 1827 (2013) 986-1002.

69 K. So, Y. Kitazumi, O. Shirai, K. Kurita, H. Nishihara, Y. Higuchi, K. Kano, Kinetic analysis of inactivation and enzyme reaction of oxygen-tolerant [NiFe]-hydrogenase at direct electron-transfer bioanode, Bull. Chem. Soc. Jpn. 87 (2014) 1177-1185.

70 K. So, R. Hamamoto, R. Takeuchi, Y. Kitazumi, O. Shirai,R. Endo, H. Nishihara, Y. Higuchi, K. Kano, Bioelectrochemical analysis of thermodynamics of the catalytic cycle and kinetics of the oxidative inactivation of oxygen-tolerant [NiFe]-hydrogenase, J. Electroanal. Chem. 766 (2016) 152–161.

71 E. Lojou. Hydrogenases as catalysts for fuel cells: strategies for efficient immobilization at electrode interfaces, Electrochim. Acta 58 (2011) 10385–10397.

72 O. Rüdiger, J.M. Abad , E.C. Hatchikian,V.M. Fernandez , A.L. De Lacey, Oriented Immobilization of Desulfovibrio gi gas Hydrogenase onto Carbon Electrodes by Covalent Bonds for Nonmediated Oxidation of H_2, J. Am. Chem. Soc. 127 *(*2005)16008–16009.

73 C.Gutiérrez-Sánchez, D. Olea, M. Marques, V.M. Fernández, I.A.C. Pereira, M.Vélez, A.L. De Lacey, Oriented immobilization of a membrane-bound hydrogenase onto an electrode for direct electron transfer, Langmuir 27 (2011) 6449–6457.

74 F. Oteri, A. Ciaccafava, A. de Poulpiquet, M. Baaden, E. Lojou, S. Sacquin-Mora, The weak, fluctuating, dipole moment of membrane-bound hydrogenase from Aquifex aeolicus accounts for its adaptability to charged electrodes, Phys. Chem. Chem. Phys. 16 (2014) 11318–11322.

75 N. Heidary, T. Utesch, M. Zerball, M. Horch, D. Millo, J. Fritsch, O. Lenz, R. von Klitzing, P. Hildebrandt, A. Fischer, M.A. Mroginski, I. Zebger, Orientation-Controlled Electrocatalytic Efficiency of an Adsorbed Oxygen-Tolerant Hydrogenase, PloS one 10 (2015) e0143101.

76 K. So, Y. Kitazumi, O. Shirai, K. Kurita, H. Nishihara, Y. Higuchi, K. Kano, Gas-diffusion and Direct-electron-transfer-type Bioanode for Hydrogen Oxidation with Oxygen-tolerant [NiFe]-hydrogenase as an Electrocatalyst, Chem. Lett. 43 (2014) 1575–1577.

77 R. Kontani, S. Tsujimura, K. Kano, Air diffusion biocathode with CueO as electrocatalyst adsorbed on carbon particle-modified electrodes, Bioelectrochemistry 76 (2009) 10–13.

78 G. Gupta, C. Lau, B. Branch, V. Rajendran, D. Ivnitski, P. Atanassov, Direct bio-electrocatalysis by multi-copper oxidases: Gas-diffusion laccase-catalyzed cathodes for biofuel cells, Electrochim. Acta 56 (2011) 10767–10771.

79 K. So, M. Onizuka, T. Komukai, Y. Kitazumi, O. Shirai, K. Kano, Binder/surfactant-free biocathode with bilirubin oxidase for gas-diffusion-type system, Electrochem. Commun. 66 (2016) 58–61.

80 Y. Higuchi, N. Yasuoka, M. Kakudo, Y. Katsube, T. Yagi, H. Inokuchi, Single crystals of hydrogenase from *Desulfovibrio vulgaris* Miyazaki F, J. Biol. Chem. 262 (1987) 2823–2825.

81 R.S. Deinhammer, M. Ho, J.W. Anderegg, M.D. Porter, Electrochemical oxidation of amine-containing compounds: a route to the surface modification of glassy carbon electrodes, Langmuir 10 (1994) 1306–1313.

82 K. Mizutai, M. Toyoda, K. Sagara, N. Takahashi, A. Sato, Y. Kamitaka, S. Tsujimura, Y. Nakanishi, T. Sugiura, S. Yamaguchi, K. Kano, B. Mikami, X-ray analysis of bilirubin oxidase from *Myrothecium verrucaria* at 2.3 Å resolution using a twinned crystal, Acta Crystallogr. F 66 (2010) 765–770.

83 A. Nagashima, Viscosity of water substance—new international formulation and its background, J. Phys. Chem. Ref. Data, 6 (1977) 1133–1166.

84 IUPAC Solubility Data Series, ed. by C. L. Young, Pergamon Press, Oxford, 1981, Vol. 5/6.

85 P. Delahay, Implications of the Kinetics of Ionic Dissociation with Regard to Some Electrochemical Processes-Application to Polarography, J. Am. Chem. Soc. 74 (1952) 3497–3500.

86 A.H.M. Cosijn, Diffusion polarisation of the hydrogen electrode: I. Theory, J. Electroanal. Chem. 2 (1961) 437–451.

87 V. Marinović, A.R. Despić, Hydrogen evolution from solutions of citric acids, J. Electroanal. Chem. 431 (1997) 127–132.

88 C. Léger, S. Dementin, P. Bertrand, M. Rousset, B. Guigliarelli, Inhibition and aerobic inactivation kinetics of Desulfovibrio fructosovorans NiFe hydrogenase studied by protein film voltammeter, J. Am. Chem. Soc. 126 (2004) 12162–12172.

89 M. Hambourger, M. Gervaldo, D. Svedruzic, P.W. King, D. Gust, M. Ghirardi, A.L. Moore, T.A. Moore, [FeFe]-hydrogenase-catalyzed H_2 production in a photoelectrochemical biofuel cell, J. Am. Chem. Soc. 130 (2008) 2015–2022.

90 F.A. Armstrong, N.A. Belsey, J.A. Cracknell, G. Goldet, A. Parkin, E. Reisner, K.A. Vincent, A.F. Wait, Dynamic electrochemical investigations of hydrogen oxidation and production by enzymes and implications for future technology, Chem. Soc. Rev. 38 (2009) 36–51.

Chapter 3-3

Interaction between D-fructose dehydrogenase and methoxy-substituent-functionalized carbon surface to increase productive orientations

Abstract

D-Fructose dehydrogenase (FDH) from *Gluconobacter japonicus* NBRC3260 catalyzes the two-electron oxidation of D-fructose to 5-keto-D-fructose, and it is widely used in biofuel cells and biosensors. In this study, methoxy-substituent-functionalized carbon electrodes are constructed by electrochemical oxidation of methoxy-aniline derivatives on Ketjen Black (KB)-modified electrodes to improve the immobilization and bioelectrocatalysis of FDH. It is proposed that the specific interaction between FDH, especially the heme *c* moiety, and methoxy substituent(s) of amines on carbon electrode increases the proportion of the productively oriented FDH molecules to the total FDHs. Consequently, the limiting catalytic current density of the D-fructose oxidation increases to as much as 23 ± 2 mA cm^{-2} in FDH/2,4-dimethoxyaniline/KB/glassy carbon electrode, for example.

1. Introduction

Immobilization of a redox enzyme onto a solid electrode for direct electron transfer (DET)-type enzymatic bioelectrocatalysis, wherein the redox enzyme acts as an electrocatalyst and communicates with the electrode without a mediator, is the first step to construct mediator-free biosensors and biofuel cells.[1,2] However, the electrochemical communication between the enzyme and electrode is limited due to the long-distance electron transfer from the active center of the enzyme to the electrode surface; also, the details of their interaction are still unclear, unlike the well-understood interaction between the enzyme and its natural substrate.[1–3] Furthermore, when the enzyme is adsorbed with a random orientation on the electrode surface, the apparent interfacial electron transfer-kinetics decreases.[4] Functionalization of the electrode surface, through, for example, modification with some specific compounds (including the natural substrate of the enzyme), can induce a favorable orientation of the enzyme due to the specific interaction (for example, electrostatic interaction,[5–9] supermolecular interaction[10–15] and enzyme–substrate interaction[16–18]) between the enzyme and the specific modifier.[5–20] However, there is no report on the use of D-fructose dehydrogenase (FDH; EC 1.1.99.11). In this study, we focus our attention on the specific affinity between FDH and some quinones.[21]

FDH from *Gluconobacter japonicus* NCBR 3260 (formerly *Gluconobacter industrius*), which catalyzes the two-electron oxidation of D-fructose to 5-keto-D-fructose, is a flavohemoprotein with a molecular mass of *ca.* 140 kDa, comprising subunits I (67 kDa), II (51 kDa), and III (20 kDa)).[22,23] Subunits I and II have covalently bound flavin adenine dinucleotide (FAD) and three

heme *c* moieties, respectively, though the function of subunit III is still unclear. FDH shows strict substrate specificity to D-fructose, and it is applied to diagnostic and food analysis.[24–26] Besides, the dioxygen-insensitive property of FDH is useful for constructing membrane-less D-fructose/dioxygen biofuel cells.[17,27–30] An important issue here is to construct an FDH-modified electrode that possesses good electrocatalytic activity and stability for technological applications.

Several approaches, such as the use of a mediator[31,32] and a conductive polymer[33], have been reported to improve the electrocatalytic performance of FDH for mediated electron transfer (MET)-type bioelectrocatalysis. In addition, high catalytic current density was also realized in DET-type bioelectrocatalysis without mediator at some porous materials[17,27,34–36] and self-assembled monolayer-modified Au-nanoparticles[37]. Two electrons in a D-fructose molecule are transferred to the FAD catalytic center of FDH and then successively to the heme *c* moieties. One of the heme *c* moieties works as an electron donating site to external electron acceptors in MET-type bioelectrocatalysis (as well as homogeneous enzyme reactions) and to electrodes in DET-type bioelectrocatalysis,[21,38,39] although non-catalytic Faradaic signal of FDH is not clearly identified.[21,34,38,39]

Ubiquinones (2,3-dimethoxy-5-methyl-6-poly prenyl-1,4-benzoquinones) were identified as the physiological electron acceptors of FDH.[23,40] Interestingly, some quinones with methoxy substituents, like 2,3-dimethoxy-5-methyl-1,4-benzoquinone and 2,3-dimethoxy-5-farnesyl-1,4-benz -oquinone, showed high affinity to FDH and functioned as good soluble electron acceptors of the reduced FDH (or good mediators between FDH and electrodes) compared with other quinones without methoxy substituent.[21] Some specific interaction between methoxy substituent and the electron-donating heme *c* moiety of FDH is expected to occur,[21,38,39] although no direct evidence was provided owing to unidentified crystal structure.

In this study, we consider that the expected attractive interactions between methoxy substituent and the electron-donating heme *c* moiety may increase the number of FDH molecules with the productive orientation on electrodes and increase the current density of the DET-type bioelectrocatalysis of FDH as in a mode depicted in Fig. 1. We attempt to construct several methoxy-substituent-functionalized surfaces by the electrochemical oxidation of methoxy aniline derivatives at carbon electrodes and assess DET-type bioelectrocatalytic performance of FDH adsorbed on the electrodes.

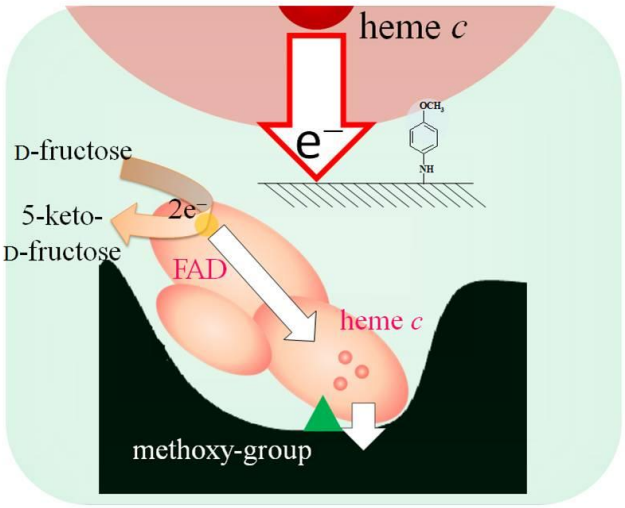

Fig. 1

Proposed scheme of the interaction between FDH and methoxy-substituent-functionalized carbon electrode surface. The electron from D-fructose is transfer to the heme *c* moiety via FAD and then to electrode in DET-type bioelectrocatalysis. Methoxy-substituent seems to play an important role to induce the productive orientation of FDH with facing the heme *c* moiety to electrode. The expected structure of the covalently bound *p*-anisidine that is electrochemically oxidized on carbon electrode is also given.

2. Experimental

2.1. Materials and regents

Ketjen Black EC300J (KB) was kindly donated by Lion Co. (Japan). Polytetrafluoroethylene fine powder (PTFE, 6-J) was obtained from DuPont Mitsui Fluorochemicals (Japan). *p*-Anisidine (4-methoxyaniline), 2,4-dimethoxyaniline, 3,4-dimethoxyaniline, methyl 4-aminobenzoate, 4-aminobenzoic acid, 4-aminophenol, and *p*-phenylenediamine (1,4-diaminobenzene) were purchased from Tokyo Chemical Industry Co. (Japan). The expression and purification of FDH were conducted as described in the literature.[21] All other chemicals used in this study were of analytical grade, and all solutions were prepared with distilled water.

2.2. Electrochemical measurements

All electrochemical measurements were performed using an electrochemical analyzer ALS 701E with a rotating disk glassy carbon electrode (GCE) (3 mm diameter, BAS) as a working electrode, a Pt wire as a counter electrode, and an Ag|AgCl|sat. KCl electrode as a reference

electrode. All potentials were referred against the reference electrode in this study. The bioelectrocatalytic activity of FDH for fructose oxidation was evaluated from the steady-state currents measured by cyclic voltammetry and chronoamperometry at 25 ± 1 °C in a pH 5.0 McIlvaine buffer (McB) at a rotation rate (ω) of 2000 rpm.

2.3. Electrochemical modification of carbon electrodes with amines

KB-modified glassy carbon electrode (KB/GCE) was prepared as described in the literature.[13] Briefly, 3 μL of a KB slurry (KB:PTFE = 4:1, in 2-propanol) were dropped on a GCE surface and dried at room temperature (about 25 °C) for 10 min to produce KB/GCE (L = dm^3). The KB/GCEs were electrochemically modified with several amines according to a previously described method.[9] In preliminary experiments, *p*-anisidine solution was electrolyzed through a five-cycle potential scan in the potential range from 0.3 to 0.7 V at a scan rate (v) of 20 mV s^{-1}. A large oxidation peak of the *p*-anisidine amino group was observed at around 0.4 V in the first cycle, but the current drastically decreased in the subsequent scan. The electrochemical oxidation of *p*-anisidine on carbon electrodes is expected to produce a methoxy-substituent-functionalized surface through a nitrogen–carbon bond (Fig. 1).[9,41] Following, a single-step electrochemical oxidation was induced at 0.4 V for 120 s to simplify the procedure. The modified electrode was washed with distilled water to remove physically absorbed amine. The *p*-anisidine-modified KB/GCE was called *p*-anisidine/KB/GCE. Similar naming was applied to the other amine-modified electrodes.

2.4. FDH adsorption on KB/GCEs and amine/KB/GCEs

FDH solution was dropped on KB/GCEs and amine/KB/GCEs and dried at 4 °C for 12 h, as previously described.[34] The electrode was washed with distilled water and used for electrochemical experiments. Then, the electrodes were called FDH/KB/GCE and FDH/amine/KB/GCEs, respectively. For long-term storage, the FDH-adsorbed electrodes were kept in a water-saturated atmosphere at 4 °C.

2.5. Determining the fructose oxidation activity of FDH adsorbed on electrodes

The enzyme activity of FDH adsorbed on electrodes was measured with $[Fe(CN)_6]^{3-}$ as an electron acceptor, based on the previously reported method.[22] Briefly, the FDH-adsorbing electrode was washed with deionized water and immersed into a reaction mixture (250 μL fructose solution 0.4 M + 250 μL $K_3Fe(CN)_6$ 0.04 M + 500 μL McB (pH 4.5)) for 5 min at 25 °C (M = mol dm^{-3}). Furthermore, 500 μL Dupanol solution (3 g L^{-1} sodium dodecyl sulfate and 5 g L^{-1} $Fe_2(SO_4)_3$) were

added to the reaction mixture to stop the enzyme reaction and the mixture was incubated at 25 °C for 20 min. The mixture was diluted to 5.00 mL with deionized water. The absorbance of the reaction solution was measured at 660 nm with a spectrometer (UV-2550, Shimadzu, Kyoto, Japan).

3. Results and discussion

3.1. DET-type bioelectrocatalysis of FDH on amine-modified electrode surfaces

Fig. 2 shows the rotating-disk cyclic voltammograms of FDH/KB/GCE and FDH/*p*-anisidine/KB/GCE at ω = 2000 rpm in McB (pH 5) containing 0.2 M D-fructose. Well-defined sigmoidal catalytic waves are observed in both cases. Such catalytic waves are not observed in the absence of D-fructose (Fig. 2, A and B). The Faradaic waves are ascribed to the D-fructose oxidation due to the DET-type bioelectrocatalysis with FDH on the electrode surface.[27,34] Note here that the rotating-disk electrode was used in this study to diminish the influence of the mass transfer of D-fructose from the bulk solution to the electrode surface. At ω > 1000 rpm, the catalytic current becomes independent of ω in both FDH/KB/GCE and FDH/*p*-anisidine/KB/GCE (Fig 2, A and B), indicating that the catalytic limiting current density at least at 2000 rpm is completely controlled by enzyme kinetics. The steady-state catalytic current density at FDH/KB/GCE is 7 ± 1 mA cm^{-2} at 0.5 V, and it is consistent with previous results.[27,34] Interestingly, at FDH/*p*-anisidine/KB/GCE, the catalytic current density reaches 17 ± 1 mA cm^{-2} at 0.5 V. In addition, the bioelectrocatalytic current increases with the electric charge for the electrochemical modification, but reach a saturated value (data not shown).

Fig. 2C is chronoamperograms (CAs) at 0.5 V with FDH/*p*-anisidine/KB/GCE and FDH/KB/GCE. Steady-state oxidation currents are obtained for at least 400 s at both electrodes. In conclusion, the *p*-anisidine-modified electrode surface provides a suitable platform for FDH to produce catalytic currents at a high density and with high stability.

However, a pair of small redox peaks were observed around 0.25 V at FDH/*p*-anisidine/KB/GCE in the absence of D-fructose (Fig. 2A). The redox wave was observed even in the absence of FDH and also after washing of the electrode with water. Therefore, the redox wave is safely assigned to a surface-confined redox species (for example, 4,4'-dimethoxyhydrazobenzene)[42] generated as a by-product during the oxidation of *p*-anisidine. Similar redox waves were also observed on other amine-modified electrodes.[9] The onset potential of the catalytic wave at FDH/*p*-anisidine/KB/GCE in the presence of D-fructose (Fig. 2A) is ca. −0.1 V and is close to the formal potential of the heme *c* moiety of FDH,[21,34,39] but far negative than the redox potential of the surface-confined by-product. In addition the surface-confined wave was not affected by the addition of D-fructose. Therefore, the catalytic wave is safely assigned to DET-type bioelectrocatalysis of FDH, and the surface-confined

by-product does not participate in MET-type bioelectrocatalysis of FDH on the electrode, most probably due to restricted movement of the surface-confined by-product. In order to verify our conclusion, $Fe(CN)_6^{3-/4-}$ was used as a soluble mediator to observe MET-type bioelectrocatalysis. $Fe(CN)_6^{3-/4-}$-mediated bioelectrocatalytic wave is simply overlapped on the DET-type wave in the potential range more positive than the redox potential of $[Fe(CN)_6]^{3-/4-}$ (ca. 0.23 V) that is close to the redox potential of the surface confined bi-product) without any change in the onset characteristics in the DET-type bioelectrocatalysis (Fig. 2B). All these results support our consideration.

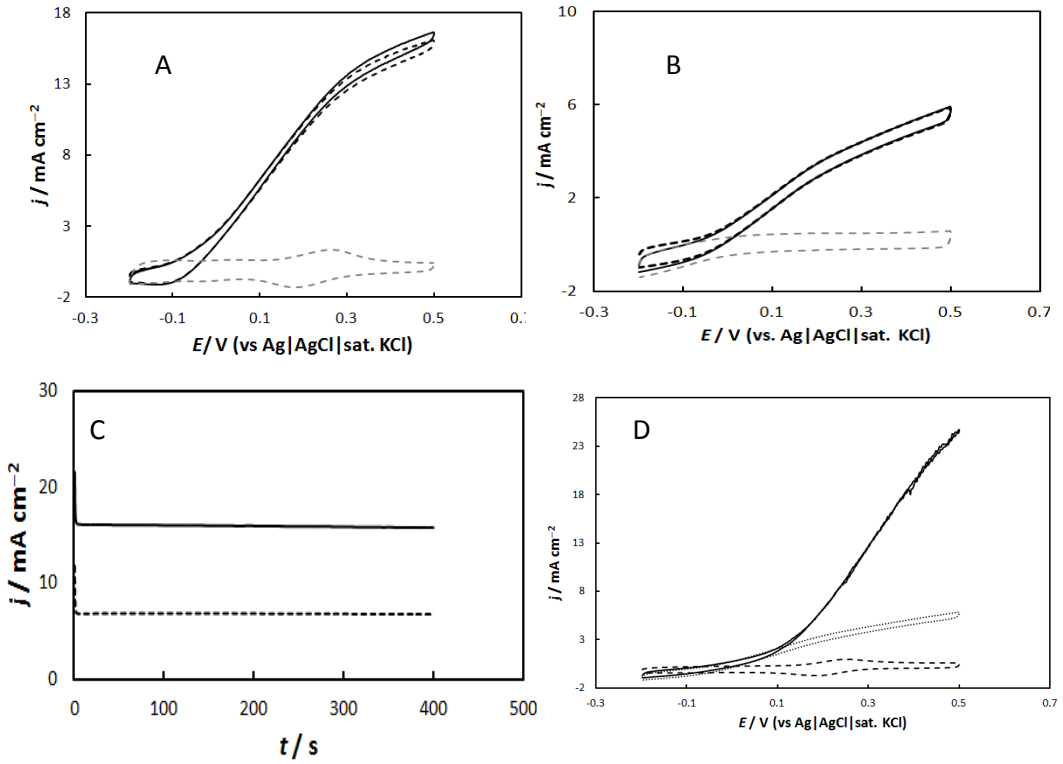

Fig. 2

CVs of (A) FDH/KB/GCE and (B) FDH/*p*-anisidine-KB/GCE in pH 5 McB in the absence (gray dash line) and presence of 0.2 M D-fructose under convective conditions at ω = 1000 rpm (black dash line) and 2000 rpm (black solid line).

(C) CAs of FDH/KB/GCE (dashed line) and FDH/*p*-anisidine/KB/GCE (solid line) at 0.5 V under the same conditions as in A and B .

(D) CVs of FDH/KB/GCE in pH 5 McB in the absence (black dash line) and presence of 0.2 M D-fructose and $[Fe(CN)_6]^{3-/4-}$ as a free mediator in solution (DET + MET reaction). A cyclic voltammogram of FDH/KB/GCE (dotted line) in pH 5 McB containing 0.2 M D-fructose and but without $[Fe(CN)_6]^{3-/4-}$ are shown as a comparison (DET reaction).

As a comparison, other amines with structures similar to *p*-anisidine (4-aminophenol, 4-aminobenzoic acid, *p*-phenylenediamine and methyl 4-aminobenenzoate) were also modified on KB as platforms for FDH. The steady-state catalytic current densities of FDH/amine/KB/GCEs at 0.5 V in McB (pH 5) containing 0.2 M D-fructose are compared with that of FDH/KB/GCE (Fig. 3).

At methoxy substituent-containing amine-modified electrodes, such as FDH/3,4-dimethoxyaniline/KB/GCE and FDH/2,4-dimethoxyaniline/KB/GCE, the steady-state current densities reach 16 ± 1 and 23 ± 2 mA cm^{-2}, respectively. However, when amines without methoxy substituent are modified, no obvious change is observed compared with FDH/KB/GCE. Therefore, we conclude that the methoxy substituent of the aromatic amines plays an important role in increasing the catalytic current density of FDH. Note here that there is no redox wave around the onset potential of DET-type bioelectrocatalysis at the amine-modified electrodes and the onset potential is almost independent of the modification. This means that the aromatic moieties with methoxy substituent are not electrochemical active and do not work as redox mediators in bioelectrocatalysis of fructose oxidation. Therefore, the aromatic moieties with methoxy substituent on the carbon electrodes seem to play a role not to improve the kinetic property but to increase the number of FDH molecules with the productive orientation convenient for DET-type bioelectrocatalysis due to the attractive interaction between the methoxy group and the electron donating heme *c* site in FDH (Fig. 1).

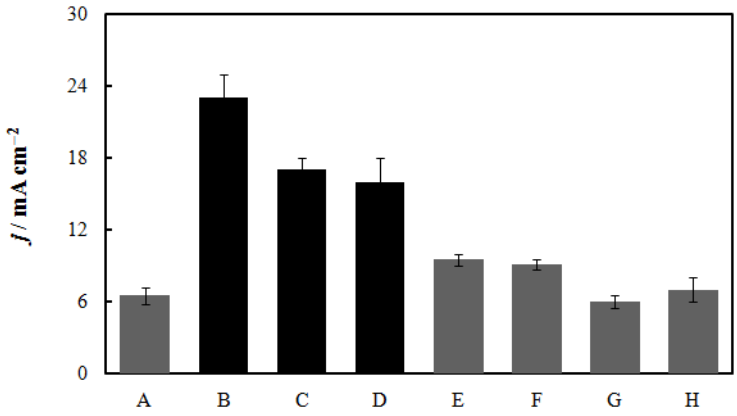

Fig. 3

Background-corrected current density of the catalytic fructose oxidation reaction of FDH in (A) pristine KB/GCE, (B) 2,4-dimethoxyaniline/KB/GCE, (C) *p*-anisidine/KB/GCE, (D) 3,4-dimethoxyaniline/KB/GCE, (E) 4-aminophenol/KB/GCE, (F) 4-aminobenzoic acid/KB/GCE, (G) *p*-phenylenediamine/KB/GCE, and (H) methyl 4-aminobenzoate/KB/GCE at 0.5 V in rotating-disk linear sweep voltammetry at ω = 2000 rpm and v = 20 mV s^{-1} in pH 5 McB containing 0.2 M D-fructose.

3.2. The state of immobilized FDH based on kinetic analysis

We attempt to assess the total activity of FDH adsorbed on the electrodes. The D-fructose oxidation activity of FDH, which is adsorbed on the electrodes, was spectrophotometrically evaluated, as described in Section 2.5. Interestingly, although FDH exhibits different limiting current densities at different electrodes, it shows almost the same level of D-fructose oxidation activity (Fig. 4). Indeed, the activity reflects the $k_c\Gamma_t$ value of the FDH adsorbed on the electrodes, where k_c is the catalytic rate constant for the soluble electron acceptor ($[Fe(CN)_6]^{3-}$) and Γ_t is the total surface concentration of FDH. Therefore, the amine-modification employed here do not seem to affect the $k_c\Gamma_t$ value of FDH; the difference in the limiting current densities on different electrodes is attributable not to $k_c\Gamma_t$ but to some other factor(s) (DET-type catalytic activity k_{cat} and/or the orientation factor λ as described below) involved in the electrochemical communication between FDH and the electrode.

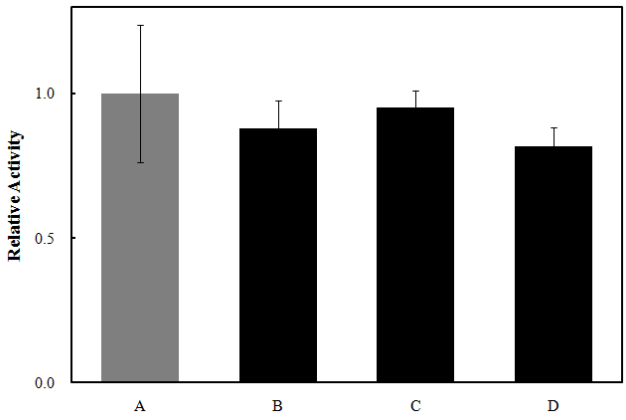

Fig. 4

Relative activity of FDH adsorbed on (A) pristine KB surface, (B) 2,4-dimethoxyaniline/KB surface, (C) *p*-anisidine/KB surface, and (D) 3,4-dimethoxyaniline-KB surface for D-fructose oxidation.

Therefore, we perform a kinetic analysis of the catalytic wave on a steady-state model without the concentration polarization of the substrate to consider random orientation :[9]

$$\frac{j}{j_{cat}^{lim}} = \frac{1}{\beta\Delta d\left(1+\exp\left\{\frac{n'_E F}{RT}\left(E-E^{\circ\prime}{}_E\right)\right\}\right)} \ln\left|\frac{\left(1+\exp\left\{\frac{n'_E F}{RT}\left(E-E^{\circ\prime}{}_E\right)\right\}\right)+\frac{k_{cat}}{k_0^{max}}\exp\left\{\frac{\alpha n'_E F}{RT}\left(E-E^{\circ\prime}{}_E\right)\right\}}{\exp\left(-\beta\Delta d\right)\left(1+\exp\left\{\frac{n'_E F}{RT}\left(E-E^{\circ\prime}{}_E\right)\right\}\right)+\frac{k_{cat}}{k_0^{max}}\exp\left\{\frac{\alpha n'_E F}{RT}\left(E-E^{\circ\prime}{}_E\right)\right\}}\right| \quad (1)$$

where n'_E is the number of electrons in the rate-determining step of the interfacial electron transfer

(the number of the electrons for heme *c* in FDH = 1 in this case), *F* is the Faraday constant, *R* is the gas constant, *T* is the absolute temperature, k_0^{max} is the standard rate constant near the best orientation position of the enzyme, Δd is the distance between the closest and the farthest position of the enzymes (that can communicate with electrode) in several orientations, α is the transfer coefficient, β is the coefficient in the long-range electron transfer, $E^{\circ\prime}{}_E$ is the formal potential of the redox center of the enzyme for electrochemical communication with the electrode, and j_{cat}^{lim} is the limiting current density given by

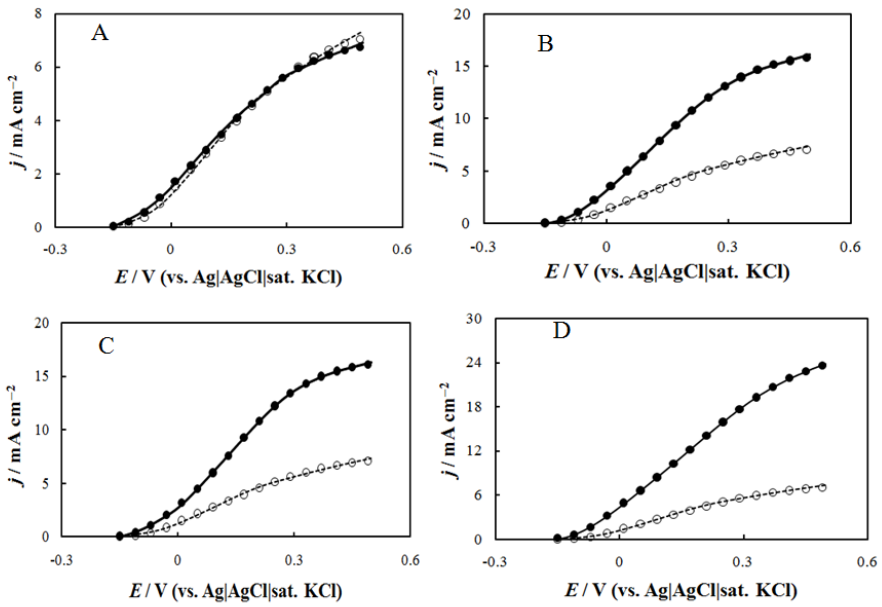

Fig. 5

Background current-corrected rotating disk linear sweep voltammograms at (A) FDH/*p*-phenylenediamine-KB/GCE, (B) FDH/*p*-anisidine-KB/GCE, (C) FDH/3,4-dimethoxyaniline-KB/GCE and (D) FDH/2,4-dimethoxyaniline-KB/GCE in pH 5 McB containing 0.2 M D-fructose at ω = 2000 rpm and v = 20 mV s^{-1}. Dashed lines represent a rotating disk cyclic voltammogram at FDH/KB/GCE taken under the same conditions for comparison. The closed and open circles represent the best fitted curves obtained by non-linear least square method.

$$j_{cat}^{lim} = (n_S / n_E) F k_{cat} \lambda \Gamma_t \qquad (2)$$

where n_S is the number of electrons in the substrate (n_S = 2 in this case), n_E is the number of

electrons in the enzyme (n_E = 1 in this case), λ is the surface concentration proportion of the productively oriented enzymes (that is the enzymes that can communicate with the electrode) to the total adsorbed enzymes. The parameter k_{cat} in Eqs. (1) and (2) is the catalytic rate constant in the DET reaction. Moreover, k_{cat} is different from the solution activity (k_c) that depends on the electron acceptor but might be in a correlation with k_c. Considering $\frac{k_{cat}}{k_0^{max}}$, $\beta\Delta d$, and $k_{cat}\lambda\Gamma_t$ as adjustable parameters, Eq. (1) is fitted to the rotating-disk voltammograms using nonlinear regression with Excel© 2007. The experimental data are well reproduced by Eq. (1), as indicated by the example results shown in Fig. 6.

Table 1. Kinetic parameters of DET-type bioelectrocatalytic oxidation of fructose for several FDH-adsorbed electrodes

Electrodes	k_{cat} / k_0^{max}	$k_{cat}\lambda\Gamma_t$/mol cm^{-2} s^{-1}	$\beta\,\Delta d$
FDH/KB/GCE	2.2 ± 0.1	(5.4 ± 0.5) × 10^{-8}	2.1 ± 0.1
FDH/*p*-phenylenediamine/KB/GCE	2.0 ± 0.6	(6 ± 1) × 10^{-8}	1.7 ± 0.1
FDH/*p*-anisidine/KB/GCE	2.3 ± 0.3	(1.8 ± 0.1) × 10^{-7}	2.0 ± 0.2
FDH/2,4-dimethoxyaniline/KB/GCE	2.4 ± 0.1	(1.6 ± 0.1) × 10^{-7}	1.2 ± 0.5
FDH/3,4-dimethoxyaniline/KB/GCE	2.1 ± 0.1	(2.7 ± 0.2) × 10^{-7}	1.6 ± 0.2

The refined data are summarized in Table 1. The parameters $\frac{k_{cat}}{k_0^{max}}$ and $\beta\Delta d$ are almost independent of the amine modification of the electrode. In contrast, $k_{cat}\lambda\Gamma_t$ significantly depends on amine-modification and it shows a clear linear correlation with the catalytic current density (j) obtained by rotating disk voltammetry at 0.5 V, as shown in Fig. 6. Since the values of $k_{cat}\Gamma_t$ ($\propto k_c\Gamma_t$) are almost independent of the amine modification, as evidenced by the results in Fig. 6, the present data indicate that the limiting current densities are mainly controlled by the orientation parameter λ. It can be reasonably accepted, therefore, that only FDH adsorbed in productive (or convenient) orientations, with heme *c* facing the electrode, can communicate with the electrode to produce the catalytic current. [43] Note here that Δd values at the four kinds of electrodes may assume values within a rather narrow range from 0.8–1.5 Å, if we assume a tentative value of β = 1.4 Å^{-1}.[44] The Δd values are much shorter than the diameter of FDH (70 Å) evaluated by atomic force microscopy[43] and are almost independent of the amine modification. These results indicate that FDH molecules that can productively communicate with the electrode are those with specific patterns of orientations. In conclusion, we propose that methoxy-substituent-functionalized surface increases the proportion of the productively oriented FDH molecules to the total FDH molecules on carbon electrodes, thus,

increasing the density of the limiting catalytic current.

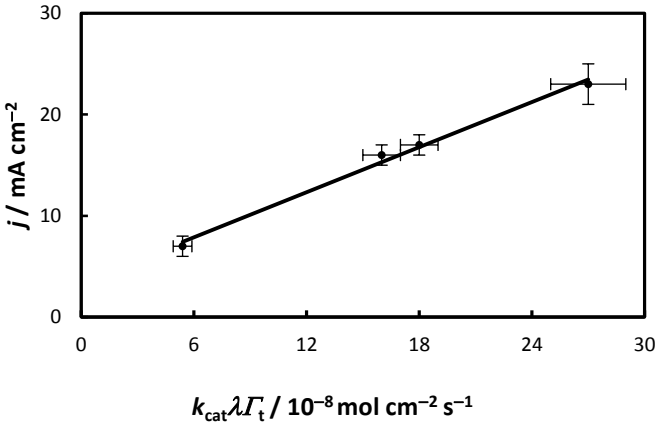

Fig. 6

Correlation between the catalytic current density (j) obtained by rotating-disk voltammetry at 0.5 V and the $k_{cat}\lambda\Gamma_t$ evaluated by the curve fitting.

4. Conclusion

In summary, the use of a methoxy-substituent-functionalized KB electrode increases the bioelectrocatalytic current density of FDH for fructose oxidation compared to a pristine KB electrode and other KB electrodes modified with aromatic compounds without a methoxy substituent. We propose here that the specific interaction between FDH and the methoxy group, which is also observed in the bimolecular rate constant between FDH and some quinones with a methoxy group in solution,[21] improves the orientation for a DET-type catalytic reaction. The highest current density of FDH for fructose oxidation is 23 ± 2 mA cm^{-2} in pH 5 McB containing 0.2 M D-fructose. This value is much higher than those reported under similar conditions.[27,34–37] Therefore, this electrode that exhibits high current density with acceptable stability could function as a bioanode in biofuel cells.

5. References

1 A.L. Ghindilis, A. Plamen, W. Ebtisam, Enzyme-catalyzed direct electron transfer: Fundamentals and analytical applications, Electroanalysis 9 (1997) 661–674.

2 J.A. Cracknell, K.A. Vincent, F.A. Armstrong, Enzymes as working or inspirational electrocatalysts for fuel cells and electrolysis, Chem. Rev. 108 (2008) 2439–2461.

3 A. Heller, Electrical connection of enzyme redox centers to electrodes, J. Phys. Chem. 96 (1992) 3579–3587.

4 C. Léger, P. Bertrand, Direct electrochemistry of redox enzymes as a tool for mechanistic studies, Chem. Rev. 108 (2008) 2379–2438.

5 F. Tasca, W. Harreither, R. Ludwig, J.J. Gooding, L. Gorton, Cellobiose dehydrogenase aryl diazonium modified single walled carbon nanotubes: enhanced direct electron transfer through a positively charged surface, Anal. Chem. 83 (2011) 3042–3049.

6 P. Olejnik, B. Palys, A. Kowalczyk, A.M. Nowicka, Orientation of laccase on charged surfaces. Mediatorless oxygen reduction on amino- and carboxyl-ended ethylphenyl groups, J. Phys. Chem. C 116 (2012) 25911–25918.

7 F. Oteri, A. Ciaccafava, A. De Poulpiquet, M. Baaden, E. Lojou, S. Sacquin-Mora, The weak, fluctuating, dipole moment of membrane-bound hydrogenase from *Aquifex aeolicus* accounts for its adaptability to charged electrodes, Phys. Chem. Chem. Phys. 16 (2014) 11318–11322.

8 L. Peng, T. Utesch, A. Yarman, J.H. Jeoung, S. Steinborn, H. Dobbek, F.W. Scheller. Surface-Tuned Electron Transfer and Electrocatalysis of Hexameric Tyrosine-Coordinated Heme Protein, Chem-Eur. J. 21 (2015) 7596–7602.

9 H. Xia, Y. Kitazumi, O. Shirai, K. Kano, Enhanced direct electron transfer-type bioelectrocatalysis of bilirubin oxidase on negatively charged aromatic compound-modified carbon electrode, J. Electroanal. Chem. 763 (2016) 104–109.

10 C.F. Blanford, R.S. Heath, F.A. Armstrong, A stable electrode for high-potential, electrocatalytic O_2 reduction based on rational attachment of a blue copper oxidase to a graphite surface, Chem. Commun. 17 (2007) 1710–1712.

11 M. Karaśkiewicz, E. Nazaruk, K. Żelechowska, J.F. Biernat, J. Rogalski, R. Bilewicz, Fully enzymatic mediatorless fuel cell with efficient naphthylated carbon nanotube–laccase composite cathodes, Electrochem. Commun. 20 (2012) 124–127.

12 F. Giroud, S.D. Minteer, Anthracene-modified pyrenes immobilized on carbon nanotubes for direct electroreduction of O_2 by laccase, Electrochem. Commun. 34 (2013) 157–160.

13 N. Lalaoui, A. Le Goff, M. Holzinger, S. Cosnier, Fully oriented bilirubin oxidase on porphyrin-functionalized carbon nanotube electrodes for electrocatalytic oxygen reduction, Chem. Eur. J. 21 (2015) 16868–16873.

14 N. Lalaoui, P. Rousselot-Pailley, V. Robert, Y. Mekmouche, R. Villalonga, M. Holzinger, A. Le Goff, Direct Electron Transfer between a Site-Specific Pyrene-Modified Laccase and Carbon Nanotube/Gold Nanoparticle Supramolecular Assemblies for Bioelectrocatalytic Dioxygen Reduction, ACS Catalysis 6(2016) 1894–1900.

15 J.A. Cracknell, T.P. McNamara, E.D. Lowe, C.F. Blanford, Bilirubin oxidase from Myrothecium verrucaria: X-ray determination of the complete crystal structure and a rational surface modification for enhanced electrocatalytic O_2 reduction, Dalton Trans. 40 (2011) 6668–6675.

16 K. So, S. Kawai, Y. Hamano, Y. Kitazumi, O. Shirai, M. Hibi, J. Ogawa, K. Kano, Improvement of a direct electron transfer-type fructose/dioxygen biofuel cell with a substrate-modified biocathode, Phys. Chem. Chem. Phys. 16 (2014) 4823–4829.

17 I. Matanovic, S. Babanova, M.S. Chavez, P. Atanassov, Protein–Support Interactions for rationally designed bilirubin oxidase based cathode: A Computational study, J. Phys. Chem. B 120 (2016) 3634–3641.

18 K. So, Y. Kitazumi, O. Shirai, K. Nishikawa, Y. Higuchi, K. Kano, Direct electron transfer-type dual gas diffusion H_2/O_2 biofuel cells, J. Mater. Chem. A 4 (2016) 8742–8749.

19 K. Murata, K. Kajiya, N. Nakamura, H. Ohno, Direct electrochemistry of bilirubin oxidase on three-dimensional gold nanoparticle electrodes and its application in a biofuel cell, Energy Environ. Sci. 2 (2009) 1280–1285.

20 M. Tominaga, A. Sasaki, M. Togami, Laccase bioelectrocatalyst at a steroid-type biosurfactant-modified carbon nanotube interface, Anal. Chem. 87 (2015) 5417–5421.

21 S. Kawai, T. Yakushi, K. Matsushita, Y. Kitazumi, O. Shirai, K. Kano, The electron transfer pathway in direct electrochemical communication of fructose dehydrogenase with electrodes, Electrochem. Commun. 38 (2014) 28–31.

22 M. Ameyama, E. Shinagawa, K. Matsushita, O. Adachi, D-fructose dehydrogenase of *Gluconobacter industrius*: purification, characterization, and application to enzymatic microdetermination of D-fructose, J. Bacterial. 145 (1981) 814–823.

23 S. Kawai, M. Goda-Tsutsumi, T. Yakushi, K. Kano, K. Matsushita, Heterologous overexpression and characterization of a flavoprotein-cytochrome *c* complex fructose dehydrogenase of *Gluconobacter japonicus* NBRC3260, Appl. Environ. Microbiol. 79 (2013) 1654–1660.

24 J. Parellada, E. Domínguez, V.M. Fernández, Amperometric flow injection determination of fructose in honey with a carbon paste sensor based on fructose dehydrogenase, Anal. Chim. Acta 330 (1996) 71–77.

25 P.A. Paredes, J. Parellada, V.M. Fernández, I. Katakis, E. Domínguez, Amperometric mediated carbon paste biosensor based on d-fructose dehydrogenase for the determination of fructose in food analysis, Biosens. Bioelectron. 12 (1997) 1233–1243.

26 R. Antiochia, G. Vinci, L. Gorton, Rapid and direct determination of fructose in food: a new osmium-polymer mediated biosensor, Food Chem. 140 (2013) 742–747.

27 Y. Kamitaka, S. Tsujimura, N. Setoyama, T. Kajino, K. Kano, Fructose/dioxygen biofuel cell based on direct electron transfer-type bioelectrocatalysis, Phys. Chem. Chem. Phys. 9 (2007) 1793–1801.

28 K. Murata, K. Kajiya, N. Nakamura, H. Ohno, Direct electrochemistry of bilirubin oxidase on three-dimensional gold nanoparticle electrodes and its application in a biofuel cell, Energy Environ. Sci. 2 (2009) 1280–1285.

29 T. Miyake, K. Haneda, N. Nagai, Y. Yatagawa, H. Onami, S. Yoshino, M. Nishizawa, Enzymatic biofuel cells designed for direct power generation from biofluids in living organisms, Energy Environ. Sci. 4 (2011) 5008–5012.

30 M. Kizling, K. Stolarczyk, J.S.S. Kiat, P. Tammela, Z. Wang, L. Nyholm, R. Bilewicz, Pseudocapacitive polypyrrole–nanocellulose composite for sugar-air enzymatic fuel cells, Electrochem. Commun. 50 (2015) 55–59.

31 T. Ikeda, F. Matsushita, M. Senda, d-Fructose dehydrogenase-modified carbon paste electrode containing *p*-benzoquinone as a mediated amperometric fructose sensor, Agric. Boil. Chem. 54 (1990) 2919–2924.

32 K. Damar, D.O. Demirkol, Modified gold surfaces by poly(amidoamine) dendrimers and fructose dehydrogenase for mediated fructose sensing, Talanta 87 (2011) 67–73.

33 D. Sarauli, C. Wettstein, K. Peters, B. Schulz, D. Fattakhova-Rohlfing, F. Lisdat, Interaction of fructose dehydrogenase with a sulfonated polyaniline: Application for enhanced bioelectrocatalysis, ACS Catalysis 5 (2015) 2081−2087.

34 Y. Kamitaka, S. Tsujimura, K. Kano, High current density bioelectrolysis of d-fructose at fructose dehydrogenase-adsorbed and Ketjen Black-modified electrodes without a mediator, Chem. Lett. 36 (2007) 218−219.

35 S. Tsujimura, A. Nishina, Y. Hamano, K. Kano, S. Shiraishi, Electrochemical reaction of fructose dehydrogenase on carbon cryogel electrodes with controlled pore sizes, Electrochem. Commun. 12 (2010) 446−449.

36 H. Funabashi, K. Murata, S. Tsujimura, Effect of Pore Size of MgO-templated carbon on the direct electrochemistry of d-fructose dehydrogenase, Electrochemistry 83 (2015) 372-375.

37 K. Murata, M. Suzuki K. Kajiya, N. Nakamura, H. Ohno, High performance bioanode based on direct electron transfer of fructose dehydrogenase at gold nanoparticle-modified electrodes, Electrochem. Commun. 11 (2009) 668−671.

38 K. Murata, M. Suzuki, N. Nakamura, H. Ohno, Direct evidence of electron flow via the heme c group for the direct electron transfer reaction of fructose dehydrogenase using a silver nanoparticle-modified electrode, Electrochem. Commun. 11 (2009) 1623−1626.

39 Y. Hibino, S. Kawai, Y. Kitazumi, O. Shirai, K. Kano, Mutation of heme c axial ligands in d-fructose dehydrogenase for investigation of electron transfer pathways and reduction of overpotential in direct electron transfer-type bioelectrocatalysis, Electrochem. Commun. 67 (2016) 43−46.

40 Y. Yamada, K. Aida, T. Uemura, Coenzyme Q_{10} in the respiratory chain linked to fructose dehydrogenase of *Gluconobacter cerinus*, Agric. Biol. Chem. 32 (1968) 532−534.

41 R.S. Deinhammer, M. Ho, J.W. Anderegg, M.D Porter, Electrochemical oxidation of amine-containing compounds: a route to the surface modification of glassy carbon electrodes, Langmuir 10 (1994) 1306−1313.

42 E.P. Koval'chuk, N.V Stratan, O.V. Reshetnyak, J. Błażejowski, M.S. Whittingham, Synthesis and properties of the polyanisidines, Solid State Ion. 141 (2001) 217−224.

43 M. Tominaga, C. Shirakihara, I. Taniguchi, Direct heterogeneous electron transfer reactions and molecular orientation of fructose dehydrogenase adsorbed onto pyrolytic graphite electrodes, J. Electroanal. Chem. 610 (2007) 1–8.

44 C.C. Moser, J.M. Keske, K. Warncke, R.S. Farid, P.L. Dutton, Nature of biological electron transfer, Nature 355 (1992) 796–802.

Conclusions

In this thesis, the author investigated the factors of electrodes and enzymes affect the performance of DET-type bioelectrocatalysis. Futhermore, based on the understanding the interaction between enzymes and electrodes, improved performance of DET-type bioelecatalysis have been realiazed by adsorption of enzymes at functionalized electrode surface.

In chapter 1, non-catalytic direct electron transfer (DET) signal of Compound I of horseradish peroxidase (POD) was first detected at 0.7 V on POD/carbon nanotube mixture-modified electrodes. Excellent performance of DET-type bioelectrocatalysis was achieved with POD immobilized with glutaraldehyde onto KB/GC electrodes for H_2O_2 reduction with an onset potential of 0.65 V (vs. Ag|AgCl|sat. KCl) without any electrode surface modification. These results indicated that the mesoporous structures play an important role for promoting the DET-type bioelectrocatalysis of POD. Furthermore, by coupling of the H_2O_2-generated oxidase (for example, glucose oxidase) with POD at such mesoporous electrode, bienzyme system has been successfully developed for detection of a variety of substrates of H_2O_2-generating oxidases. The developed DET-type bienzyme system can be applied in a variety of analytes detection by just changing the corresponding H_2O_2-generated oxidase.

In chapter 2, the author has found that electrostatic interaction between the enzymes and electrode surfaces affect the performance of DET-type bioelectrocatalysis. In the case of BOD, the O_2 reduction current increased with decreasing the CNT length and almost diffusion-controlled bioelectrocatalytic reduction of O_2 was realized with CNTs of an average length (L) of 1 μm at pH 7.0, 25 °C, and a rotating rate of 4000 rpm. In contrast, the almost opposite tendency was obtained when CueO was utilized as a biocatalyst despite both BOD and CueO having similar sizes and a net negative charge in neutral solutions. Several factors affect the performance of DET-type bioelectrocatalysis have been investigated and discussed, and the electrostatic interaction between the enzyme, especially the portion near the redox active center, and the electrode is one of the most important factors controlling the orientation of the redox enzyme for DET-type bioelectrocatalysis.. This assumption was reinforced using hydrogenase (H_2ase) as a model enzyme.

In chapter 3, improved DET-type bioelectrocatalysis of BOD has been realized at 4-aminobenzoic acid modified KB electrode, while H_2se at *p*-phenylenediamine modified KB electrode, thanks to the electrostatic interaction between the enzymes (BOD or H_2ase) and the charged electrodes. The developed BOD-based biocathode and H_2ase-based bioanode have been used to constructe a dual gas-diffusion membrane- and mediatorless H_2/air-breathing gas-diffusion H_2/air biofuel cell operatin under room temperature and quiescent condition with a very high power density (P_{max}=6.1 mW cm^{-2}). On the other hand, methoxy-functionalized carbon surface was developed to increase the productive orientation of D-fructose dehydrogenase (FDH) for efficient

DET-type bioelectrocatalysis, due to the specific interaction between FDH, especially the heme c moiety, and methoxy substituent on the electrode surface. The developed FDH-based bioanode with very high current density (23 ± 2 mA cm^{-2} in FDH/2,4-dimethoxyaniline/KB/GCE, for example) is expected to be applied in biofuel cell.

Acknowledgments

The author would like to express his sincere gratitude to Dr. Kenji Kano, Professor of Kyoto University for providing him with his continuous guidance, valuable discussion, and encouragement throughout this study. The author would like to thank Dr. Osamu Shirai, Associate Professor of Kyoto University, for a number of helpful suggestions and criticisms. The author would like to thank Dr. Yuki Kitazumi, Assistant Professor of Kyoto University, for his kind supports and a number of critical comments. Speical thanks to Ms. Toshie Koyama, the secretary in the lab, for her kindness and support in the laboratory life.

The author gratefully thanks to the members of Kano's laboratory, Dr. Shota Kawai, Dr. Keisei So, Dr. Yu Sugimoto, Mr. Issei Hirata, Mr. Masahiro Hori, Mr. Keisuke Kimura, Mr. Kento Sakai, Mr. Yasunari Takano, Mr. Yuya Hibino, Mr. Masaki Motoike, Mr. Arato Suzuki, Mr. Yutaka Takeuchi, Mr. Kebin Xu, Mr. Ryutaro Katsube, Mr. Ryosuke Takeuchi, Mr. Takuya Yamaguchi, Ms. Yuko Fukao, Ms. Yukina Matsui, Mr. Eisaku Nakao, Ms. Saeko Shiraiwa, Ms. Maiko Kaji, Ms. Akiho Kojima, Ms. Yui Takahashi, Mr. Masaki Takaishi, Ms.Toshie Koyama, Mr. Taiki Adachi, Mr. Harunori Kawai, Mr. Yuya Kaida, Mr. Issei Kasai and Ms. Kyoko Kisida for their kind support during the three years.

The author thanks professors, doctors and friends, the author have ever met in conferences and events for their kind advices and encouragement.

Finally, the author would like to express his greatest thanks to his family for their continuous encouragement.

Hong-qi Xia

Kyoto

September 2017

List of publications

1 **H.-Q. Xia**, Y. Kitazumi, O. Shirai, and K. Kano
Direct electron transfer-type bioelectrocatalysis of Peroxidase at mesoporous carbon electrodes and its application for glucose determination based on bienzyme system
Anal. Sci., in press (Chapter 1 1-1)

2 **H.-Q. Xia**, Y. Kitazumi, O. Shirai, H. Ohta, S. Kurihara, and K. Kano
Mesoporous microelectrode for diffusion-controlled amperometric detection of putrescine based on co-immobilization of peroxidase and putrescine oxidase without a mediator
In preparation. (Chapter 1 1-2)

3 **H.-Q. Xia**, Y. Kitazumi, O. Shirai, Hiroki Ozawa, Maki Onizuka, Takuji Komukai, and K. Kano
Factors affecting the interaction between carbon nanotubes and redox enzymes in direct electron transfer-type bioelectrocatalysis
Bioelectrochemistry, submitted (Chapter 2 2-1)

4 **H.-Q. Xia**, Y. Kitazumi, O. Shirai, and K. Kano
Enhanced direct electron transfer-type bioelectrocatalysis of bilirubin oxidase on negatively charged aromatic compound-modified carbon electrode
J. Electroanal. Chem., **763**; 104–109 (2016) (Chapter 3 3-1)

5 **H.-Q. Xia**, K. So, Y. Kitazumi, O. Shirai, K. Nishikawa, Y. Higuchi, and K. Kano
Dual gas-diffusion membrane- and mediatorless dihydrogen/air-breathing biofuel cell operating at room temperature
J. Power Sources, **335**; 105–112 (2016). (Chapter 3 3-2)

6 **H.-Q. Xia**, Y. Hibino, Y. Kitazumi, O. Shirai, and K. Kano
Interaction between D-fructose dehydrogenase and methoxy-substituent-functionalized carbon surface to increase productive orientations
Electrochim. Acta, **218**; 41–46 (2016). (Chapter 3 3-3)